A STUDY ON FLING STEPS IN THE TURKISH STRONG GROUND MOTION DATASET

by

Emrecan Adanır

B.S., Civil Engineering, Ondokuz Mayis University, 2019

Submitted to Kandilli Observatory and Earthquake Research Institute in partial fulfillment of the requirements for the degree of Master of Science

Graduate Program in Earthquake Engineering

Boğaziçi University

2023

To my family,

ACKNOWLEDGEMENTS

First of all, I would like to express my special thanks of gratitude to my supervisor Assoc. Prof. Gülüm Tanırcan for her limitless support, patience, and guidance during the preparation of my thesis. Her mentoring contributed to not only a full understanding of my research area but also shaping my career path. In addition to being an excellent mentor, she is one of the nicest people I have ever met. Her recommendations will always shed light on my life.

In addition, I would like express my gratitude to Prof. Ayşe Edinçliler for her time and encouragement.

I would like to thank Prof. Sinan Akkar, Assoc. Prof. Ufuk Hancılar and Prof. Ali Pınar for their valuable lectures and guidance.

I am also thankful to my classmates, in the Earthquake Engineering department for their invaluable friendship and for great times we spent together.

Lastly, I am eternally grateful to my parents, Metin Adanır and Zülfi Adanır, for their unconditional support. I owe my entire life to them. I also wish to thank my niece Buse Ak, who supported me motivationally throughout this process.

ABSTRACT

A STUDY ON FLING STEPS IN THE TURKISH STRONG GROUND MOTION DATASET

In this study, the existing methodologies on fling step calculation from strong ground motions have been investigated and improvements on the most recent data processing scheme eBASCO (Schiappapietra et al., 2021) have been proposed. Capability of the proposed scheme is verified through comparison of permanent displacements that obtained on the processed records and those derived from the co-located GPS data both from Türkiye and worldwide earthquakes. For the first time, Türkiye permanent displacement inventory is created through processing both horizontal and vertical components of the Turkish strong motion dataset. For this purpose, 288 recordings (Rjb $\leq$ 50 km) of 20 shallow crustal earthquakes (Mw $\geq$ 6) occurred between 1983-2023 are utilized. In addition, 36 recordings of the 2023 Kahramanmaraş (Mw 7.7) earthquake are also processed and included in this thesis. Performance of evaluation of two global prediction models for fling amplitudes (Kamai et al. (2014) and Burks and Baker (2016)) are performed using Turkish permanent displacement inventory. Then, fling step prediction model of Burks and Baker (2016) is adjusted and the Türkiye-adjusted equation has been further compared with the recordings of the 6 February 2023 Kahramanmaraş (Mw 7.7) earthquake. Lastly, the permanent displacements in vertical components from Turkish strong motion database and NESS 2.0 database are inspected. Performance of the Kamai et al. (2014) prediction equation for this component is evaluated through residual analyses. In addition, based on the empirical dataset, a new predictive model for this component is proposed. This study will contribute to both seismic design of new structures and more accurate evaluation of existing structures in the vicinity of faults. The presented inventory will greatly help to identify the fling-containing ground motion records to be used in the seismic design of the structures through selecting and scaling procedures. Furthermore, the presented fling inventory will augment to fling values of normal and strike-slip earthquakes in the worldwide fling database by 22% and 33%, respectively.

ÖZET

TÜRKİYE KUVVETLİ YER HAREKETİ VERİ TABANI İÇERİSİNDE KALICI YER DEĞİŞTİRMELER ÜZERİNE BİR ÇALIŞMA

Bu çalışmada kalıcı atım hesaplanması için mevcut olan yöntemler incelenmiş ve en güncel veri işleme şeması olan eBASCO (Schiappapietra vd., 2021) iyileştirilmiştir. Önerilen veri işleme şemasının kalıcı deplasmanları yakalama yetkinliği bu şema ile işlenmiş Türkiye ve dünya depremlerine ait kayıtlardan ve onlara yakın konumlanmış GPS verilerinden elde edilen kalıcı yer değiştirmelerin kıyaslanmasıyla doğrulanmıştır. Türkiye güçlü yer hareketleri veri setindeki deprem kayıtlarının işlenmesiyle ilk kez kalıcı yer değiştirme envanteri oluşturulmuştur. Bu amaçla, 1983'den 2023 yılına kadar oluşmuş 20 sığ kabuk depreme ($Mw \geq 6$) ait 288 deprem kaydı ($Rjb \leq 50$) kullanılmıştır. Ayrıca, 2023 Kahramanmaraş (Mw 7.7) depreminin 36 deprem kaydı proses edilmiş ve çalışmaya eklenmiştir. Kamai vd. (2014) ve Burks ve Baker (2016) küresel kalıcı yer değiştirme tahmin denkleminin Türkiye için tahmin performansları envanter üzerinde değerlendirilmiştir. Burks ve Baker (2016) kalıcı yer değiştirme tahmin denklemi Türkiye'ye uyarlanmış ve uyarlanmış denklemin tahminleri 2023 Kahramanmaraş (Mw 7.7) depremi kayıtları ile test edilmiştir. Son olarak Türkiye güçlü yer hareketleri veri tabanı ile NESS 2.0 veri tabanında bulunan dikey bileşen kayıtlarının kalıcı yer değiştirmeleri incelenmiştir. Bu bileşen için Kamai vd. (2014) tahmin denklemi kalıntı analizleri ile değerlendirilmiştir. Ayrıca bu bileşen için ampirik veri setine dayalı yeni bir kalıcı atım tahmin denklemi sunulmuştur. Bu çalışma hem fay yakınlarına yapılacak yapıların sismik dizaynlarına hem de mevcut yapıların daha kesin değerlendirilmesine katkı sağlayacaktır. Sunulan envanter yapıların sismik tasarımında kullanılacak kayıtları seçme ve ölçeklendirme aşaması için gerekli olan kalıcı atım içeren deprem kayıtlarının belirlenmesine büyük katkı sağlayacaktır. Sunulan envanter küresel kalıcı atım veri tabanı normal ve doğrultu atımlı depremler açısından %22 ve %33 oranında artıracaktır.

TABLE OF CONTENTS

LIST OF FIGURES

LIST OF TABLES

LIST OF SYMBOLS/ABBREVIATIONS

AFAD	Earthquake Research Department of General Directorate of Disaster Affairs
ANN	Artificial neural network
AUST	Geoscience Australia
BAP	Basic Accelerogram Processing, Converse, 1984
BBP	Broadband Platform
CSEM	Centre Sismologique Euro-Mediterraneen
eBASCO	Extended Baseline Correction
ESM	Engineering Strong Motion Database
EW	East-West
FN	Fault Normal
FP	Fault Parallel
FW	Foot Wall
GCMT	Global Centroid Moment Tensor project
GMM	Ground motion model
GMPE	Ground motion prediction equation
GNSS	Global Navigation Satellite Systems
GPS	Global Positioning System
HW	Hanging Wall
ICBO	International Conference of Building Officials
IDA	Incremental Dynamic Analysis
IRIGM	Universite Joseph Fourier, Grenoble, France
ISC	International Seismological Center
ITU	Istanbul Technical University
KOERI	Boğaziçi University- Kandilli Observatory and Earthquake Research Institute
LDEO	Lamont Doherty Earth Observatory of Columbia University
M0	Seismic moment
Mw	Moment magnitude
N-TSMD	New Turkish strong ground motion dataset of Türkiye

N.m	Newton-meter
NESS	Near Source Strong Motion flat file
NESS 2.0	Second Version of Near Source Strong Motion flat file
NGAW2	Next Generation Attenuation Relationships for Western United States of America 2
NS	North-South
NTH	Nonlinear time history
PD	Permanent displacement
PE&A	Pacific Engineering and Analysis
PEER	Pacific Earthquake Engineering Research Center
PGA	Peak Ground Acceleration
PGD	Peak ground displacement
RotD100	Rotated motion which yields the maximum horizontal permanent displacement
Rjb	Joyner and Boore distance that corresponds to the closest distance from the fault rupture projection
Rrup	Closest distance to the fault
Rx	Horizontal strike-normal distance from the fault
S	Rupture area
SCEC	Southern California Earthquake Center
Sd	Displacement response spectra
SDOF	Single Degree of Freedom
TBYD 2018	Turkish Building Design Code 2018
UBC	Uniform Building Code
UD	Up-Down

1. INTRODUCTION

Fling step is a distinct characteristic of near-field strong ground motions which can be detected as a half cycle pulse on the velocity waveforms. Fling step is originated by a permanent dislocation of the ground and therefore it is also known as permanent displacement. Previous observations demonstrated that fling step has a great potential to damage the structures. Therefore, it should be taken into account in the seismic design of structures. Nevertheless, on account of the fact that widely utilized data processing procedures such as filtering camouflage the permanent displacements, the records containing fling step cannot be identified. In addition, performances of the existing permanent displacement predictive models, which are based on earthquake simulations, for Türkiye earthquakes are not clear. Hence, these ambiguities and missing fling inventory in Türkiye have been the main motivations of this study.

1.1. Contributions of the Study

In most of the design codes, it is allowed to use spectrally matched accelerograms. However, in the case of near fault sites, records should be carefully selected to include the near fault effects (directivity and fling). Therefore, in the selection of the strong ground motions for the structural design purposes, fling-containing motions should be identified. Although some studies proposed an alternative way to obtain fling-containing records by including synthetic fling step onto filtered records, Burks and Baker (2014) demonstrated that it causes a conservative estimate of the collapse capacity. For this reason, a new comprehensive data processing scheme, which is going to meet the need in the literature, is proposed in this thesis. In addition, the acquired permanent displacement inventory of Türkiye will be a guidance for engineers to clearly identify the records whether the fling does exist or not. Fling step database of Türkiye consists of 288 ground motion records from 20 earthquakes. In the dataset, the largest permanent displacement is found as 264 cm from 1999 Düzce (Mw 7.1) earthquake. Another point of the study is that apart from the three main components (East-West (EW),North-South (NS),Up-Down (UD)), the Fault Normal

(FN) and Fault Parallel (FP) components of the ground motion stations are also processed. It is observed that the fling in the slip direction component of the earthquake record is not always larger than that in the perpendicular component. Moreover, performances of the Kamai et al. (2014) and Burks and Baker (2016) fling predictive models for Türkiye earthquakes are evaluated. Based on the results of the residual analyses, Burks and Baker (2016) prediction model is improved for the permanent displacements on the horizontal components of Türkiye earthquakes is presented. Adjusted model is also tested by 6 February 2023 Kahramanmaraş (Mw 7.7) earthquake. Lastly, permanent displacements in vertical components are inspected and a new predictive model for this direction of the motion is proposed.

1.2. Scope of Work

- Previous studies on fling step are presented in Chapter 2.
- Existing processing schemes, proposed scheme, differences between proposed and previous schemes, and the prove of the effectiveness of the proposed scheme are given in Chapter 3.
- Detailed description of Türkiye strong motion database utilized in this study is given in Chapter 4.
- Permanent displacement database of Türkiye is demonstrated in Chapter 5.
- Evaluations of performance of the fling step prediction models for Türkiye earthquakes, proposed Türkiye adjusted Burks and Baker (2016) prediction model, and evaluation of performance of the adjusted model for the 6 February 2023 Kahramanmaraş (Mw 7.7) earthquake are presented in Chapter 6.
- Evaluation of Kamai et al. (2014) prediction model for vertical components from worldwide earthquakes and proposed new global fling step prediction model for vertical components are presented in Chapter 7.
- Conclusions and future works of the study are given in Chapter 8.

2. PREVIOUS EFFORTS ON FLING STEP

One of the earliest studies on permanent displacement determination from strong motion accelerogram has been performed by Iwan et. al (1985). They stated that a digital instrument has much lower noise than the analog instrument and its capability of recording the pre-event motions disqualifies the ambiguity in the initial conditions of the data. In order to examine the nature of the errors associated with integration of acceleration time histories obtained from digital instruments, they conducted a series of laboratory tests. Test results demonstrated that the integrated acceleration time history can give a well accurate measure of the permanent displacement. Based on test results they stated that the integrated acceleration time history, recorded in digital seismograph, may result in a well accurate measure of the permanent displacement. For this purpose, based on the test results, they presented a correction algorithm which consists of the evaluation of the baseline offsets in the strongest portion of the motion and the following end part. To define these parts of the motion, Iwan et al. (1985) introduced time correction points T_1 and T_2 that corresponds to starting and end points of the strongest part of the motion respectively. Detailed explanation about the algorithm and laboratory tests can be found in Chapter 3.1.

Later, Boore (1999) studied the displacement waveforms that are derived from the acceleration time histories of the 1999 Chi-Chi earthquake at stations TCU 078 and TCU 129. After removing a simple baseline which was derived from the pre-event portion of the motion, drifts appeared on the derived displacement waveforms. With this finding, he suggested that changes in the zero-level of the acceleration trace are responsible for the drifts. Studied stations were specifically chosen because of the quality of their data and close distances to the earthquake location. However, shifts in the acceleration baselines made it difficult to determine the permanent displacements from the records. Baseline was obtained from the average of the pre-event portion of the motion and removed by utilizing BAP (Basic Accelerogram Processing, Converse, 1984).

Since the Global Positioning System (GPS) stations exhibited 340 cm horizontal and 180 cm vertical static offset in the epicentral area, it is understood that very large displacements, that reach up to 15 m, seen on the horizontal components of TCU 129 were unrealistic even after simple baseline removal. Moreover, the displacements exhibit no signs of leveling off at the end of the recorded duration. Similar trends were also seen on vertical component of that station as well as on the all records of the other station. Therefore, it is decided that a processing scheme was needed to be executed on the records. It was stated that a reasonable constraint on any strong ground motion record was that the ground velocity must be zero after the strong shaking ended, which was not the case for some of the components of the TCU 129 and the TCU 078. Based on the almost linear trend observed on the velocity traces of the records of station TCU 129, Boore (1999) also mentioned that the baseline of the acceleration time history is not the same as the pre-event portion. To be able to evaluate the records appropriately, he used a processing scheme for baseline correction and presented the processed EW component of the station TCU 129. As a first step in the processing scheme, the average of the pre-event portion on the acceleration time history is removed. Then, a line which fits to the acceleration trace between the onset of the shaking and the end of the motion is removed from the beginning at the onset of the shaking. Third step in the scheme is defined as applying an acausal low-cut filter (Butterworth filter) with an order of 2 and a corner of 0.05 Hz to the corrected trace. Fourth step is applying a 2nd order causal low-cut (Butterworth filter) filter with corner frequency of 0.05 Hz to the corrected trace. As a last step, Boore (1999) recommended applying the Iwan et al. (1985) scheme. In the last part of the study, the effect of the baseline correction on displacement response spectra was inspected. Boore (1999) concluded that for periods less than about 20 second, baseline-correction scheme did not affect the displacement response spectra.

Boore (2001) was published as a follow-up study to Boore (1999). The findings of the previous study were restated with more data on the 1999 Chi-Chi earthquake by Boore (2001). Boore (2001) illustrated the effects of several baseline correction procedures for accounting for the baseline shifts on the ground velocity, ground displacement and response spectra. In the study, a generalization of the scheme presented by Iwan et al. (1985) was mainly used. However, Boore (2001) neither made an assumption for the source of the baseline shifts as found by Iwan et al. (1985) nor defined a threshold for baseline occurrence. After performing a few tests, he stated that the corrected velocity and displacement traces

are not very sensitive to the selection of the correction point T_1. Nevertheless, he recommended testing this finding for cases in which the records cease recording immediately after the strong shaking. Boore (2001) also found that if the recorded motion is not very long where the changes in acceleration baseline might lead to a non-linear trend in velocity trace, T_2 is generally chosen to be end of the motion. In the study, the condition that the final velocity should be equal to zero was satisfied by fitting a baseline correction at the end of the T_1 - T_2 interval. Boore (2001) redefined the time correction points T_1 and T_2 as free parameters rather than relying on the acceleration amplitude threshold like Iwan et al. (1985). For instance, T_2 can be any point between T_1 and the end of the record to meet the zero condition of the velocity close to the end of the record. However, it was acknowledged that assigning T_2 as a free parameter causes in a wide range of values for permanent displacements. For this reason Boore (2001) recommended to utilize a more appropriate correction scheme based on the long-time behavior of the velocity time histories from the raw acceleration waveform.

Abrahamson (2002) described a method for incorporating fling into design ground motions by modeling the fling time history as a sine wave for sites located close to the fault, like within 10 km. His model is composed of three parameters: the period and amplitude of fling as well as the arrival time of the sine wave with respect to the vibratory ground motion. In his model the acceleration time history of the fling-step, amplitude of fling and the amplitude of the tectonic deformation at the site are parameterized. However, the arrival time of the sine wave is described only if the site located close to fault than 10 km, T_1 is very close to arrival time of S-wave and for more distant sites T_1 is between the arrival of P and S waves. Moreover, he also presented a fling amplitude prediction equation for the fault parallel components of the strike slip earthquakes.

Hisada and Bielak (2003) presented a mathematical method for computation of the near fault strong ground motions in a layered half-space by taking into consideration permanent displacement due to surface faulting. In their study they found that the Green's function demonstrated near singularities for near fault motions. After the investigation of the singularities, they stated that the dynamic Green's functions required to be distributed very densely for these singularities. Therefore, a new form of the representation theorem is

introduced by Hisada and Bielak (2003). In the proposed Green's function form, dynamic and the static Green's functions separated and thus the computation load decreased. In addition they investigated the combined effects of the fling step and the rupture directivity on the ground motion. It was found that the fling effects mainly stem from the static Green's function while the directivity effects mainly stem from the dynamic Green's function. In addition, after investigating the attenuation relation of the permanent displacement by utilizing a circular fault model with a radius of 10 km in a homogenous full-space, Hisada and Bielak (2003) stated that the permanent displacement attenuates quickly on the order of $1/r^2$ at distances larger than a fraction of the radius.

Kalkan and Kunnath (2006) inspected the consequences of well-known characteristics of near-fault ground motions on the seismic response of steel moment frames. Their fundamental findings are; the waveforms which contain forward directivity do not contain fling causing higher modes to be activated and records with fling effects were found to excite systems primarily in their fundamental mode. In their study, a set of near-fault ground motions having forward directivity and fling step are assembled. These records are used in nonlinear time history (NTH) analyses and their results are compared to the response of buildings to typical far-fault ground motions. Additionally, artificial fling-step effects are synthesized into typical near-fault motions having forward directivity, and the structural response of the same buildings is reexamined. Kalkan and Kunnath (2006) utilized a total of 21 records which were selected to cover a range of frequency content, duration and amplitude. Records were divided into three sub categories with the aim of obtaining the effects of the fling and directivity on the buildings separately. The first set contains seven ordinary far-fault ground from earthquakes with the magnitude of ranging between Mw 6.4 to Mw 7.5 at soil or stiff soil sites. The second set includes seven near-fault ground motions characterized with forward-directivity effect which recorded the earthquakes having a magnitude between Mw 6.7 and Mw 7.1. The third set, a total of seven near-fault ground motions characterized with fling-step displacement were collected. The last set was created from the records of 1999 Kocaeli (Mw 7.6) and 1999 Chi-Chi (Mw 7.6) earthquakes at distances of 2.2 to 13.8 km. Kalkan and Kunnath (2006) specifically processed the records in the third set by mainly utilizing Iwan et al. (1985) and Boore (2001) to reveal the permanent displacements. They considered 4-story building designed according to Uniform Building Code (UBC), International Conference of Building Officials, (ICBO 1988) , 6- and

13-story buildings designed with the UBC (ICBO 1973) requirements for the analyses. They found that far-fault motions produce nearly uniform inter-story drift for most records; however, in case of near-fault records, they impose higher and the maximum drift is generally concentrated at the lower story levels. Additionally, they found that demands in the lower levels for records with fling step were much higher than records with forward-directivity. Moreover, responses of the buildings to records with predominant flings found in the first mode. Therefore, Kalkan and Kunnath (2006) concluded that near-fault records with fling can be more damaging than far-fault records but they tend to accentuate first-mode behavior. They also inspected the effect of the fling on acceleration response spectrum and found that the effect of the inherent pulse tends to augment the long-period part of the spectrum. With this outcome Kalkan and Kunnath (2006) suggested that amplifying the design spectrum with explicit near-source factors as in UBC may not be always conservative.

Wu and Wu (2007) presented a baseline correction procedure for ground motion records. Based on the works of Iwan et al. (1985) and Boore (2001), they developed a new scheme for the baseline correction and validated it by shake-table tests of a known “step” displacement on a set of accelerographs. Their method recovered some 97% of the observed displacement on the shake table. Although their method is mainly validated against shake table tests, Wu and Wu (2007) also tested the scheme with the limited ground motion records, from 1999 Chi-Chi (Mw 7.6) and 2003 Chengkung (Mw 6.8) earthquakes, by comparing the findings with GPS measurements at close sites. Differently from the Iwan et al. (1985), Wu and Wu (2007) proposed separating the ground motion records into three parts. For this purpose, they redefined the time correction points T_1 and T_2 and introduced the third correction point T_3 in the proposed baseline correction scheme. In addition, to make sure the permanent displacement is defined on the flat portion of the record, they introduced a flatness indicator that exhibits the fade level of displacements in the last portion of the motion starting from T_3. Detailed information about Wu-Wu (2007) data processing scheme can be found in Chapter 3. Moreover, Wu-Wu (2007) also presented a fling step predictive model only based on some of the records of the 1999 Chi Chi (Mw 7.6) earthquake.

Chao et al. (2010) updated the Wu and Wu (2007) baseline correction procedure by taking into consideration the energy distribution in accelerograms for the selection of the correction points. In the study, the estimation of the permanent displacement was made quicker by defining the selection of the correction points with the cumulative energy distribution rather than opting manually. Chao et al. (2010) utilized the 1999 Chi-Chi (Mw 7.6), 2003 Chengkung (Mw 6.8) and the 2006 Taitung (Mw 6.1) earthquakes to demonstrate the effectiveness of their approach. Firstly, from the definitions of the T_1 and T_3 correction points, Chao et al. (2010) interpreted that these points should be in the first 50% and the last 50% of the energy distribution of the accelerogram. Then, with the findings of the study T_1 and T_3 were assigned as the points which correspond to the 25% and the 65% of the energy dissipation of the strong shaking respectively. In addition, T_1 was redefined as a point after the point at which the ground starts to move. Moreover, due to the fact that the final displacement values changed more closely with the T_3, Chao et al. (2010) stated that the permanent displacement is more sensitive to the T_3 point than T_1. Lastly, they also inspected the Peak Ground Acceleration (PGA) constraint of the previous processing schemes by a combination of acceleration limit and the ratio of the energy dissipation. It was found that limiting the acceleration did not give rise to favorable results.

Burks and Baker (2014) presented an evaluation of a nonlinear Single Degree of Freedom (SDOF) system using ground motion records with varying fling properties, including records with static offsets preserved via baseline correction, records with static offsets removed via filtering, and records with artificial static offsets added. For this study, they utilized the strong ground motion records from Pacific Earthquake Engineering Research Center (PEER)- Next Generation Attenuation Relationships for Western United States of America 2 (NGAW2) database. Firstly, each set of pulses was high-pass filtered at a cutoff frequency of 0.2 Hz and 0.5 Hz to investigate the effect of record filtering on collapse capacity. They found that the collapse capacity of a degrading nonlinear SDOF is similar for two versions of the same ground motion: one with the static offset preserved via baseline correction and the other with the static offset removed via filtering. Burks and Baker (2014) also stated that even though the static displacement is removed by filtering processing, the dynamic component of the fling is preserved. Due to the scarcity of data, they only considered three record that already contain fling: the 1999 Chi Chi earthquake North-South (NS) component of the station TCU 068 from; the 2010 Darfield (Mw 7)

earthquake East-West component of GDLC station; and the 1999 Kocaeli earthquake NS component of YPT station. These records were processed by utilizing Boore (2001) and Wu-Wu (2007) without filtering. After conducting Incremental Dynamic Analysis (IDA), they found that filter cutoff frequency of 0.2 Hz has a negligible effect on the collapse capacity, while the cutoff frequency of 0.5 Hz causes an increase in collapse capacity for all pulse types. They stated that filtering at a low cutoff frequency outside the range of pulse or structural periods has a negligible effect on collapse capacity. However, filtering at a high cutoff frequency that approaches the pulse or structural period can increase the collapse capacity, leading to an un-conservative estimate. Lastly, after adding artificial fling pulses to filtered records, it was observed that as displacement amplitude increases or pulse period decreases, the collapse capacity decreases.

Rather than processing the raw data containing the fling step, Kamai et. al (2014) presented an update to the Abrahamson (2002) fling-step models for recreating synthetic fling-containing ground motion by adding the fling step onto any processed time history. Parameterization of the fling step was performed using the wavelet type that adopted the form proposed by Abrahamson (2002). For this purpose they presented a fling step prediction model and tailored it for the records of the horizontal components of strike-slip earthquakes and both horizontal and vertical components of reverse earthquakes. The model for the horizontal components were constructed based on the rotated motion which yields the maximum horizontal permanent displacement, also known as RotD100. For the derivation of the predictive model, they conducted an extensive set of finite-fault simulations on Southern California Earthquake Center (SCEC) broadband platform by utilizing the hybrid broadband methodology of Graves and Pitarka (2010). After presenting the simulation-based fling step model, Kamai et. al (2014) utilized 84 records from 7 events, which were available in NGAW2, to validate their findings. For this purpose, the records were specifically processed by Pacific Engineering and Analysis (PE&A). Kamai et al. (2014) stated that although empirical data exhibited a wide scatter, fling amplitudes attenuated similarly between the simulations and the available strong ground motion records. In this study, we evaluated the performance of the fling step predictive model of Kamai et al. (2014) for Türkiye earthquakes. Detailed explanation of this model and the evaluation results can be found in Chapter 6.3 and 6.4.

Burks and Baker (2016) extracted fling pulses from the data sources which are GPS, earthquake simulations and specially processed earthquake records to create a fling step predictive model. Their dataset consists of 67 processed ground motion records, 44 high-rate GPS records and nearly 2.2 million ground motion simulations. The defined real records were processed by utilizing Boore (2001) and Wu and Wu (2007) baseline correction scheme to reveal the permanent displacements. For the simulations, Burks and Baker (2016) focused on kinematic and hybrid simulations as these methods include earthquake source and wave propagation path information. Kinematic simulations of earthquake scenarios used in the study were similar to San Francisco earthquake, Hayward fault and hybrid broadband simulations of earthquake scenarios on generic reverse faults. Since the displacement time histories from the GPS were located far from the source or had very little permanent displacements, they were used to evaluate fling characteristics only at large distances. Burks and Baker (2016) evaluated the fling amplitude as a function of closest distance to the fault and moment magnitude. Therefore, differently from Kamai et al. (2014), fling predictive model of Burks and Baker (2016) depends on neither rupture mechanism nor dip angle. In this study, the performance of the fling step prediction model of Burks and Baker (2016) for Türkiye earthquakes is evaluated and its adjusted version is presented. Further information for the evaluation results and the adjusted equation can be found in Chapter 6.1 and 6.2.

D'Amico et al. (2018) presented a semi-automatic baseline correction scheme named Extended Baseline Correction (eBASCO) for near-source records by utilizing the Wu and Wu (2007) and Chao et al. (2010). They tested the scheme with the records of the 2016 Norcia (Mw 6.5) earthquake and compared the results with the geodetic measurements as well as the ground motion simulations. In addition, D'Amico et al. (2018) also tested the scheme with 6 records from the worldwide earthquakes and found good agreement between obtained permanent displacements and those were measured from nearby GPS data. eBASCO processing scheme was based on a baseline correction of the strong ground motion records by virtue of piecewise linear detrend. Unlike the previous schemes, in eBASCO a trilinear detrend is applied instead of bilinear one. In other words, the acceleration time history is subdivided into three parts named pre-event, transient and post-event windows by correction points T_0, T_1, T_2 and T_3. T_0 correction point was defined as the first sample after subtracting the first sample of recorded motion to guarantee that the velocity starts from 0. Further details of this scheme can be found in the Chapter 3. Moreover, in this study, the

recovered fling step amplitudes of the 2016 Norcia earthquake by eBASCO compared with that of predicted ones by Kamai et al. (2014) and Burks and Baker (2016) were compared. It was stated that, in general, both of the prediction models were in agreement with the permanent displacements recovered by eBASCO.

Satoh (2020) inspected the permanent displacements and the long period velocity pulse of the near fault records of the crustal earthquakes that occurred in Japan and compared them with prediction equations. In addition to comparisons, he also updated the Kamai et al. (2014) fling predictive model prediction equation for the permanent displacement by inspecting the effect of seismic moment (M_0) and rupture area relationship on the model. It was found that the rupture area (S) of homogenous-slip models from the geodetic data is smaller than the rupture area of fault models from the strong motion records and that of M_0-S relations by Wells and Coppersmith (1994), which results in the smaller average slip. Satoh (2020) stated that substituting the M_0-S relation obtained by utilizing homogenous-slip models from geodetic data into the prediction equation of Kamai et al. (2014) results in closer estimates. Further details for the M_0-S relation and its effect on Kamai et al. (2014) fling predictive model can be found in Chapter 6.2 and 6.3.

Dhanya and Raghukanth (2020) presented a probabilistic fling hazard map for India and adjoined regions. For this purpose, they developed a region-specific ground motion prediction equation (GMPE) based on the artificial neural network (ANN) by utilizing 556 scenario events consistent with the regional characteristics. They stated that the simulated permanent displacements were valid for rock type soil class. The developed GMPE was tested with the records of 1999 Chi-Chi and the 2015 Nepal (Mw 7.9) earthquakes. After classifying the faults in the region with the predominant mechanism, Dhanya and Raghukanth (2020) performed half of the probabilistic seismic hazard analysis with the developed GMPE, and the one quarter of it with Burks and Baker (2016) and the one quarter of it with Kamai et a. (2014) in a logic tree approach to account for the epistemic uncertainties. In the study, resultant probabilistic fling hazard maps for 10%, 2%, 1% and 0.5% probability in 50 years for the region were reported. In addition, they found that the active regions experience higher permanent displacements than the stable regions.

Schiappapietra et al. (2021) updated the eBASCO processing scheme that was introduced by D'amico et al. (2018). They processed some 600 records by updated version of eBASCO to test the capability of the scheme as well as to compile a dataset for the sake of calibrating attenuation models for peak ground displacement (PGD), 5% damped displacement response spectra (Sd), and permanent displacement amplitude (PD). Schiappapietra et al. (2021) updated the eBASCO scheme by modifying the selection range of T_3 correction point and comparisons of the amplitudes of the acceleration in the correction points. Detailed information about the updated scheme can be found in Chapter 3.1. The data processed by this scheme was compared with that of NESS, which was obtained by applying a second-order acausal time-domain Butterworth filter to the zero-padded acceleration time series and a cosine taper at both the beginning and the end of the signal. It was found that the PGAs are insensitive to the different low-frequency treatment of the signal. However, Peak Ground Displacements (PGDs) obtained by eBASCO were found larger than those obtained by Near Source Strong Motion flat file (NESS). Moreover, Schiappapietra et al. (2021) also compared the displacement response spectra (Sd) and found that eBASCO results in larger spectral ordinates. In addition, they presented recovered the worldwide permanent displacement dataset consists of the processed near source ground motions records by the updated version of eBASCO, named NESS 2.0. Schiappapietra et al. (2021) tested the capability of the proposed scheme by comparing some of the obtained permanent displacements with corresponding geodetic measurements. Based on the comparisons, they stated that updated version of eBASCO generally successful to obtain permanent displacements. Schiappapietra et al. (2021) also inspected the consistency of the created dataset with the Burks and Baker (2016) and Kamai et al. (2014) predictive models. They stated that estimates of Burks and Baker (2016) are in agreement only for Joyner and Boore (Rjb) distances larger than 10 km and for magnitudes greater than Mw 6. It was also stated that the observed permanent displacements decay faster with the distance than Burks and Baker (2016) prediction curves while those at the stations with close distances to the fault trace were underestimated. Schiappapietra et al. (2021) found Kamai et al. (2014) model reasonably well for the horizontal permanent displacements of strike slip earthquakes.

Hisada and Tanaka (2021) explained the fling step and introduced a theoretical method for the simulation of the near-field strong ground motions containing fling steps. In the study, the theory that had been introduced by Hisada and Bielak (2003) was validated by utilizing the theoretical solutions of a circular fault model. Moreover, they compared the static amplitudes between circular fault and a point source. It was found that the point source approximation is now valid within a distance approximate to the fault radius. Then, they applied the theory to layered half-spaces and introduced the simulation techniques for the ground motion records containing fling steps. In addition to previous theory, their approach involved subdivision of the fault and the Gauss-Legendre quadrature scheme to resolve the singularity behavior of the static Green's function. For the sake of proving the effectiveness of their approach, Hisada and Tanaka (2021) simulated 1992 Landers (Mw 7.3), 1999 Chi-Chi, 2014 Kamishiro (Mw 6.2), and 2016 Kumamoto (Mw 7) earthquakes and found successful results. Based on their findings, they concluded that calculation of the fling step requires evaluation of the fault surface integral rigorously and paying attention to both the singularity of the static Green's function and the quick fluctuations in the radiation pattern of the nearest point source.

Schiappapietra et al. (2022) utilized the recently released dataset NESS 2.0 to create a new ground motion model (GMM) for the fling-step and to add an adjustment factor of the spectral displacements predicted by a reference GMM to account for the contribution of the fling step at long periods. Differently from Kamai et al. (2014), their fling step predictive model contains normal faulting earthquakes. Schiappapietra et al. (2022) also compared their model with the Kamai et al. (2014) and found that the permanent displacement estimates of Kamai et al. (2014) attenuates faster than proposed model for both strike slip and thrust faulting events with magnitudes ranging between Mw 6 and Mw 7. In addition, it was also found that the Kamai et al. (2014) predicts larger values for strike slip events at short distances than Schiappapietra et al. (2022). They also compared some of the predicted permanent displacements with those of obtained from Global Navigation Satellite Systems (GNSS) and stated that attenuation of the prediction with distance, especially at higher magnitude values, aligned with the GNSS values. For their additional adjustment factor of the spectral displacements comparison with GNSS observations done and it was stated that the standard deviation of the updated model was always lower than that of the previous version of Cauzzi et al. (2015).

3. METHODOLOGY

In this chapter, existing data processing schemes for fling step, Iwan et al. (1985), Wu and Wu (2007), D'Amico et al. (2018), and Schiappapietra et al. (2021) are evaluated. Since the Iwan et al. (1985) and Wu and Wu (2007) defined the time correction points as trial of the all points and contained PGA limits, the feasibility of these procedures are found less to create a dataset. For instance, Kalkan and Kunnath (2006) revealed permanent displacements only on 7 records from worldwide earthquakes by utilizing Iwan et al. (1985) and Boore (2001). Similarly, Burks and Baker (2016) processed only 67 records from worldwide earthquakes by using Wu and Wu (2007). On the other hand, D'Amico et al. (2018) contains the PGAs comparison of the raw and processed data for accuracy; however, Schiappapietra et al. (2021) demonstrated that PGAs are insensitive to the different low-frequency treatment of the signal. Moreover, both D'Amico et al. (2018) and Schiappapietra et al. (2021) assign a very limited number of samples to time correction points among their defined ranges and ignores the most of the possible samples. Therefore, instead of utilizing one of these procedures, creating a new automatic data processing scheme for recovering the fling steps from the records is found more efficient.

In this section, previous data processing schemes, newly proposed schemes, their comparisons and the proof of the effectiveness of the new scheme are presented.

3.1. Existing Base Line Correction Procedures for Fling Step

As stated in Chapter 2, Iwan et al. (1985) was one of the earliest studies on the fling step in the literature. They made an attribution for the source of the baseline shift to a hysteresis in the transducer which occurs when acceleration exceeds some 50 cm/s^2 and presented a baseline correction procedure. According to Iwan et al. (1985), firstly, the acceleration time history is corrected by performing a time average solely on the first one-half of the pre-event data to eliminate the probability of including any actual earthquake data. Secondly, the last offset of the acceleration is determined and it is expected to be zero if there are no anomaly. Apart from the final offset, Iwan et al. (1985) also defined individual

baseline shifts in the strongest part of the motion and proposed to replace this shift by a single rectangular acceleration correction. In other words, they defined two portions of the records: (1) intermediate range correction acceleration, A_m, between times T_1 and T_2, where T_1 and T_2 are the start and end times of the strongest shaking interval, respectively, and (2) final part correction acceleration, A_f, from time T_2 to the end of the record. For this purpose, T_1 and T_2 correction points are defined by two approaches. In the first approach, T_1 and T_2 are defined as the first and the last times when the acceleration exceeds 50 cm/s^2. However, in the second approach, while T_1 is defined as the time of the first significant acceleration pulse, higher than 50 cm/s^2, T_2 is defined as the value which minimizes the permanent displacement. They stated that if the existence of the permanent displacement is known prior to correction, the first approach is more useful to define the correction points. However, if it is not known, the use of the second approach is recommended in the procedure. In the procedure, intermediate acceleration correction A_m is defined so as to make velocity correction continuous over the entire record with the following form:

$$A_m = \frac{V_f(T_2)}{(T_2 - T_1)} \tag{3.1}$$

They found that estimating the final acceleration offset from the last slope of the velocity record gives a more accurate result. Hence, the correction for the final offset, the level A_f, is determined from the slope of a linear fit to a part of the velocity time history as:

$$V_f(t) = V_0 + A_f t \tag{3.2}$$

V_f is found by a least-squares fit of the final part of the velocity time history, which is from T_2 to the end of the record. Overall correction procedure is given Figure 3.1.

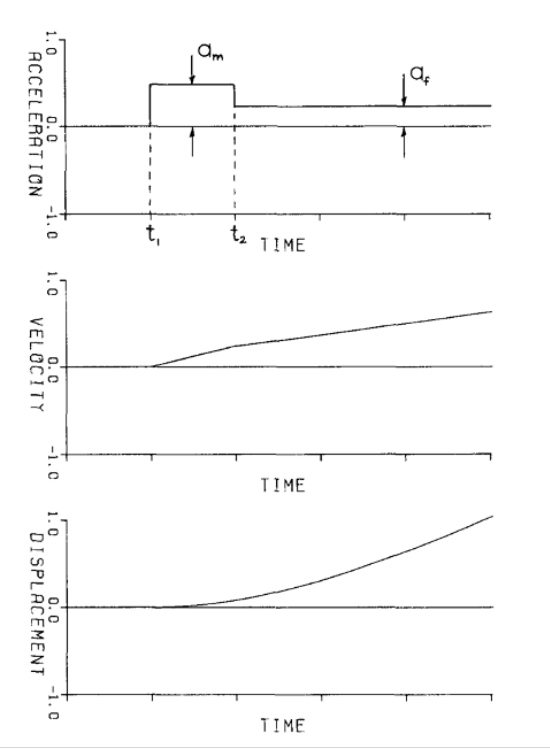

Figure 3.1. Iwan et al. (1985) baseline correction scheme in (top) acceleration, (middle) velocity and displacement (bottom) time histories

This baseline correction scheme was modified by Boore (2001) in that the selection of the correction point T_1 is set as a free parameter. Iwan et al (1985) and its modified version by Boore (2001) were used in the fling retrieving studies, such as Kalkan and Kunnath (2006), until the new schemes were introduced.

Wu and Wu (2007) data processing procedure for retrieving the fling step from the strong ground motion record was tested against shake table tests as well as 1999 Chi Chi (Mw 7.6) and 2003 Chengkung (Mw 6.8) earthquakes. This scheme was constructed by utilizing the Iwan et al. (1985)'s procedure and is valid only for the records whose PGA is higher than 60cm/s^2. First of all, based on their previous experiences and the results of Boore (2001), they stated that the displacement time history takes the shape of a ramp function. Aligned with this statement, in their procedure the T_1 is defined as the time when the ground starts moving from zero displacement, with the condition of being no earlier than that determined by utilizing Iwan et al. (1985). In addition, they also stated that the last portion of the corrected displacement history should be highly flat where the permanent

displacement is seen. Therefore, a new correction point T_3 at which the ground moves to the permanent displacement level and an "f-value" which was determined by utilizing the portion from T_3 to the end of the record are introduced in this procedure. Based on the dispersion of the displacement amplitudes at the last portion of the corrected waveform from the displacement level, where the motion fades is defined as follows:

$$f = \frac{|\, r \,|}{|\, b \,|.\, \sigma} \tag{3.3}$$

where r is the linear correlation coefficient and b is the slope of the least-squares regression line of the corrected displacement time history from T_3 to the end of the record. In the Wu and Wu (2007) processing scheme, the permanent displacement is assumed as the mean value of the last portion of the corrected displacement trace and its variance is shown as σ in the Equation (3.3). According to this procedure, correction point T_2 is defined as a time between T_3 and the end of the record such that the "f-value" becomes maximum. Wu and Wu (2007) justified themselves by the following explanation. Due to the fact that the displacement waveform should be very flat at the end portion of a well processed strong ground motion record, the absolute value of r gets close to 1, b approaches to 0, and σ takes its minimum value. For these conditions, the f reaches to its maximum value. Figure 3.2 demonstrates the Wu and Wu (2007) data processing scheme.

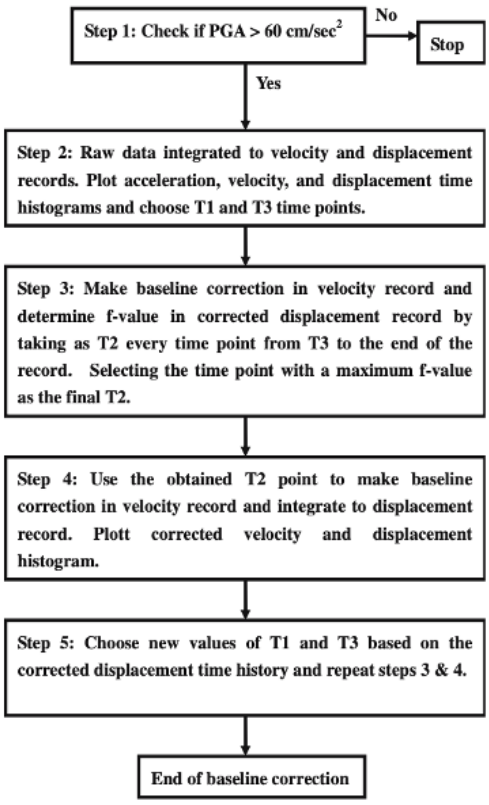

Figure 3.2. Schematic diagram of Wu and Wu (2007) data processing scheme

As seen in Figure 3.2, correction points T_1 and T_3 are approximately assigned by inspecting the integration results; therefore, executing more than one recurrence of the procedure are needed for reliable results. As aforementioned, T_2 is set to a time point between T_3 and the end of the record based on the fade level of the corrected waveform.

D'Amico et al. (2018) presented a processing scheme named eBASCO. This scheme relies on a baseline adjustment of the strong ground motion records by means of piecewise linear detrend. Different from the previous schemes, they applied a trilinear detrend. Analysis steps are as follows:

-The amplitude of the first sample is subtracted from the acceleration time history in order to make the velocity equals zero at T_0. Then baseline shift of an acceleration time history is subdivided into three windows as follows: (1) pre-event window between the time

of the first sample T_0 and the time T_1; (2) transient window between T_1 and T_2; and (3) post-event window from T_2 to the end of the signal.

-After defining the T_0, the pre-event baseline (V_i) is removed by subtracting a regression line which crosses the origin from the velocity time history. The baseline of the pre-event window is computed as:

$$V_{\mathrm{i}}(t) = A_{\mathrm{i}}t \tag{3.4}$$

where t is the time and A_i is the slope of the line that fits the velocity trace in the pre-event window. Another least-squares fitting is used to remove the linear trend V_f in the post-event window of the velocity time history, which is defined as:

$$V_f(t) = V_{0,f} + A_f t \tag{3.5}$$

where A_f is the slope of the line fitting the post event window velocity and $V_{0,f}$ is the intercepting ordinate. In the scheme, the baseline correction A_m , which was defined as the intermediate range correction acceleration by Iwan et al. (1985) in the form of Equation 3.1 is used in the acceleration transient window to satisfy that the velocity oscillates around zero at the end of the transient window. D'Amico et al. (2018) stated that aim of using A_m as to satisfy the requirement that the velocity at the end of the transient window oscillates around zero after baseline correction. Based on this statement, the velocity of the baseline correction at the end of the transient window should be equal to the velocity amplitude acquired from the Equation 3.5 as V_f (T_2). The transient-window velocity is obtained by integrating the corresponding corrected acceleration. Corrected velocity time history is created by the combination of the pre-event, transient and post-event windows.

-At last, the corrected displacement and the acceleration waveforms are obtained by integration and the derivation of the corrected velocity trace, respectively. Figure 3.3 illustrates the flowchart of D'Amico et al. (2018) processing scheme.

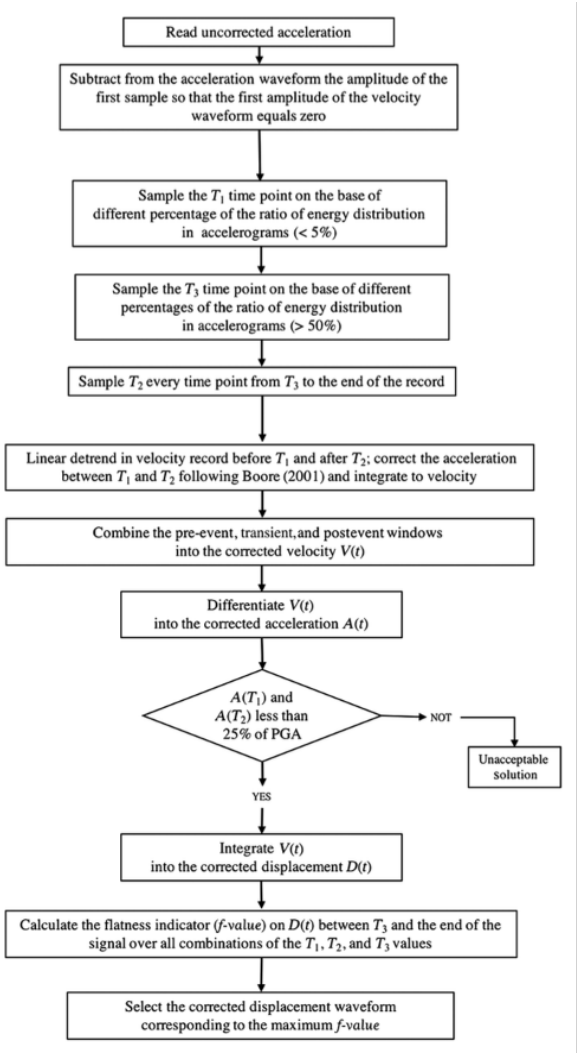

Figure 3.3. The schematic illustration of eBASCO, D'Amico et al. (2018), processing method.

For the correction points, D'Amico et al. (2018) stated that executing the scheme with the inappropriate combinations of T_1 and T_2 can result in spurious spikes in the corrected acceleration. With the aim of reducing the subjectivity of the correction points, findings of Chao et al. (2010) are taken into consideration and the selection of these points are presented as follows:

- T1 is selected as one of the five points of correspondence which are logarithmically spaced from 0.0001% to 5% of the cumulative energy dissipation of the record.

- T_3, introduced by Wu and Wu (2007), is set to linearly spaced five samples between 50 % and % 95 of the cumulative energy dissipation of the motion.

- In this scheme, the corrected displacement time histories are estimated for all the combinations of T_1 and T_3 by using baseline corrections introduced in Equations 3.4 and 3.1. For this purpose, the third correction point T_2 is sampled as 20 points that are logarithmically spaced from T_3 to the end of the record.

- D'Amico et. al (2018) stated that the acceleration amplitudes in T_1 and T_2 of the corrected waveform should be less than 25% of the PGA. This threshold is introduced to avoid the generation of spurious spikes in the acceleration time history at times T_1 and T_2 due to the inappropriate combinations of the time correction points.

- In addition, this scheme considers the statement of Wu and Wu (2007) that the corrected displacement trace should be flat at the last portion of the signal. With this statement, D'Amico et al. (2018) also utilized the "f value" introduced by Wu and Wu (2007) after modifying it as:

$$f = \frac{r}{|\,b\,|.\sigma} \tag{3.6}$$

- Finally, the best values for the correction points that give the most accurate estimation of the fling among all the combinations of them is pinpointed as the one that results in the maximum f-value.

All the inputs of Equation 3.6 stand for the same definitions as those in Equation 3.3. Moreover, D'Amico et al. (2018) stated the same point that higher the absolute value of r and b tends to 1 and 0, respectively, and s tends to lower values, the flatter displacement time history. However, as can be seen in Equation 3.6, r, the linear correlation coefficient is included as it is in contrast to Wu and Wu (2007), in which the absolute r value was placed in the f value equation.

Schiappapietra et al. (2021) updated the eBASCO processing scheme which was presented by D'Amico et al. (2018). They summarized the correction steps of the modified scheme as: (1) cutting the uncorrected acceleration time history; (2) assigning the time correction points; (3) executing tri-linear detrend on the velocity trace; (4) determining the best solution. As the first step of the updated version of eBASCO, a preliminary cutting of the acceleration time history is applied. Secondly, the first acceleration amplitude is

subtracted from the acceleration time history to make the velocity zero in T_0. Just like the second step, time windows and the time correction points are defined in the same way as the previous version of the eBASCO procedure. Moreover, the applied baseline corrections to pre-event and transient windows given by a linear trend between $V_i(T_1)$ and V_f (T_2) in Equations 3.4 and 3.5, respectively, were not changed in this scheme. However, to eliminate the unsuccessful combinations of the time correction points that result in spurious spikes on acceleration traces, Schiappapietra et al. (2021) proposed a different condition from the previous version of the scheme. For this purpose, they stated that the relative differences of the acceleration amplitudes in correction points T_1 and T_2 on the corrected and the raw data should be less than 25%. As the last step of the procedure, among all the combinations of the correction points, which meet the relative difference condition, the best solution is determined in the same way as the previous version of eBASCO. Figure 3.4 exhibits the updated version of eBASCO procedure by Schiappapietra et al. (2021). They utilized Python 2.7 and presented the code as an electronic supplement. Although not seen in the flowchart of the procedure, it was stated that after defining the best solution, a second-order low pass filter, acausal Butterworth, is applied before the recursive integration to obtain the corrected displacement and velocity time histories. Moreover, Schiappapietra et al. (2021) recommended applying a cosine taper at the beginning of the waveform in each of these integration steps.

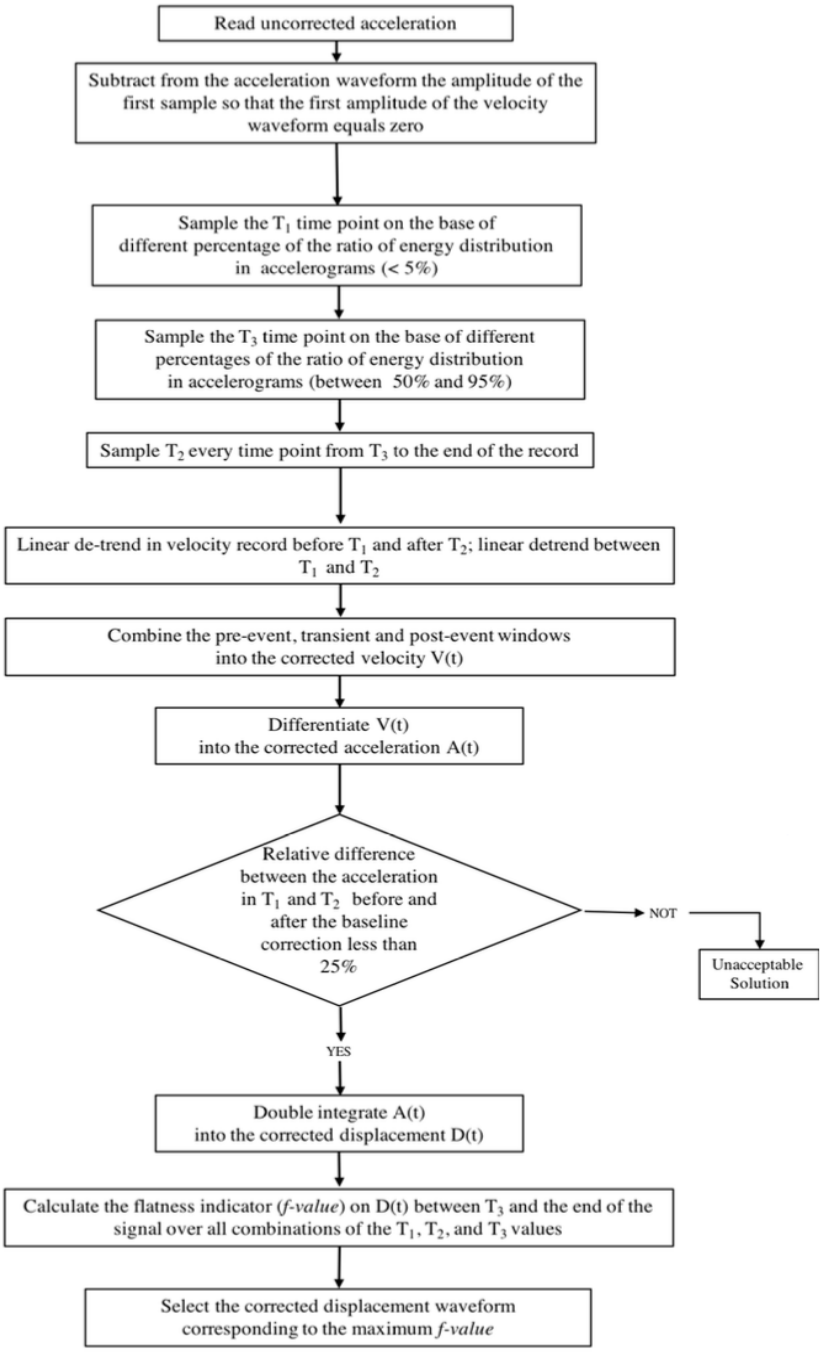

Figure 3.4. Demonstration of the updated version of eBASCO by Schiappapietra et al. (2021)

3.2. Proposed Processing Scheme and Differences From the Previous Ones

As aforementioned, constructing an improved processing scheme is considered more effective to recover the fling steps from Türkiye earthquakes. For this purpose, previously proposed schemes, especially the updated version of eBASCO is utilized. The processing steps of the created procedure are presented as follows:

Step1: After reading the raw earthquake data, slightly different from the Schiappapietra et al. (2021), the first amplitude of the acceleration time history is assigned as zero to make sure that the velocity oscillates around zero at the beginning of the motion.

Step 2: Normalized Arias Intensity is calculated to illustrate the cumulative energy distribution of the record, which is required for the following step.

Step 3: The motion is divided into three time windows, namely pre-event, ephemeral, post-event, by the time correction points T_1, T_2, T_3. Similar to the eBASCO procedure, time correction points are defined based on the cumulative energy dissipation of the record. Different from Schiappapietra et al. (2021) , the time correction points are assigned as seconds to increase the possible combinations and thus the accuracy of the obtained corrected waveform.

Step 4: For the preparation of the baseline correction sequence, velocity time history is obtained by integrating the acceleration waveform. In both the pre-event, from the beginning of the record to T_1, and the ephemeral windows, between T_1 and T_2 where the strongest portion of the motion takes place, linear trends are found in baseline shifts, just like D'Amico et al. (2018). Therefore, the same approach is utilized to remove the baselines from these windows by implementing a least-linear fitting. For the post-event window which is defined from T_2 to the end of the signal, on the other hand, the third baseline correction is defined as applying constant de-trend which is calculated as follows:

$$V_f = \frac{\sum_{j=T_2}^{T_{end}} V_{f,2}(j)}{n} \tag{3.7}$$

where j is the time, T_{end} is the end time of the record, T_2 is the second correction point, n is the number of the records. V_f is the baseline shift in the post-event window of the velocity time history.

Step 5: After implementing baseline corrections, the next step is defined as concatenating the three windows to acquire the partly corrected velocity time history. Since the motion is not intact and the procedure is not completed in this step, the obtained velocity waveform is named partly corrected one. Then, another baseline is defined in the part of the motion from T_3, where the strongest pulse of the motion finishes, to the end of the motion. This baseline correction is applied to check the conformity of the previous baseline corrections, the exceptions and details are going to be mentioned at the end of this section. This additional baseline correction is defined as:

$$V_{f,2} = \frac{\sum_{j=T_3}^{T_{end}} V_{f,2}(j)}{n} \tag{3.8}$$

where $V_{f,2}$ is the last baseline defined on the partly corrected velocity waveform between T_3 and the end of the trace, and other symbols are defined as in Equation 3.7.

Step 6: Next step of the proposed processing scheme is differentiating the corrected velocity trace into acceleration time history. In this step, the unexpected spurious spikes on the acceleration time history are unveiled. Following step is defined as eliminating the erroneous spurious spikes on the obtained acceleration time history. Based on Boore and Bommer (2005), the correction of the spurious spikes is done by assigning the means of the nearest acceleration amplitudes to the amplitude corresponding to time correction points as follows:

$$A(T) = \frac{(A(T-5) + A(T+5))}{2} \tag{3.9a}$$

$$A(T+1) = \frac{(A(T-6) + A(T+6))}{2} \tag{3.9b}$$

$$A(T-1) = \frac{(A(T-4) + A(T+4))}{2} \tag{3.9c}$$

$$A(T-2) = \frac{(A(T-3) + A(T+3))}{2} \tag{3.9d}$$

where the T stands for the correction points, and A stands for the corresponding acceleration amplitudes. This correction is applied to all correction points T_1, T_2, and T_3. Observations in this study demonstrated that existence of spurious spikes are not perceived from the

corrected displacement trace and therefore skipping this step may pave the way for erroneous interpretations.

Step 7 : The next step in the scheme is defined as the comparison of the acceleration amplitudes of the raw and processed data corresponding to T_1. The detailed explanation for this step is explained in Chapter 3, Section 3.3.

Step 8: The corrected waveform among over all combinations of the correction points is selected. For this decision, just like the previous studies, Wu and Wu (2007), D'Amico et al. (2018), and Schiappapietra et al. (2021) the f value, whose maximum value demonstrates the minimum dispersion of the last portion of the motion from T_3 to the end of the record, from the fade level is utilized. For the fade level indication value, Wu and Wu (2007) defined as absolute value for the correlation coefficient r; however, both D'Amico et al. (2018) and Schiappapietra et al. (2021) incorporated this coefficient into the equation as it is. After inspection of the effect of this difference, that coefficient is introduced to the proposed scheme as it is rather than its absolute value.

$$f = \frac{r}{|\,b\,|.\sigma} \tag{3.10}$$

Figure 3.5 illustrates the comparisons of the corrected and raw waveforms of the 1999 Düzce earthquake EW component of station TK 8101. In addition, displacement time histories, in the below, presented along with some of the invalid combinations of time correction points.

Step 9 : As the last step, after obtaining the corrected waveform, the permanent displacement is assigned. Based on the Significant Duration theorem, presented by Trifunac and Brady (1975), we made the assumption that after 95% of the cumulative energy of the strong ground motion is dissipated, the ground displacement fades by oscillating around the permanent displacement level. Figure 3.6 demonstrates the flowchart of the proposed data processing scheme.

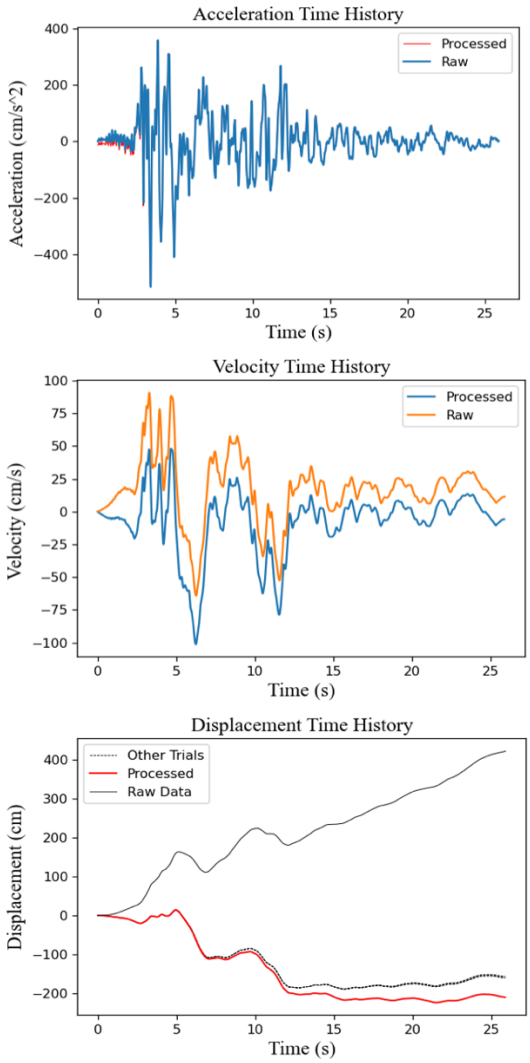

Figure 3.5. The acceleration, velocity and displacement time histories of 1999 Düzce earthquake EW component of station TK 8101

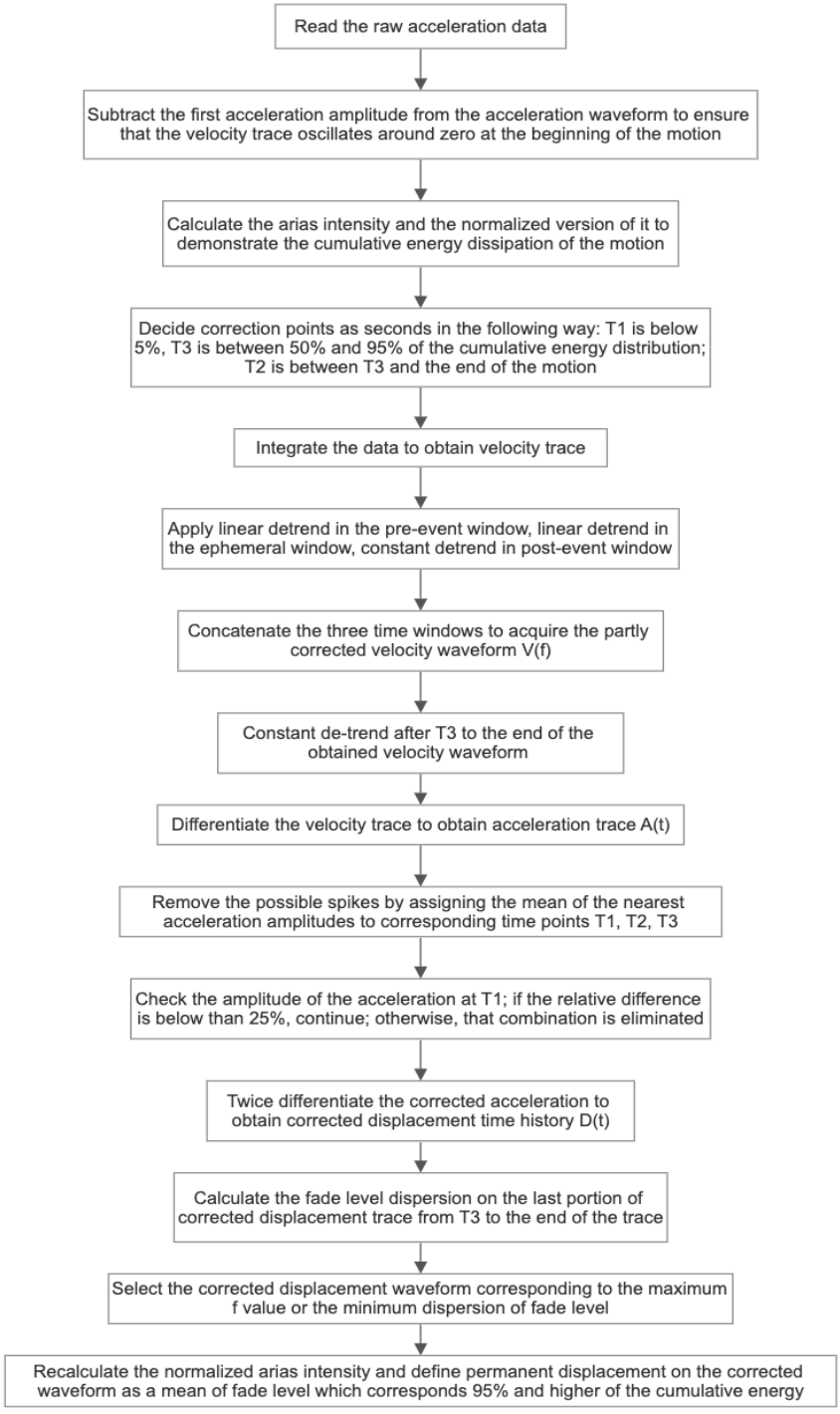

Figure 3.6. The schematic illustration of the proposed data processing scheme

Although the updated eBASCO processing scheme is utilized more than other previous ones while creating the proposed scheme, there are some differences that make the proposed scheme advantageous. For instance, in contrast to updated version of eBASCO procedure, scheme applying cosine taper at each step is not found required in the proposed scheme. Moreover, the primarily cutting of the motion is also not recommended unless it is

inevitable. In addition, to preserve the low frequency content of the motion, the Butterworth filter at the end of the processing scheme is not recommended, as opposed to Schiappapietra et al. (2021). Other influential differences of the proposed scheme from the previous ones are presented as follows:

1) Chao et al. (2010) proposed to select the correction points based on the cumulative energy distribution of the data. Then D'Amico et al. (2018) added this method in the eBASCO procedure. However, how to calculate the cumulative energy distribution of the data was not clear on that scheme, which may pave the way for complexities to utilize the procedure by engineers and the scientists. In the proposed scheme, it is recommended to utilize the normalized arias intensity to opt the correction points based on the cumulative energy distributions.

2) In addition to energy distribution, in the proposed scheme much more possible time correction points and thus combinations are introduced through assigning them as seconds. The reason behind our sample modification decision stem from the differences of findings for the same records by D'Amico et al. (2018) and Schiappapietra et al. (2021). Although the time correction points are defined in the same cumulative energy distribution ranges, there were some differences in possible values between these two procedures. Former procedure defined T_1 in logarithmically distributed samples between 0.0001% and 5% of the cumulative energy dissipation whereas in the latter procedure T_1 is sampled logarithmically from 0.001% to 5% of the cumulative energy distribution. Secondly, according to Schiappapietra et al. (2018), correction point T_3 is sampled in a set of five logarithmically spaced points from 50% to 95% of the energy while D'Amico et al. (2018) defined it in the same range but with linearly distribution points. Table 3.1 demonstrates the obtained static displacements from the D'Amico et al. (2018) and Schiappapietra et al. (2021) for the same records of the 2016 Norcia earthquake. In this study, because the flowcharts of these procedures (Figure 3.3 and 3.4) are highly similar, it is considered that the differences of the obtained permanent displacements originated from the mentioned differences in the selection of the time correction points. Therefore, it is considered that the permanent displacements are susceptible to the selection of the correction points and the more the possible sample points assigned to time correction points the more the accurate result can be obtained. Aligned with this statement, firstly an attempt to assign all the sample points to the time correction points was made while

creating the procedure. However, it was found that the computational load extensively increased with that approach. Moreover, assigning the seconds results in quite similar results with assigning the sample points. For instance, for the 1999 Kocaeli earthquake, the EW component of the SKR station was processed by both samples and seconds approaches and the permanent displacement was found as 185 cm and 186.85 cm, respectively. Assigning each sample approach took 8 hours in Python 3.9 which is run in an MacOS Ventura operation system to reveal the permanent whereas the assigning seconds approach lasted only a minute. For the same record, Kalkan and Kunnath (2006) revealed the permanent displacement as 186.76 cm based on the Iwan et al. (1985) and Boore (2001). Consequently, in this study, the seconds approach is found not only enough to reveal the permanent displacements on the records but also time efficient. Figure 3.7 demonstrates the obtained displacement time history by the two approaches.

Table 3.1. Comparison of the obtained permanent displacements with procedures of D'Amico et al. (2018) and Schiappapietra et al. (2021) as well as GPS stations for the 2016 Norcia earthquake. All the permanent displacements are in cm. *(Cont.)*

Station	Component	D'Amico et al. (2018)	Schiappapietra et at. (2021)	GPS Station	GPS (cm)
CLO	EW	-61.7	-46.57	VTW5	-41.8
CLO	NS	-14.5	-33.57	VTW5	-35.3
CLO	UD	-85	-81.84	VTW5	-70.7
T 1214	EW	-12.4	-8.61	RIFP (HRGPS)	-10.02
T 1214	NS	-7.2	-9.18	RIFP (HRGPS)	-13.97
T 1214	UD	-38.6	-43.44	RIFP (HRGPS)	-40.15
T 1213	EW	-15.7	-24.44	-	
T 1213	NS	-10	-10.48	-	
T 1213	UD	-4.7	-4.72	-	

ACC	UD	-3.8	-9.91	ACCU	-7.4
T 1216	UD	1.8	1.37	MUVI	-0.4
AMT	UD	2.4	0.04	AMAT	1

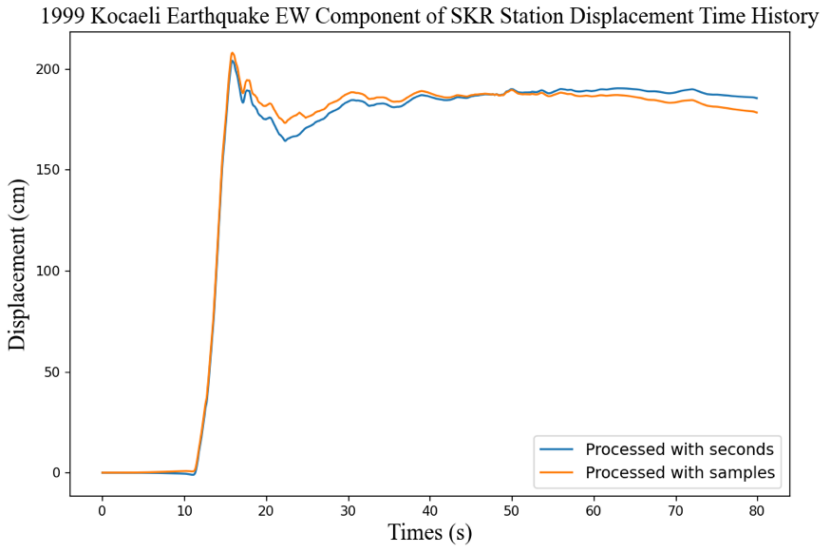

Figure 3.7. Comparison of the acquired displacement time histories by assigning the time correction points as seconds and assigning them as samples on 1999 Kocaeli earthquake EW component of SKR station

3) Assigning the first acceleration amplitude to zero and subtraction of the first acceleration amplitude from the whole record to meet the criteria that at the beginning the velocity trace of the motion oscillates around zero does not give rise to important differences. Therefore, only setting the first acceleration amplitude to zero is found enough for this purpose. Table 3.2 demonstrates the comparisons of the first amplitudes of the velocity time histories calculated according to eBASCO and the proposed scheme.

Table 3.2. The comparison of the first velocity amplitudes of eBASCO and Proposed Scheme; $V(0)_{eBASCO}$: First amplitude of the velocity based on eBASCO; $V(0)_{Proposed\ Scheme}$: First amplitude of the velocity based on the proposed scheme

Earthquake	Station-Component	$V(0)_{eBASCO}$ (cm/s)	$V(0)_{Proposed\ Scheme}$ (cm/s)
1999 Kocaeli	YPT-EW	$2.24x10^{-5}$	$4.48x10^{-5}$
1999 Kocaeli	YPT-NS	$1.54x10^{-5}$	$1.66x10^{-5}$
1999 Düzce	C 1060-NS	-0.0001	$2.78x10^{-5}$
1999 Düzce	C 1060-EW	0.00010	0.00017
2003 Bingöl	TK 1201-EW	$4.89x10^{-6}$	0
2020 İzmir-Samos	GMLD-UD	$3.01x10^{-6}$	$8.55x10^{-7}$
2020 İzmir-Samos	TK 3516-EW	$-9.94x10^{-5}$	$-9.53x10^{-6}$

4. In contrast to previous ones, in this scheme it is recommended to apply a constant type detrending in the post-event window rather than linear one. The reasons behind this decision are: (1) some of the fling-containing data did not exhibit linear detrend behavior such as the 1999 Kocaeli earthquake EW component of the SKR station as seen in Figure 3.8; (2) since the strongest portion of the motion is defined between T_1 and T_2, it is assumed that after this interval, the motion might become somehow stable and thus not cause linearly continuous baseline shift; (3) execution of constant detrending in this portion together with the last detrend in the follow-up step of the procedure shows a reliable trend that was defined as a ramp function in the literature.

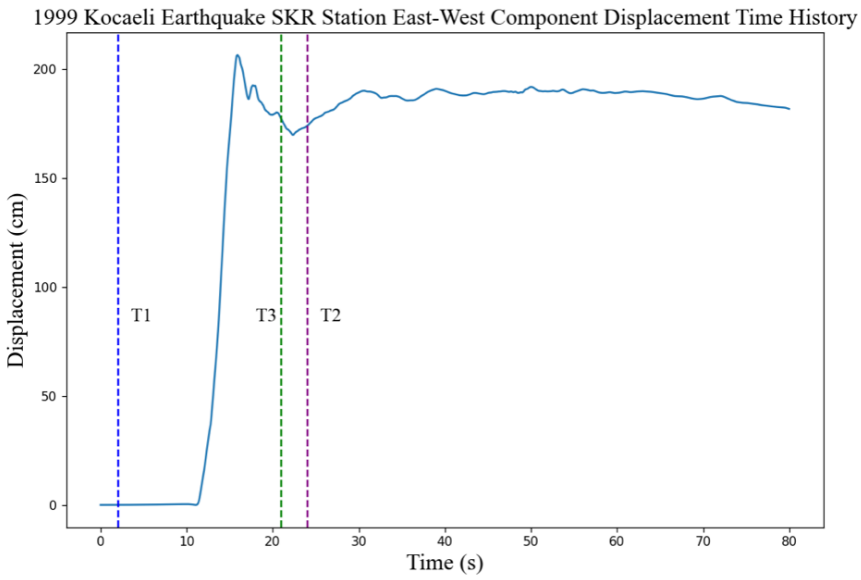

Figure 3.8. 1999 Kocaeli earthquake raw displacement time history of EW component of the SKR station with the assigned time correction points.

5. Since the applied baseline correction in post-event is different from the others, to check the conformity of them, the correction in this step starts from correction point T_3. It is expected that if the previous detrending did not work, there will still be a baseline shift on the data. Although, any inconsistency, or continued shift, is not encountered in the analyses of the records in this study, it is decided to include this step for worldwide users to make sure. Figure 3.9 demonstrates the obtained velocity time history (a) and the very small window of the displacement time history (b) of the 2014 Aegean Sea earthquake NS component of station TK 1701 the after and the before the last correction is applied.

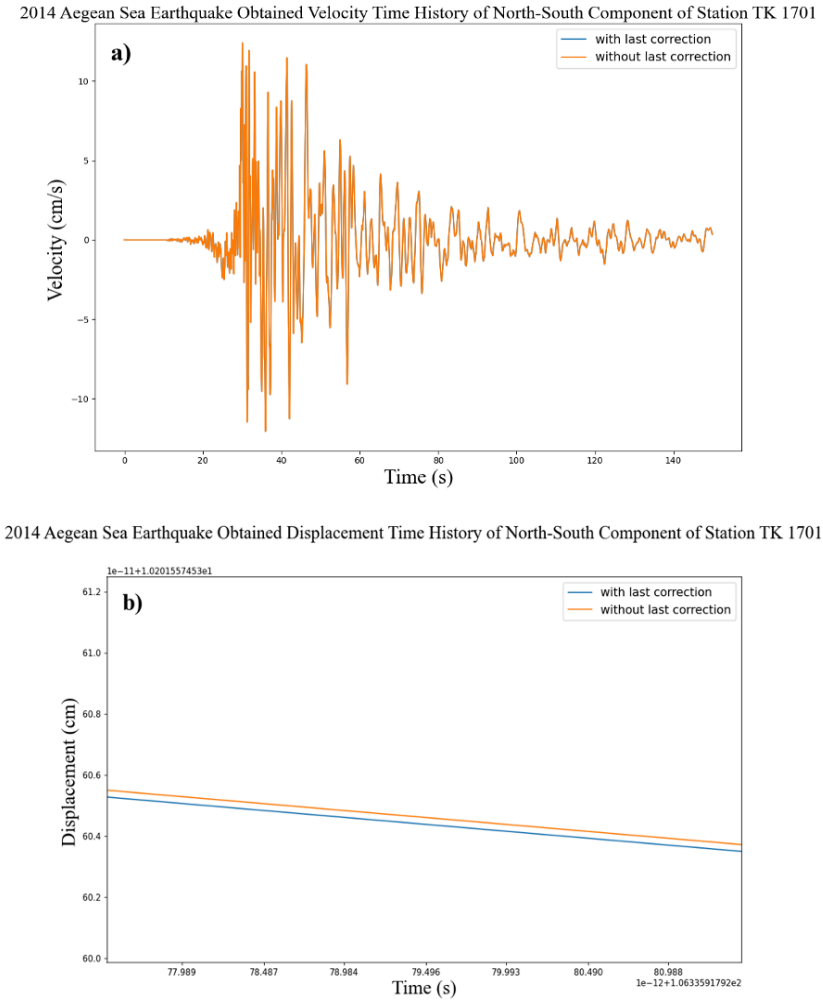

Figure 3.9. Comparisons of the corrected waveforms with the last correction and without it; a: the velocity waveform comparisons; b: very small window of the displacement time history of the 2014 Aegean Sea earthquake NS component of station TK 1701

6. Another difference is eliminating possible spurious spikes on the acceleration time history. Previously, both D'Amico et al. (2018) and Schiappapietra et al. (2021) warned for selection points to avoid spurious spikes in acceleration trace. For this purpose, D'Amico et al. (2018) utilized PGA comparison and Schiappapietra et al. (2021) utilized comparisons of the acceleration amplitudes at the correction points after and before the procedure applied. In the proposed scheme, however, acceleration correction step is introduced here by utilizing the Boore and Bommer (2005) which stated that if the spikes are identified as erroneous, they should be removed from the record and one of the methods for this purpose is defined as replacing the acceleration amplitudes of the spikes with the mean of the data points either side. In Figure 3.10, the comparisons of the

recovered waveforms of 1999 Kocaeli earthquake EW component of MSK station with the acceleration spike correction step (left), and without it (right). As can be seen, if the acceleration trace is not cleaned by the erroneous spikes, only looking at the velocity or displacement time histories misleads the users of the procedure.

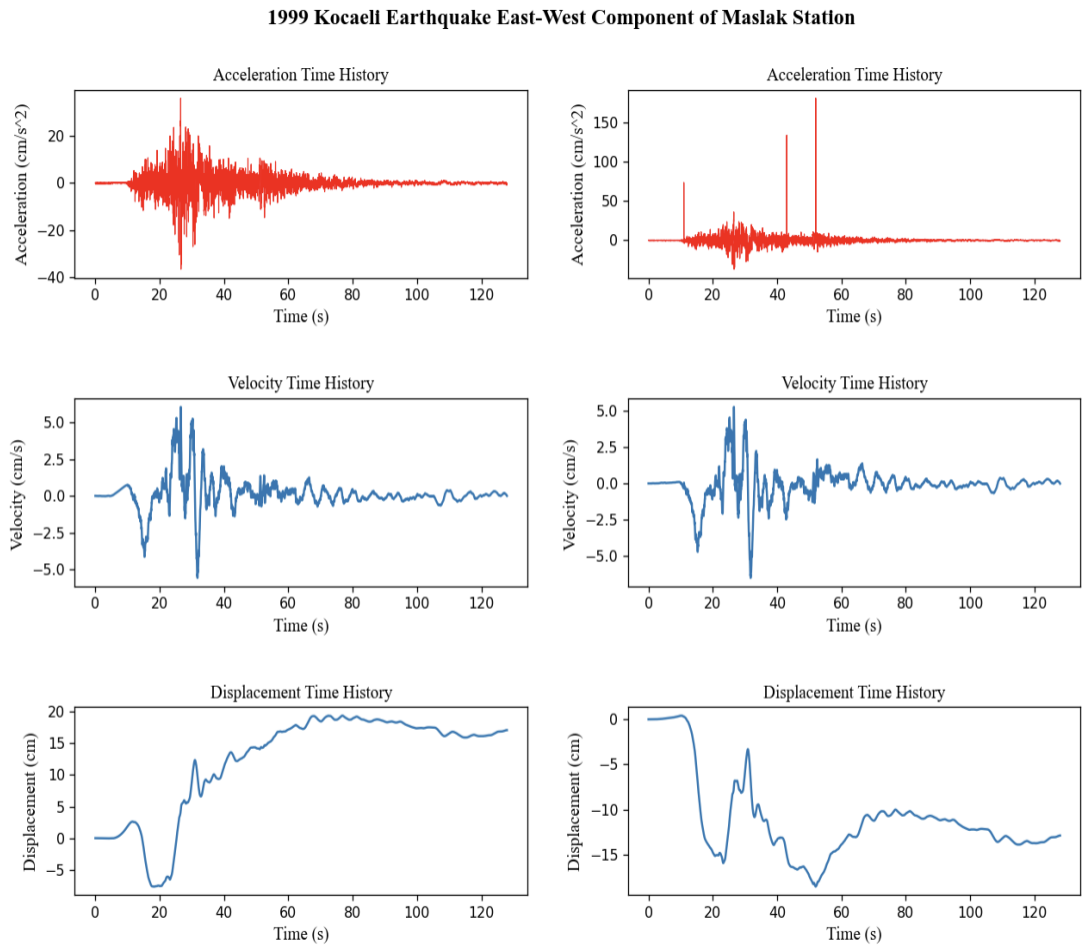

Figure 3.10. Comparisons of the corrected waveforms of the 1999 Kocaeli earthquake EW component of MSK station with the acceleration spikes correction step (right) and without this step (left).

7. In addition to the acceleration correction step, an elimination step based on the comparison of the acceleration amplitudes before and after the processing the data is placed in the proposed data processing scheme, similar to eBASCO, Although it was stated that this step was included due to the possible spurious spikes in the acceleration time history in eBASCO, in this study it is found that there could still be differences in the acceleration amplitudes after spikes. Therefore, to avoid the extensive alterations in

the earthquake data, this elimination step is included in the scheme. It is found that both the PGA differences and the acceleration amplitude differences in T_2 demonstrate almost the same differences as those in T_1. Thus, only the comparison of the acceleration amplitudes in T_1 is found enough. Figure 3.11 illustrates the comparison of the corrected displacement time histories of 1999 Kocaeli earthquake EW component of ARC corrected with elimination step only based on T_1, with elimination step based on both T_1 and T_2, and without elimination step. As can be seen in Figure 3.11, the elimination step based on $A(T_1)$ is quite enough and subtracting this step causes more than 25% of relative alteration in the acceleration amplitudes in time points. In addition, Figure 3.12 shows the differences of the displacement waveforms of the 1999 Kocaeli earthquake NS component of YPT station corrected with and without the elimination step. Table 3.3 presents the comparison of the PGAs of the raw and processed data. As can be seen, comparison of $A(T_1)$ is enough for PGAs as well.

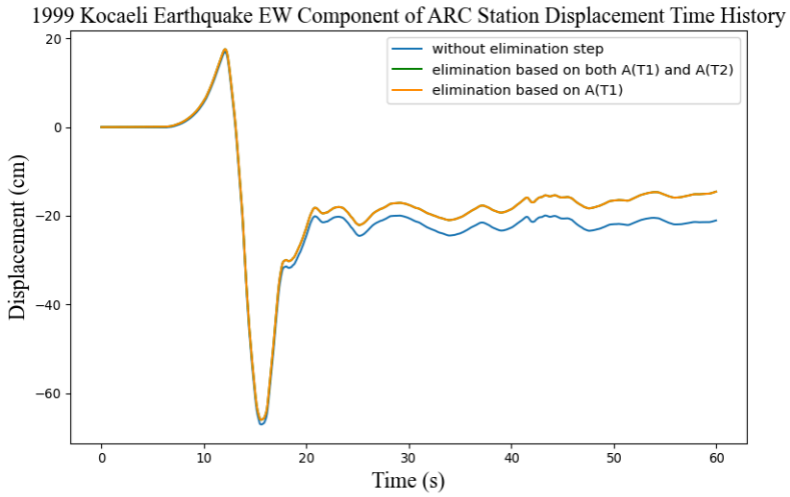

Figure 3.11. The corrected displacement time histories of 1999 Kocaeli earthquake EW component of ARC station.

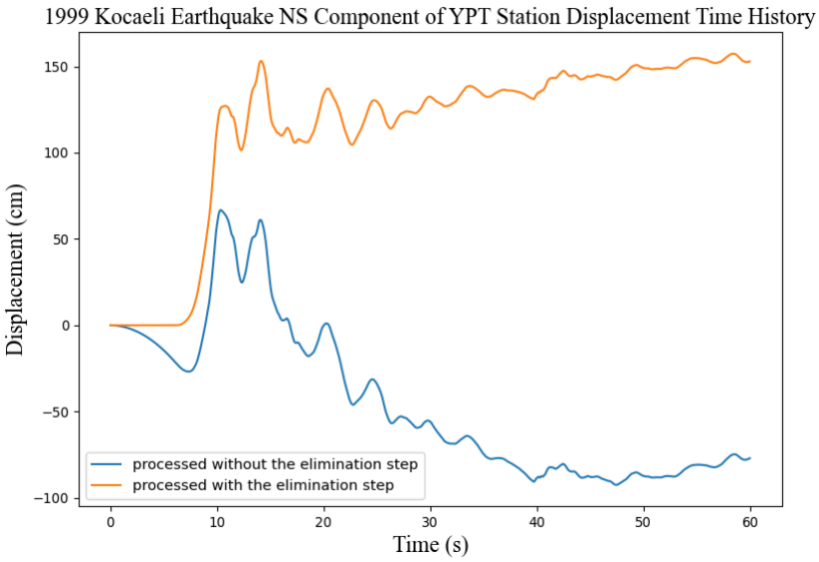

Figure 3.12. The corrected displacement time histories of 1999 Kocaeli earthquake NS component of YPT station.

Table 3.3. Comparison of PGA, $A(T_2)$, and $A(T_1)$ differences before and after the processing scheme. $PGA_{Processed}$: Peak ground acceleration of the processed data; PGA_{Raw}: Peak ground acceleration of the raw data; $A(T_1)_{Processed}$: Acceleration amplitude of the processed data at T_1 ; $A(T_1)_{Raw}$: Acceleration amplitude of the raw data at T_1 ; $A(T_2)_{Processed}$: Acceleration amplitude of the processed data at T_2 ; $A(T_2)_{Raw}$: Acceleration amplitude of the raw data at T_2

Earthquake	Station/Component	$PGA_{Processed}$	PGA_{Raw}	Relative difference	$A(T_1)_{Processed}$ (cm/s^2)	$A(T_1)_{Raw}$ (cm/s^2)	Relative difference	$A(T_2)_{Processed}$ (cm/s^2)	$A(T_2)_{Raw}$ (cm/s^2)	Relative difference
1999 Kocaeli	YPT/EW	224,7	225,26	-0,0025	25,75	25,1	0,0252	57,97	64,67	0.1036
1999 Kocaeli	TK 8101/EW	370	373,76	-0,0102	-1,66	-1,58	0,0482	10,35	11,87	0.1281
1999 Düzce	C 1061/UD	49,35	52,17	-0,0571	-0,015	-0,018	-0,2	0,71	0,94	0.234
2017 Bodrum	TK 4810/NW	38,73	39,99	-0,0325	0,0034	0,004	0,15	-0,078	-0,074	0.0512
2020 Elazığ	TK 4404/UD	139,77	149,48	-0,0695	0,0021	0,0021	0	0,85	0,79	0.0706

8. Just like the behavior of a damped SDOF system under an excitation, it is assumed that the ground displacement fades by oscillating around the permanent displacement level after the most of the excitation energy is dissipated. Based on the oscillating assumption, in this study, the fade level, also known as permanent displacement, is defined as the mean of the 95% of the dissipated cumulative energy to the end of the record. Therefore, at the end of the processing scheme, after determining the most reliable combination of the time correction points by the fade level indication (Equation 3.10), permanent displacement is determined in this way. Although not shown in the flowchart (Figure 3.2), Wu and Wu (2007) stated that in their study the permanent displacement was assigned as the mean of the displacement amplitudes after T_3 to the end of the motion. More or less the fling step is considered the same in this study; however, the difference comes from the definitions of the correction point T_3. To exemplify, while they defined this point as where the ground just reaches to the permanent displacement, in this study, T_3 is defined as the point where the strongest pulse finishes based on the results of the analyses. For this reason, it is considered that even after T_3, motion causes displacement changes, relatively less though. Figure 3.13 demonstrates corrected wave forms of the 1999 Kocaeli earthquake EW component of ARC station with the T_3 point and fade level.

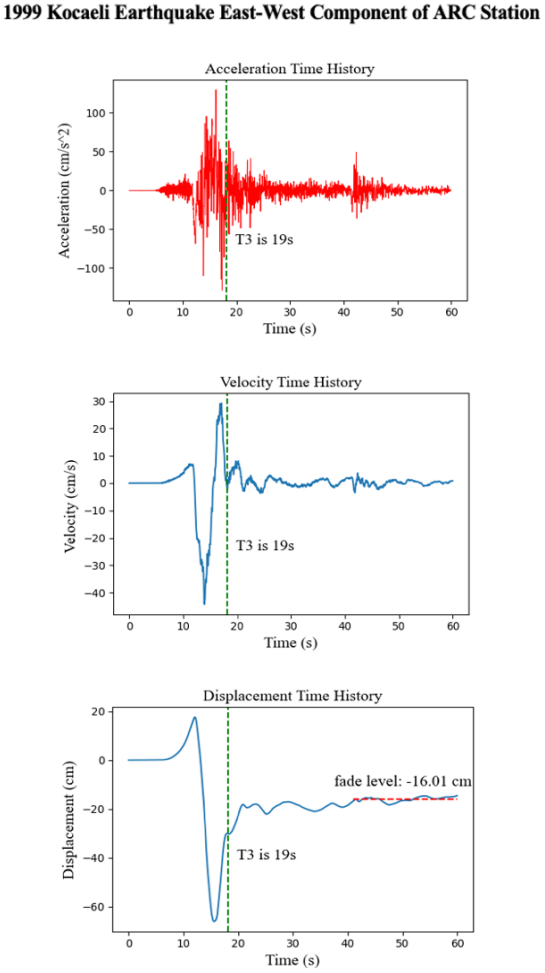

Figure 3.13. Corrected waveforms of 1999 Kocaeli earthquake EW component of ARC station

As aforementioned there is an exception in the proposed scheme for some earthquake records. Although the automatic process successfully worked and recovered most of the data, 8% of the data needed extra baseline correction at the end of the procedure. After the last correction of the procedure is applied, an additional baseline correction also applied for these records. It can be considered that some of the records had a distinct, unexplained source of baseline shifts, which is out of the scope of this study. Type of the additional baseline correction is linear baseline correction; in other words, a least-squares if it is found appropriate for this correction, which is defined as Equation 3.4. The extra correction is based on the velocity shift and where the shift start is defined by visual inspection at the end of the process. To decide whether the extra correction is required, firstly the procedure is applied and if there is a shift in the velocity time history, by visual inspection the diverging point (as seconds) is defined and the procedure is reapplied with additional baseline

correction. 23 records that needed the additional correction, most of these records belong to pre-millennial earthquakes (Further information can be found in Table A.1. in Appendix A). Therefore, the proposed scheme without additional correction is also highly successful, in general. Figure 3.14 demonstrates the 1999 Kocaeli earthquake EW component of station TK 1404 as an example of the additional baseline correction required record.

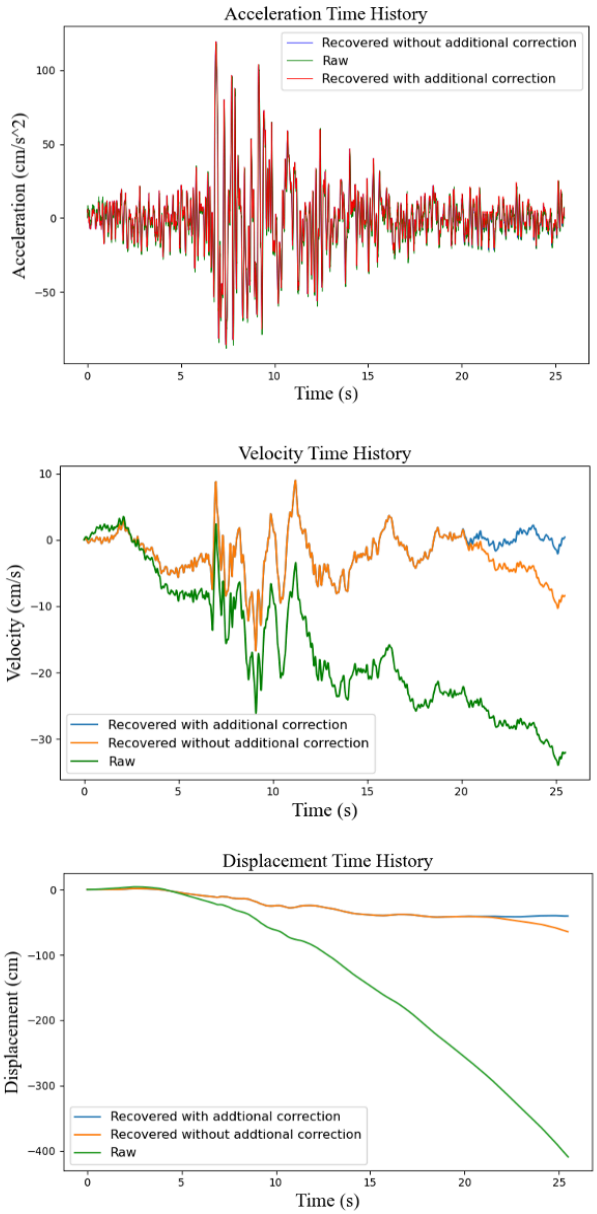

Figure 3.14. Acceleration (above), velocity (middle), and displacement (below) time histories of 1999 Kocaeli earthquake EW component of station TK 1404 that required additional baseline correction

In this part of the study, the proposed data processing scheme for revealing the fling step is introduced. The different aspects of the proposed scheme from the previous procedures are explained with the examples. Following section illustrates the accuracy of the proposed scheme by comparisons of the static displacements from the processed data and derived ones from the GPS data. Note that there is no additional correction applied in these records.

3.3. Proof of the Effectiveness of The Proposed Scheme by Comparison of GPS Data

25 records from Türkiye and worldwide earthquakes are processed and the obtained permanent displacements are compared with the those derived from the nearby GPS stations. To test the capability of the scheme the earthquakes are selected similar to the dataset in that the magnitudes of them range from Mw 6.6 to Mw 7.6 and the Rjb distances of the stations are below 50 km. It is found that the proposed processing method is highly effective to reveal the permanent displacements, especially in the sites near to the fault. Table 3.4 exhibits the comparison with the detailed information. The data selected for proof of the procedure are also based on nearby GPS data availability of the earthquakes. The derived permanent displacements from the GPS stations are compared with the estimated ones from the earthquake records of the stations which are co-located. To evaluate the proposed procedure in a wide perspective, records from the earthquakes including three styles of faulting are evaluated: 10 records from 7 stations from 1999 Chi Chi earthquake (Mw 7.6) as Reverse (Thrust) Faulting; 5 records from 4 stations from the 2014 Aegean Sea (Mw 6.9), 2015 Lefkada (Mw 6.5), and 2020 Elazığ-Sivrice (Mw 6.7) earthquakes as Strike Slip faulting; 10 records from 8 stations from the 2016 Norcia (Mw 6.6), 2017 Bodrum-Kos (Mw 6.6), 2020 İzmir-Samos (Mw 7) earthquakes as Normal Faulting. The proposed procedure is managed to retrieve the permanent displacement from some 2 millimeters to 2.66 meters successfully. Figure 3.15 shows the corrected displacement time history of the 2014 Aegean Sea earthquake NS component of the station TK 1714 with the findings from GPS data. As can be seen in Figure 3.15, the proposed method is effective for the low magnitude earthquakes so that the permanent displacements observed on the processed data and derived from the GPS station CANA are almost overlapping. Likewise, the effectiveness of the proposed

procedure on higher magnitudes is demonstrated by Figure 3.16, which demonstrates the 1999 Chi Chi earthquake EW, NS and UD components of the station TCU 074 with the findings from the GPS data. Briefly the proposed data processing scheme is found effective for both lower and larger magnitude earthquakes.

Table 3.4. The comparisons of the revealed flings with the those derived from GPS stations: Rjb, Joyner and Boore distance; PD, Permanent displacement; SoF, Style of faulting. Y01:Yu et al. (2001), K18:Konca et al. (2018), C16: Chousianitis et al. (2016), INGV16: INGV (2016), K19: Konca et al. (2019), D21: Doğru et al. (2021), B21: Aktuğ et al. (2021) *(Cont.)*

Date	Earthquake	Magnitude (Mw)	SoF	Station	Rjb (km)	Rup (km)	Latitude (°)	Longitude (°)	Component	PD (cm)	GPS Station	Latitude (°)	Longitude (°)	PD (cm)	Reference
20.09.1999	Chi Chi	7,6	TF	TCU 137	0	13,9	24.18	120.92	EW	-264,78	G099	24.173	120.887	-260	Y01
20.09.1999	Chi Chi	7,6	TF	TCU 074	0	16,4	23.962	120.962	EW	-191,03	HTZS	23.976	120.974	-187,7	
20.09.1999	Chi Chi	7,6	TF	TCU 074	0	16,4	23.962	120.962	NS	131,41	HTZS	23.976	120.974	128,40	
20.09.1999	Chi Chi	7,6	TF	TCU 074	0	16,4	23.962	120.962	UD	-65,48	HTZS	23.976	120.974	-60,30	
20.09.1999	Chi Chi	7,6	TF	TCU 076	0	1,9	23.908	120.676	UD	-15,63	AF11	23.896	120.676	-17,70	
20.09.1999	Chi Chi	7,6	TF	TCU 102	0	3,5	24.249	120.721	NS	-74,56	G103	24.262	120.710	-59,20	
20.09.1999	Chi Chi	7,6	TF	TCU 102	0	3,5	24.249	120.721	UD	-13,56	G103	24.262	120.710	-10,00	
20.09.1999	Chi Chi	7,6	TF	TCU 078	0	10,7	23.812	120.845	NS	72,73	M408	23.799	120.841	83,2	

Date	Earthquake	Magnitude (Mw)	SoF	Station	Rjb (km)	Rup (km)	Latitude (°)	Longitude (°)	Component	PD (cm)	GPS Station	Latitude (°)	Longitude (°)	PD (cm)	Reference
20.09.1999	Chi Chi	7,6	TF	TCU 078	0	10,7	23.812	120.845	UD	-22,7	M408	23.799	120.841	-16,3	Y01
20.09.1999	Chi Chi	7,6	TF	TCU 120	3,1	3,1	23.980	120.613	UD	-14,03	M365	23.968	120.619	-15,90	
24.05.2014	Aegean Sea	6,9	SS	TK 1714	46,07	46,76	40.11	26.42	EW	-3,03	CANA	40.11	26,41	-2,63	K18
24.05.2014	Aegean Sea	6,9	SS	TK 1714	46,07	46,76	40.11	26.42	NS	1,53	CANA	40.11	26,41	1,49	
17.11.2015	Lefkada	6,5	SS	KASA	**	**	39,746	19,935	EW	0,22	KASI	39,746	19,936	0,28	C16
17.11.2015	Lefkada	6,5	SS	LXRA	**	**	38,199	20,437	NS	0,17	KEFA	38,196	20,438	0,25	
30.10.2016	Norcia-Central Italy	6,6	NF	IV T 1214	0	4,5	13.208	42.76	UD	-40,81	RIFP (HRGPS)	13.176	42,76	-40,15	INGV16
30.10.2016	Norcia-Central Italy	6,6	NF	IV T 1214	0	4,5	13.208	42.76	EW	-11,8	RIFP	13.176	42,76	-10,02	

Date	Earthquake	Magnitude (Mw)	SoF	Station	Rjb (km)	Rup (km)	Latitude (°)	Longitude (°)	Component	PD (cm)	GPS Station	Latitude (°)	Longitude (°)	PD (cm)	Reference
30.10.2016	Norcia-Central Italy	6,6	NF	IV T 1216	3,1	9,2	13.019	42.891	EW	-10,83	MUVI	13.033	42.907	-6,90	INGV16
12.06.2017	Bodrum-Kos	6,6	NF	TK 4809	10,09	11,75	37.033	27.44	NS	15,79	BOD2	37.03	27,42	20,51	K19
12.06.2017	Bodrum-Kos	6,6	NF	TK 4809	10,09	11,75	37.033	27.44	UD	1,14	BOD2	37.03	27,42	0,80	
12.06.2017	Bodrum-Kos	6,6	NF	TK 4812	15,56	15,56	36.712	27.688	NS	-2,83	DATC	27.69	36.71	-3,5	
24.01.2020	Elazığ-Sivrice	6,7	SS	TK 2104	49,27	49,36	38,2644	39,759	EW	1,69	ERGN	38,269	39,758	2,01	D21
30.10.2020	İzmir-Samos	7	NF	TK 3528	43,59	44,89	38.304	26.373	NS	8,7	CESM	26.372	38.303	5,1	B21
30.10.2020	İzmir-Samos	7	NF	TK 3536	30,47	32,3	38.197	26.838	NS	6,7	SFRH	26.820	38.206	9,74	
30.10.2020	İzmir-Samos	7	NF	TK GMLD	14,20	18,60	38.076	26.9157	NS	12,61	HZUR	26.900	38.068	13,66	
30.10.2020	İzmir-Samos	7	NF	TK KUSD	36,70	39,50	37.8606	27.2868	EW	-0,8	KUSD	27.268	37.869	-0,7	

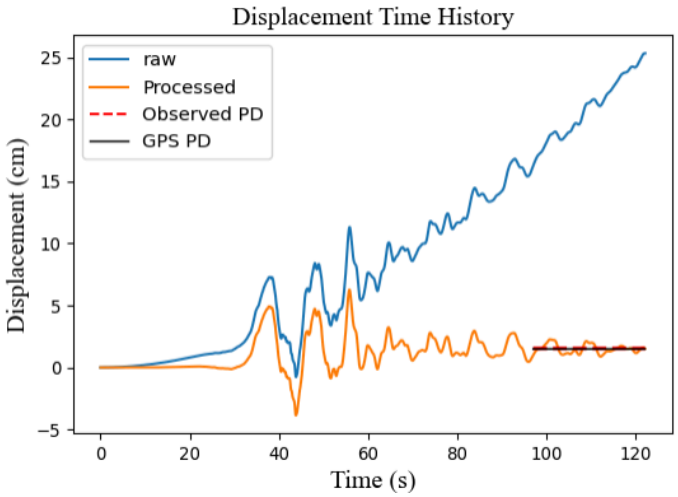

Figure 3.15. Displacement time history of the 2014 Aegean Sea earthquake NS component of the station TK 1714 with the findings from GPS data

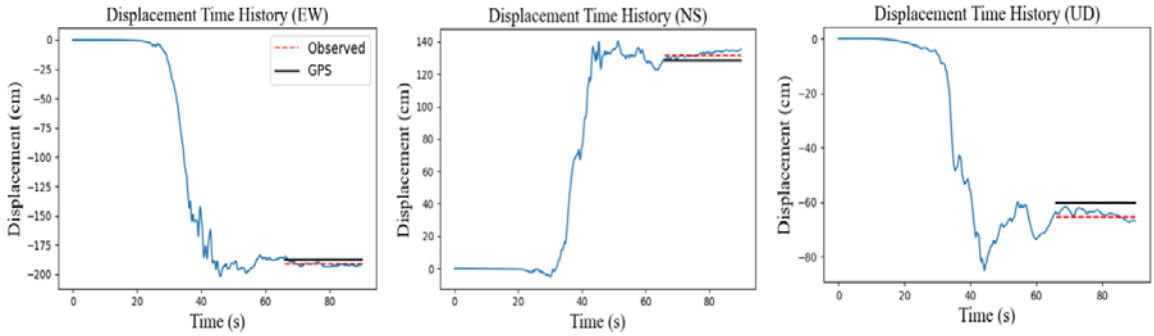

Figure 3.16. Displacement time history of 1999 Chi Chi earthquake EW, NS and UD components of the station TCU 074 with the findings from GPS data.

In addition to GPS data, the permanent displacements of the 1999 Kocaeli earthquake NS component of YPT station and EW component of SKR station are also compared with the findings of Kalkan and Kunnath (2006), which utilized Iwan et al. (1985) and Boore (2001) for processing. Since the approaches are similar and all the samples are considered for the time correction points in that study, the corresponding findings of this study are compared with theirs. They found that the permanent displacement of the NS component of YPT station is equal to

145.79 cm, whereas it is found in this study as 149 cm. Moreover, the real time data that Burks and Baker (2016) obtained by using Wu and Wu (2007) to utilize them in the predictive equation, found the permanent displacement of the same record as 148.11 cm. Similarly, for the EW component of SKR station was found as 186.76 cm in their study and it is found as 186.84 cm in this study. The proposed scheme is highly effective to recover the static displacements on the waveforms and the possible values for the time correction points are found quite enough instead of sample points.

4. TURKISH STRONG MOTION DATABASE

The new Turkish strong ground motion dataset of Türkiye (N-TSMD, Akbas et al., 2023) was utilized to detect records containing fling-steps. The criteria for selecting the records of the earthquakes occurred 1983 to 2023 in Türkiye are defined as follows:

- Magnitude range was set to Mw 6 and above with the fact that the stronger the ground motion the higher the capability of producing fling step.
- The depths of the events were limited to 30 km and below to determine the shallow crustal earthquakes producing fling such as the 1999 Chi-Chi and the 1999 Kocaeli earthquakes.
- Although there has not been a standardized distance to define the near fault area in the literature, in the previous studies approximated different distances for this purpose; for instance, while Abrahamson (2002) states the area that fling steps can be seen as around 10 km from fault, D'Amico et. al (2018) assumed it as 50 km. Likewise, it is decided that the distances of ground motion stations which might be exposed to the fling effects are within 50 km from the fault (Rjb≤50km).

In addition, the utilized earthquake data is taken from Earthquake Research Department of General Directorate of Disaster Affairs (AFAD, https://tadas.afad.gov.tr/list-waveform, last accessed December 2022) and Engineering Strong Motion Database (ESM, https://esm-db.eu/#/waveform/search, last accessed December 2022). Previous to processing, an inspection of all the stations and their components is done to eliminate the highly erroneous records which are not appropriate to evaluate the event and thus pave the way for wrong interpretations. The eliminated earthquake records and the elimination reasons are found as:

- The 1983 Biga earthquake whose two stations (TK 1012 and TK 1014) had met the criteria was removed from the database because the stations had not fully recorded the earthquake motion.

- Station TK 8108 for the 2022 Düzce earthquake was removed due to lack of data in the beginning of the earthquake.
- TK 110 station for 27 June 1998 Adana-Ceyhan earthquake, TK 4101 station for the 1999 Kocaeli earthquake, TK 1404 and TK 1406 for the 1999 Düzce earthquake, and TK 8101 stations for the 2022 Düzce earthquake, were also removed due to their highly erroneous data.
- North South and Vertical components of TK 2402 for the1992 Erzincan earthquake, North South and Vertical components of TK 2402 for 1995 Dinar earthquake, North South component of TK4106 (Gebze -Marmara TÜBİTAK) for the 1999 Kocaeli earthquake were not revealed as these records did not meet the procedure criteria that will be explained in later sections.

Finally, obtained dataset consists of 288 records of 98 stations from 14 strike slip, 5 normal faulting and 1 reverse faulting earthquakes. All the gathered data were, then, exposed to the proposed data procedure scheme explained in Chapter 3 to reveal their permanent displacements. Source parameters strike, dip and rake angles of the earthquakes are mainly taken from N-TSMD. However, due to they are not found in N-TSMD, those of four earthquakes are taken from following sources:

- International Seismological Center (ISC) catalog was utilized for the parameters of the three earthquakes which are the 1992 Erzincan and 1992 Doğanbey-İzmir are taken from The Global Centroid Moment Tensor project (GCMT) inputs in the catalog, and those of the 1998 Adana-Ceyhan and taken from the Centre Sismologique Euro-Mediterraneen (CSEM)
- The parameters of the 2022 Düzce-Gölyaka earthquake are taken from the Geoscience Australia (AUST)

Obtained parameters of the earthquakes involved in this study including seismic moments with the references, and the number of the stations and the records for the earthquakes are summarized in Table 4.1.

Table 4.1. Summary of Earthquakes and Number of Data Incorporated to the study. SoF: Style of Faulting; Mw: Moment Magnitude; SS: Strike Slip; N: Normal; R: Reverse; M_0: Seismic Moment *(Cont.)*

Date	Location	SoF	Mw	Depth (km)	Strike/Dip/ Rake (°)	M_0 (Nm)	Reference	Number of Stations/ Records
30.Oct.83	Horasan-Narman	SS	6,60	16,1	231/80/21	$1.37x10^{19}$	Pınar (1995)	1/3
13.Mar.92	Erzincan	SS	6,60	22,6	123/86/175	$1.16x10^{19}$	ISC-GCMT	1/1
6.Nov.92	Doğanbey-İzmir	SS	6,00	17,2	143/83/-21	$1.61\ x10^{18}$	ISC-GCMT	2/6
1.Oct.95	Dinar	N	6,10	15	136/43/273	$3.1\ x10^{18}$	Wright et al. (1999)	3/7
27.Jun.98	Adana-Ceyhan	SS	6,20	25	58/79/11	$2.3\ x10^{18}$	ISC-CSEM	1/3
31.Jul.98	Adana	SS	6,20	32	53/81/15	$2.96\ x10^{18}$	GCMT	6/18
17.Aug.99	Izmit (Kocaeli)	SS	7,60	20,7	91/87/164	$2.88\ x10^{20}$	GCMT	13/37
12.Nov.99	Düzce	SS	7,10	15,7	268/65/-170	$4.1x10^{19}$	ISC-CSEM	14/42
6.Jun.00	Ankara-Çankırı	SS	6,00	10	2/46/-29	$1.3x10^{18}$	Taymaz and Tan(2000)	1/3
3.Feb.02	Afyon-Sultandağ	N	6,50	10	277/60/-51	$1.1x10^{18}$	ISC-CSEM	1/3
1.May.03	Bingöl	SS	6,30	10	333/67/-171	$3.85x10^{18}$	GCMT	1/3
8.Mar.10	Elazığ	SS	6,10	5	54/80/-10	$1.2x10^{18}$	Tan et al. (2011)	1/3
23.Oct.11	Van-Erciş	R	7,10	15	246/38/60	$6.3x10^{19}$	GCMT	1/3
10.Jun.12	Fethiye	SS	6,10	24	212/78/3	$1.96x10^{18}$	Dogan et al. (2016)	2/6
24.May.14	Aegean Sea	SS	6,90	12	73/85/-177	$2.5x10^{19}$	GCMT	6/18

12.Jun.17	Midilli	N	6,30	7	125/42/-71	$4.23x10^{18}$	Kiratzi (2018)	3/9
20.Jul.17	Bodrum	N	6,60	7	275/37/-80	$1.04x10^{19}$	Karasozen et al. (2018)	9/27
24.Jan.20	Elazığ-Sivrice	SS	6,70	12	244/68/-9	$1.47x10^{19}$	Taymaz et al. (2021)	10/30
30.Oct.20	Izmir(Isle of Samos)	N	7,00	8,2	270/45/-89	$4.01x10^{19}$	Cetin et al. (2020)	11/33
23.Nov.22	Düzce	SS	6,00	6,81	255/83/178	$1.61x10^{18}$	ISC-AUST	11/33

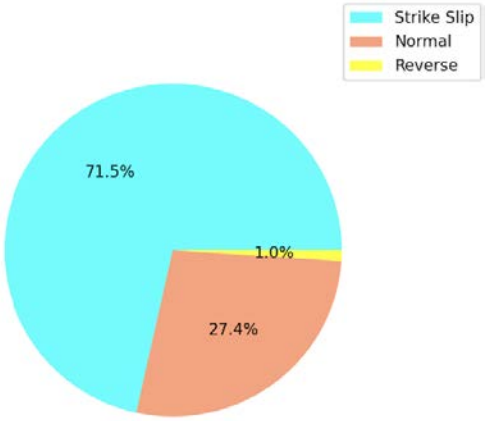

Figure 4.1. Distribution of the earthquakes in the dataset in terms of style of faulting

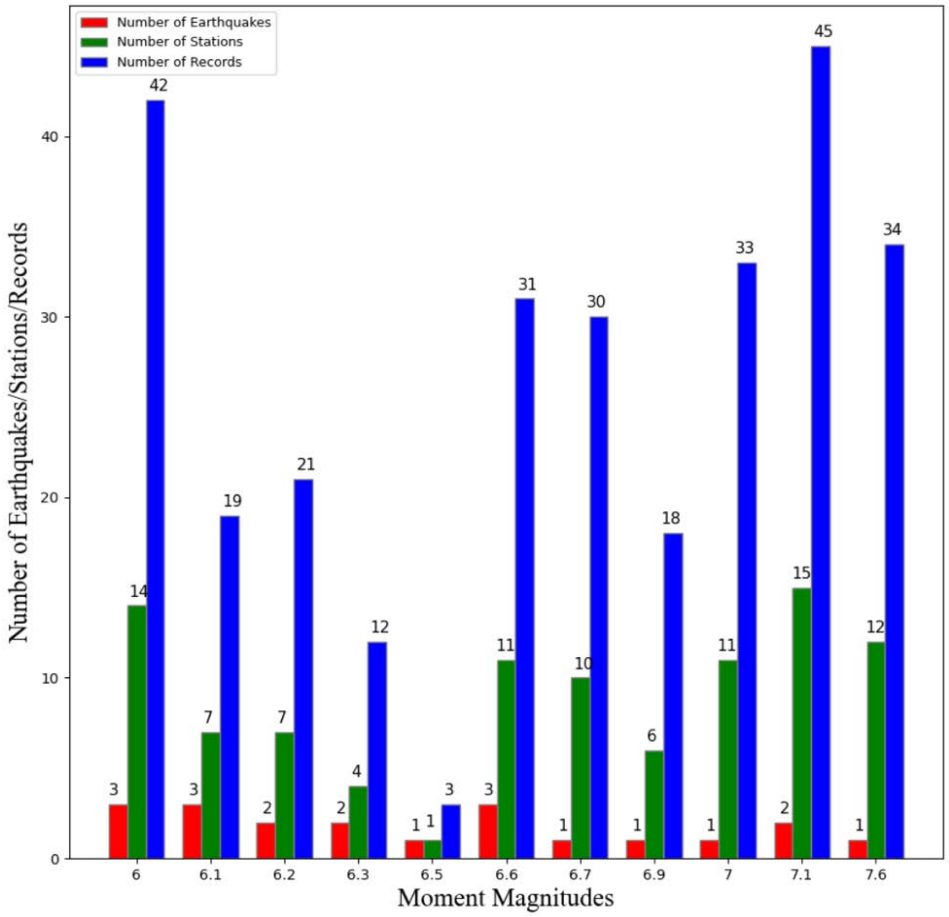

Figure 4.2. Distribution of the data with respect to moment magnitudes

Figure 4.1 and Figure 4.2 demonstrate the distribution of the data that was involved in this study. As can be seen from Figure 4.1, the strike slip earthquakes dominated the data and only one reverse faulting earthquake, the 2011 Van-Erciş earthquake, involved. Normal faulting earthquakes were not common in the previous studies; for instance, although Schiappapietra et al. (2021) considered worldwide data, their dataset contained 120 stations from 15 normal faulting earthquakes. As this study contains 26 stations from 5 normal faulting earthquakes, it is expected that this study augments the literature. Another aspect of this study is that, as can be seen in Figure 4.2, the dataset contains 30 stations from 11 earthquakes with magnitudes ranging between Mw 6 and Mw 6.5 and by considering the fact that Schiappapietra et al. (2021) contained 188 stations from 24 earthquakes in the same magnitude bin, dataset created in this study will contribute the literature.

Stations with Rjb distances closer than 30 km and 10 km correspond to 50% and 20% of the data, respectively. The records taken from the AFAD constitute 80% of the data and the rest of them are taken from the ESM. Although the earthquake stations are operated mainly by AFAD, there are also some stations operated by Boğaziçi University- Kandilli Observatory and Earthquake Research Institute (KOERI) and Istanbul Technical University (ITU). Moreover, in the dataset, there are some temporary stations operated by the institutions outside Türkiye. These stations were installed in the region to screen the behavior of NAF after 1999 Kocaeli earthquake and recorded 1999 Düzce earthquake. The codes of the earthquake stations, their Joyner and Boore (Rjb), closest distance to the horizontal projection of the earthquake rupture plane, and the rupture distances (Rrup), the closest distance to the earthquake rupture plane, sources of the data, and the operator institutions are listed in Table A.2. in Appendix A.

Among the data, 5 stations do not meet the Rjb distance criterion of the study, (two stations from the 1999 Kocaeli earthquake, and one station from each of 2020 Izmir (Samos), 2017 Bodrum, 2017 Midilli, and 2012 Fethiye earthquakes). However, since the one sided velocity pulse behavior is observed in their velocity time histories, it is decided to include these stations.

Figure 4.3 presents the distribution of the earthquakes and their recorded stations on the Türkiye map, further information for stations can be found in Table A.3. in Appendix A.

Figure 4.3. Distribution of the earthquakes and the stations which are utilized in this study

Since the 1999 Kocaeli earthquake has been widely studied and the observed flings on the waveforms were reported by different researchers, a special attention is given to the records of this earthquake. For instance,

-Rathje et al. (2000) stated that the East-West (EW) component of the SKR station demonstrated permanent displacements of roughly 200 cm and the North-South (NS) component of the YPT station exhibited that of 150 cm.

-Kalkan and Kunnath (2006) calculated permanent displacement by implementing the data processing technique of Iwan et al (1985) and they found 186.76 cm for the EW component of SKR station and 145.79 cm for the NS component of YPT station.

In this study, the obtained permanent displacements compared those from previous studies in Chapter 5.1. Another special attention is given to the 1999 Düzce earthquake. Because, although the specially processed ground motion record from this earthquake is not found, fling existence is mentioned in the previous studies. For instance,

-Yılmaz and Türer (2002) indicated that the earthquake caused 2-2.5 m fling step in the vicinity of the rupture. Moreover, 100 cm displacement in the region of the Bolu viaduct which made the dampers (Energy Dissipating Unit) of the viaduct dysfunctional since they had been designed to allow 48 cm displacements.

-KOERI report (1999), stated that the offsets are around 1.5 m at western Düzce and some 3 m towards Bolu.

-Rathje et al. (2006) reported that one of the temporary stations C-1058, installed by the LDEO, displayed 20 to 40 cm permanent displacement.

5. PERMANENT DISPLACEMENTS OF TURKISH STRONG MOTION DATABASE

The records of Türkiye earthquakes are exposed to the proposed data processing scheme of this study in Python 3.9 and the permanent displacements are revealed. Resulting static displacements found in wide range from 0.03 mm to 2.64 m. Outputs of this study presents a fling step database for Türkiye earthquakes, with 288 records from 98 seismic stations recorded 20 earthquakes, for the first time, which can contribute to the update of the structural design procedures of TBYD 2018 (Turkish Building Design Code, 2018) in terms of near fault structures. List of the prepared fling step database for Türkiye earthquakes, which also contains the FN and FP components of the stations in addition to 288 (EW,NS,UD) records and the earthquake and stations parameters is placed in Table A.3. in Appendix A.

To be able to totally evaluate the general behavior of the created dataset, firstly, the distribution of the absolute values of the obtained permanent displacements with the magnitudes of the events are presented in Figure 5.1 (EW,NS,UD components) and in Figure 21 (FN and FP components). Secondly, in the same way the distribution of the data with Rjb distances are presented in Figure 5.3 and Figure 5.4.

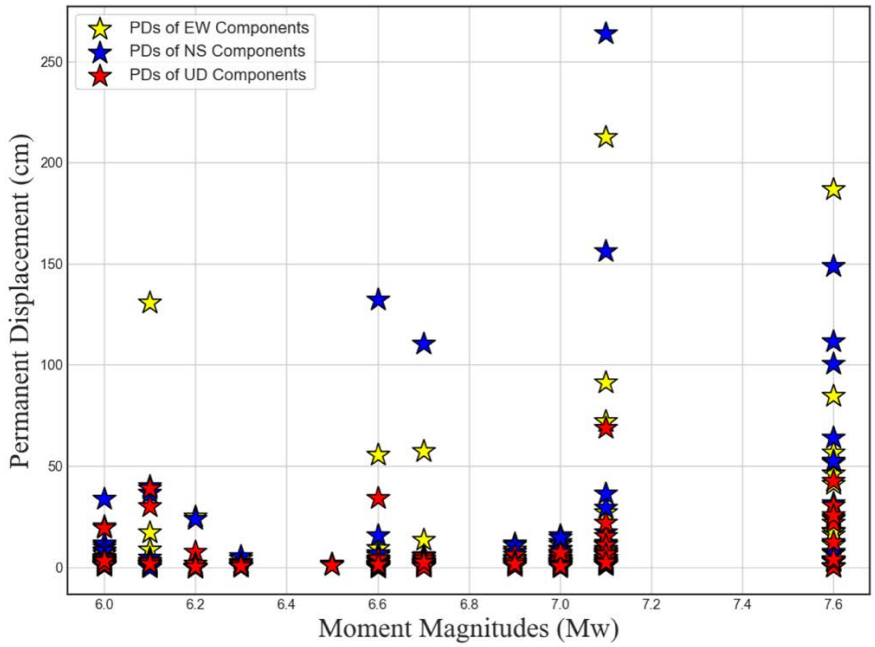

Figure 5.1. Distribution of the obtained permanent displacements (PD) at EW, NS, and UD components with moment magnitude

As can be seen on Figure 5.1, the obtained permanent displacements on the vertical components are relatively less than the horizontal ones. The highest permanent displacements occurred on the records of the Mw7.1 1999 Düzce earthquake. Apart from exceptions, the general trend can be observed that the higher the magnitude of the event the higher the resulting permanent displacement.

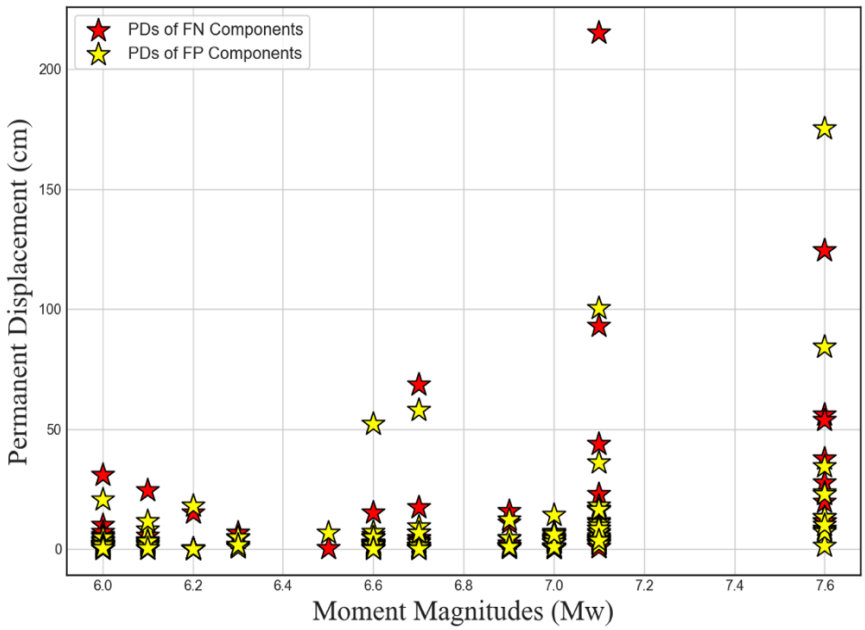

Figure 5.2. Distribution of the obtained permanent displacements (PD) on the FN and FP components of the earthquake recordings with the moment magnitudes of the events

As aforementioned, the statement of Abrahamson (2002) for the fling expected component is disproved in this study. It is found not the permanent displacement occurs on FN component of the stations of strike slip earthquakes but also it can be higher than the FP. For instance, in Figure 5.2 it is seen that while the maximum permanent displacement from the 1999 Kocaeli earthquake is available in one of the FP components of the stations, that of observed in 1999 Düzce earthquake is found on the FN components of the stations.

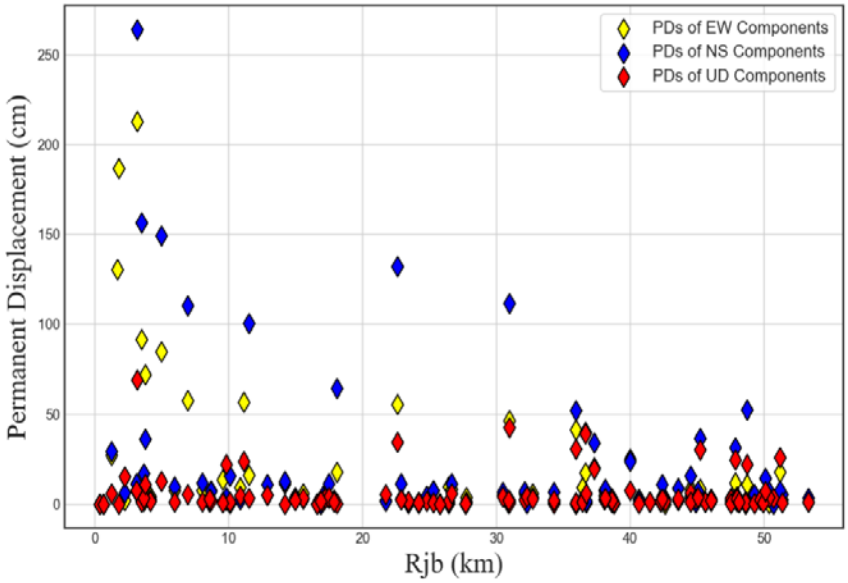

Figure 5.3. Distribution of the obtained permanent displacements (PD) on the EW, NS and UD components of the earthquake stations with the Rjb distances of the stations

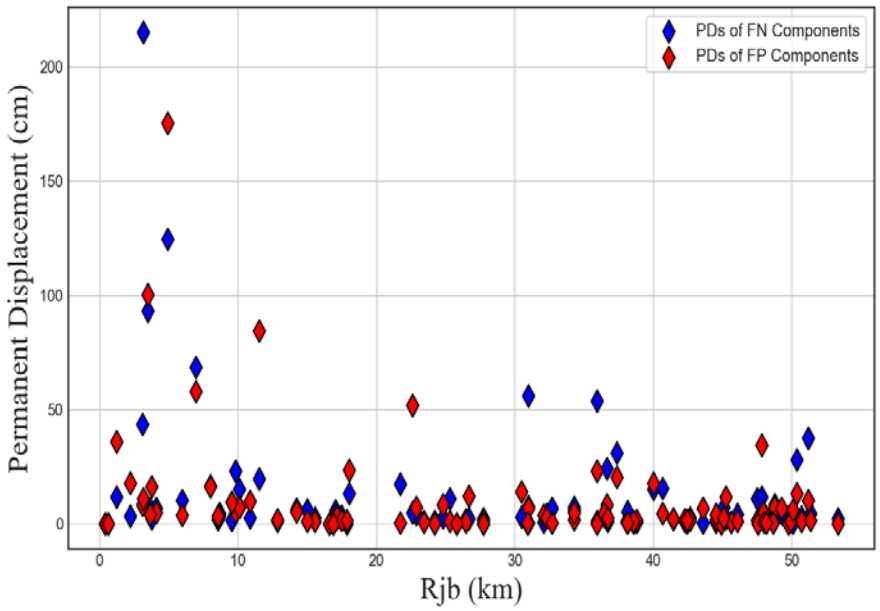

Figure 5.4. Distribution of the obtained permanent displacements (PD) on the FN and FP components of the earthquake stations with the Rjb distances of the stations

As can be seen on Figure 5.3 and 5.4, the closer the earthquake station to the fault rupture, the higher the observed permanent displacement. It is observed that the permanent displacements in the first 10 km of the fault rupture are sharply higher than the others. In addition, Figure 5.3 also supports that the UD component of the stations contain relatively small permanent displacements.

To be able to see the effect of the dip angle on the fling occurrence, the distribution of the obtained static displacements on the FP and FN components of the stations against dip angles of the earthquakes are presented in Figure 5.5. In the figures, Rjb windows are created for each 10 km distance.

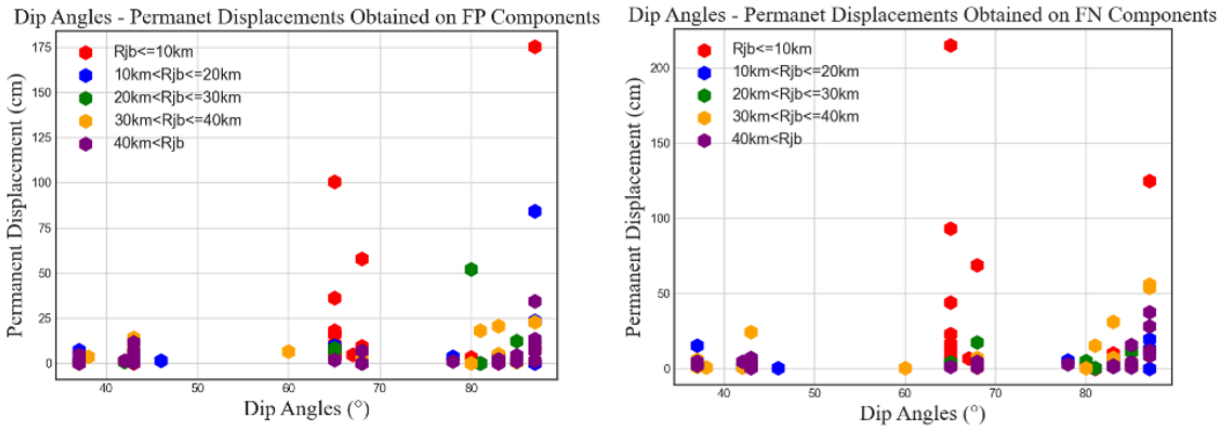

Figure 5.5. Distribution of the permanent displacements obtained on the FP (left) and FN (right) components of the stations versus dip angles of the earthquakes in each Rjb distance window.

Based on Figure 5.5, it can be stated that the permanent displacements are slightly higher in the earthquakes with higher dip angles regardless of the FP or FN direction. Nevertheless, since the difference is not as apparent as that of Mw distribution or Rjb distribution, more data from the different earthquakes with more different dip angles should be studied to get the more accurate insights into the effect of the dip angle on the fling step existence.

General Findings:

Most of the previous fling step studies were confined with the Reverse (Thrust) faulting earthquakes by virtue of the abundant data of 1999 Chi-Chi (Mw7.6) earthquake. In terms of normal faulting earthquakes, there are only limited studies. However, recent studies demonstrated the fling occurrence during the normal faulting earthquakes; for instance, D'Amico et al. (2018) studied the 2016 Norcia (Central Italy) earthquake and found permanent displacements up to 85 cm. Moreover, Schiappapietra et al. (2021) found 11 normal faulting earthquakes among the worldwide data. Nevertheless, taking into consideration of the earthquake selection criteria of the Schiappapietra et al. (2021), which are the magnitude of the event is higher than Mw 5.5 and the stations with R_{JB} distances lower than 140 km for the worldwide earthquake data from 1952 to 2020, the number of the fling identified normal faulting earthquake records is very limited in the literature. What is more, none of these earthquakes is from Türkiye. In this study, permanent displacements on 81 records of 27 stations from 5 normal faulting earthquakes in the N-TSMD are identified. It is expected that if the outputs of this study are incorporated in NESS 2.0, the number of normal faulting earthquake data will be augmented 22%. Strike slip earthquakes are relatively more studied. The number of strike slip earthquakes containing fling is defined as 26 in the fling step database NESS 2.0, 4 of which are from Türkiye earthquakes. One of the reasons behind the low number of Türkiye earthquakes in that database might be that the eBASCO procedure became insufficient for recovering the fling from these earthquakes. Nevertheless, if the outputs of this study are included in NESS 2.0, the database will be increased by 33% in terms of strike slip earthquakes.

Another point of this study is that the general acceptance of the statement of Abrahamson (2002) which is that the fling step occurs in the slip direction of the earthquake is disproved. Based on that hypothesis, permanent displacements should be observed in FP components of strike slip earthquake stations. However, fling also occurs in the FN component of the earthquake station of strike slip earthquakes. Likewise, starting from Wu and Wu (2007), previous studies demonstrated that the fling can occur in any direction including vertical components. Moreover, in this study it is found that the amount of fling in FN components can be higher than in FP components. To exemplify, for strike slip earthquakes the FN and FP

components are compared and it is found that in 41 stations the amount of permanent displacements observed in FN is higher than that in FP among the 67 stations. Some of the stations and absolute values of the permanent displacements in FP and FN are presented in Table 5.1. Similarly, strike slip earthquakes data in NESS 2.0 are also inspected and in 113 stations among 203 stations from strike slip earthquakes, the permanent displacements in FN components are found higher than those in FP components. The same inspection is also done for the normal faulting earthquakes. Likewise, for the normal faulting earthquakes, the amount of fling in the FP component of 10 stations, among 26 stations from the presented dataset in this study, is found higher than those in FN. In the NESS 2.0, 52 stations among 121 stations also demonstrated the same behavior. Figure 5.6 (left) illustrates 1999 Düzce earthquake displacement time histories of processed FN and FP components of station C 1058, which obey the Abrahamson (2002) statement. On the other hand, Figure 5.6 (right) demonstrates the 2020 İzmir-Samos earthquake displacement time histories of processed FN and FP components of station TK 3536, which is an example of the disproving the statement of Abrahamson (2002).

Table 5.1. The comparisons of some of the obtained flings in FP and FN components. *(Cont.)*

Date	Earthquake	SoF	Mw	Station	FN (cm)	FP (cm)
6.11.1992	Izmir (Doğanbey)	SS	6,6	TK 3501	31,07	20,59
27.06.1998	Adana-Ceyhan	SS	6,2	TK 105	15,36	18,05
17.08.1999	Kocaeli	SS	7,6	YPT	124,62	59,28
17.08.1999	Kocaeli	SS	7,6	FTH	27,92	13,42
17.08.1999	Kocaeli	SS	7,6	MCD	8,39	7,2
12.11.1999	Düzce	SS	7,1	C 1058	11,71	36,17
12.11.1999	Düzce	SS	7,1	D 531	16,75	16,46

1.05.2003	Bingöl	SS	6,3	TK 1201	6,91	5
20.07.2017	Bodrum-Kos	NF	6,6	TK 918	4,69	4,90
20.07.2017	Bodrum-Kos	NF	6,6	TK 4809	15,31	7,23
24.01.2020	Elazığ-Sivrice	SS	6,7	TK 2308	68,67	57,92
30.10.2020	Izmir-Samos	NF	7	TK 905	3,68	4,65
30.10.2020	Izmir-Samos	NF	7	GMLD	6,61	5,31
30.10.2020	Izmir-Samos	NF	7	TK 3536	3,15	14,23
23.11.2020	Düzce (Gölyaka)	SS	6	T 8110	7,33	5,10

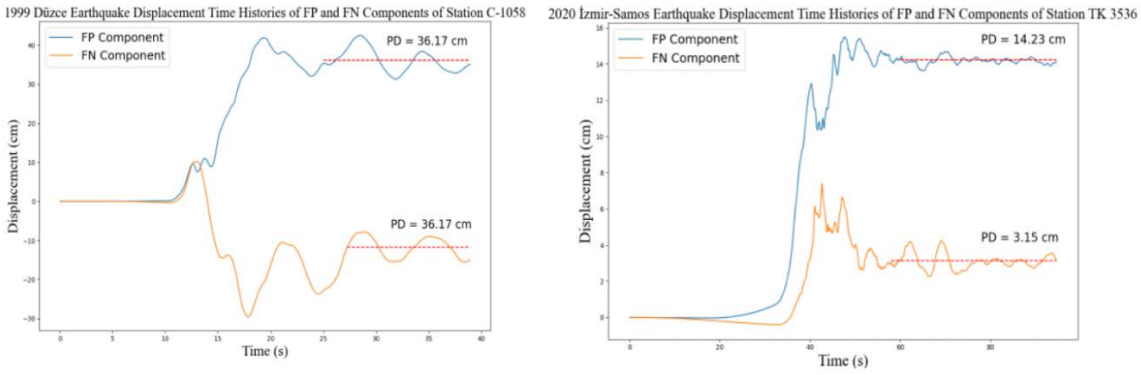

Figure 5.6. Displacement time histories of processed FN and FP components of (left) 1999 Düzce earthquake station C 1058 and (right) 2020 İzmir-Samos earthquake components of station TK 3536 (PD is permanent displacement)

The largest earthquakes included in this study are the 1999 Kocaeli, 1999 Düzce earthquake, 2011 Van-Erciş and 2020 İzmir-Samos earthquakes. Since the 2011 Van-Erciş earthquake is only represented by one station, inspection of the findings is not done for this earthquake. For the other three earthquakes, following points are found:

- Permanent displacements of the 1999 Kocaeli earthquake, which is the second most studied earthquake in terms of fling after the 1999 Chi Chi (Mw 7.6) earthquake, revealed on 34 records of 12 stations. Apart from the NS component of SKR station, which is not available, the NS component of TK 4106 also cannot be processed due to the fact that this record could not transcend the acceleration comparison limit of the procedure. Among the processed records of this earthquake, the highest permanent displacement is observed on the EW component of the SKR station as 186.84 cm and the smallest fling is found in the UD component of station TK 8101 as -0.30 cm.

- The maximum permanent displacement is observed on 1999 Düzce earthquake NS component of station TK 8101, which is located on relatively soft materials south of the D-100 highway, based on the Özmen (2000), as 263.89 cm. Although this station is not involved in the previous studies, the findings of Yılmaz and Türer (2002), in which the 2-2.5 m permanent displacement observation is stated, supports the revealed fling value. In addition, the EW component of the same station demonstrated -212.66 cm permanent displacement after being processed with the proposed scheme. The large permanent displacement in this station is also studied by Roussis et al. (2002). Because of the scarcity of the fling revealing data processing scheme, they simulated this station by hybrid approach and found a similar result of this study. Processed waveforms of 1999 Düzce earthquake NS component of station TK 8101 and simulation result of Roussis et al. (2002) for it are demonstrated in Figure 5.7. In addition to the TK 8101, 12 other stations of the 1999 Düzce earthquake, a total of 39 (EW, NS, UD) records are processed. Rathje et al. (2006) stated that the station C 1058 might have caused the 20 to 40 cm permanent displacement. Their estimation is found reasonable since the permanent displacement of the EW, NS and UD components of this station are found as -27.05 cm, -29.5 cm and -6 cm, respectively. Rathje et al. (2006) also stated that the six of the temporary stations, named C 375, D 531, C 1058, C 1059, C 1061 and C1062, were located on shallow sites close to the fault; however, the station C 375 demonstrated much higher peak ground acceleration. Moreover, they also stated that in relatively longer periods this station demonstrated much higher spectral values. Their findings are found aligned with the outcomes of this study so that the permanent displacements are found quite higher in station C 375. For instance, in EW and NS

components of this station, the permanent displacements are found as 91.49 cm and -156.24 cm, respectively. Although other stations were also very close to the fault, these differences may be explained by another observation of Rathje et al. (2006) which is that the this was located upslope from the landslide and the downslope movement of the soil in the landslide might have affected records of this station.

- Since there is not a near field station within the 10 km Rjb distance, the highest fling in the 2020 İzmir-Samos earthquake is observed on the NS component of station TK 3533, with Rjb distance of 44.54 km, as 15.74 cm. Aktuğ et al. (2021) presented some of the permanent displacements from GPS data which are close to the stations TK 3528, TK 3536, GMLD, KUSD. The revealed permanent displacements of the records of these stations are compared with those derived from GPSs in Table 3.4. In addition to this earthquake, the highest fling from the 2017 Bodrum earthquake, which is another NF earthquake, is observed on the NS component of the station TK 4809 as 15.79 cm and verified with the findings of by Konca et al. (2019), which was found as 20 cm by derivation of the GPS data, as seen in Table 3.4.

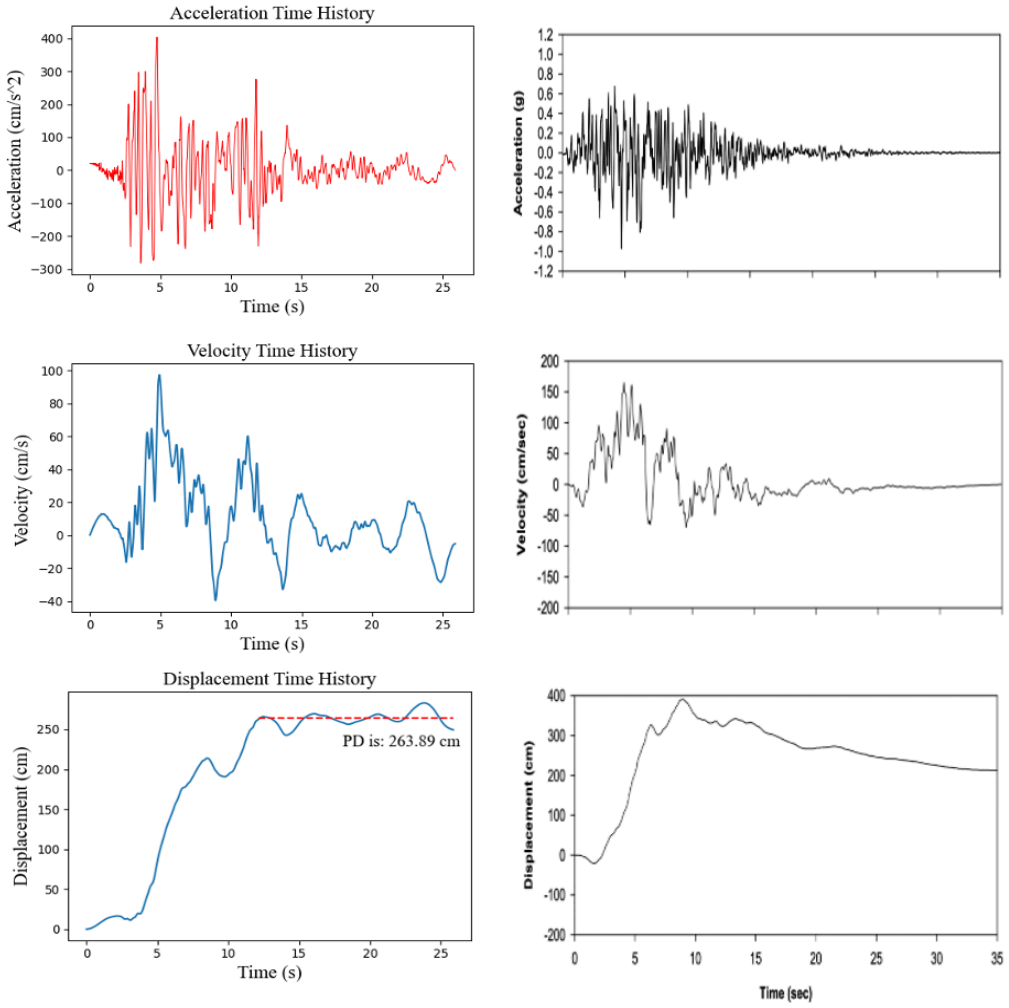

Figure 5.7. (left) Processed version of the 1999 Düzce earthquake NS component of station TK 8101 (red line shows the permanent displacement calculated as a mean of the motion after 95% of the cumulative energy is dissipated; PD is permanent displacements), (right) simulation results for the station TK 8101 by hybrid approach (Roussis et al. (2002))

Since it is not mentioned in the previous studies, another interesting result is obtained in the 1983 Horosan-Narman earthquake NS component of the station TK 2503. In this record, the permanent displacement is found as -132.18 cm, which is higher than the similar earthquake records with the similar distances such as 2020 Elazığ-Sivrice horizontal components of station TK 2301. Figure 5.8 demonstrates the acceleration, velocity and displacement waveforms of the raw and processed version of this record.

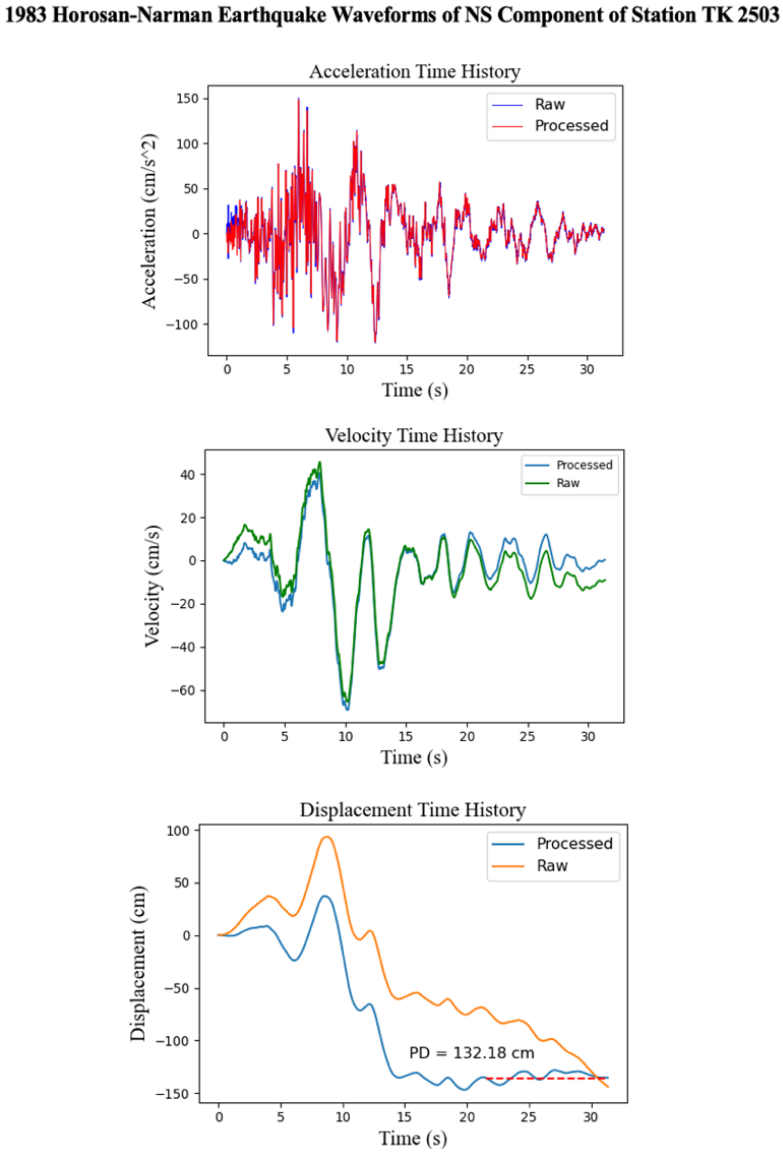

Figure 5.8. 1983 Horosan-Narman earthquake acceleration, velocity and displacement waveforms of NS component of station TK 2503 (PD is permanent displacement)

There are some records on which the fling amount is quite little, or unobservable. As expected, generally these records belong to earthquake magnitudes lower than Mw 6.5 or the stations which have great distances. For instance, the fling of the 2012 Fethiye (Mw 6.1) earthquake processed motion of the NS component of station TK 4811, whose Rjb distance is 50.6 km, is found as -0.01 cm. Another example is shown in Figure 5.9 (left) as the displacement time history of the processed waveform of the 2017 Bodrum (Mw 6.6) earthquake EW

component of station TK 4810, which has a Rjb distance of 48.67 km and a permanent displacement of 0.038 cm. Similarly, very low fling values also found UD components of some of the large earthquake records such as permanent displacement in 2020 İzmir-Samos earthquake that of GMLD station is pinpointed as 0.06 cm, as shown in Figure 5.9 (right). These kinds of examples, encountered in this study, demonstrate that the procedure might also be executed to the ground motion records at far distances.

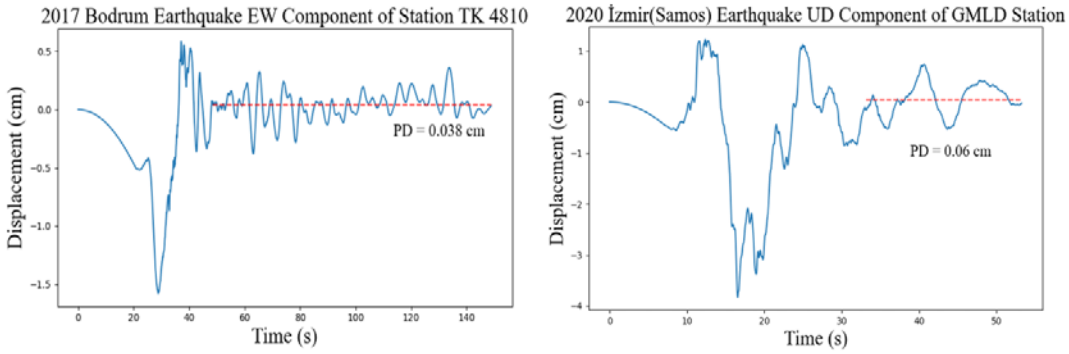

Figure 5.9. The displacement time histories of (left) 2017 Bodrum earthquake EW component of station TK 4810 and (right) 2020 İzmir-Samos earthquake UD component of GMLD station (PD is permanent displacement)

In this study, it is also found that both the directivity effect and the fling effect can be seen on the earthquake records. For instance, 1999 Düzce earthquake station TK 1401, also known as BOLU station, contains both directivity and the fling effects. On the velocity time history of the FN component, which is calculated by Somerville (2002), firstly a full cycle large wave and immediately after a half cycle large wave which is an indicator of fling existence are seen. Rathje et al. (2006) also stated the existence of a directivity effect on the FN component of the same station. Figure 5.10 illustrates the processed waveforms of the 1999 Düzce earthquake FN component of the station TK 1401.

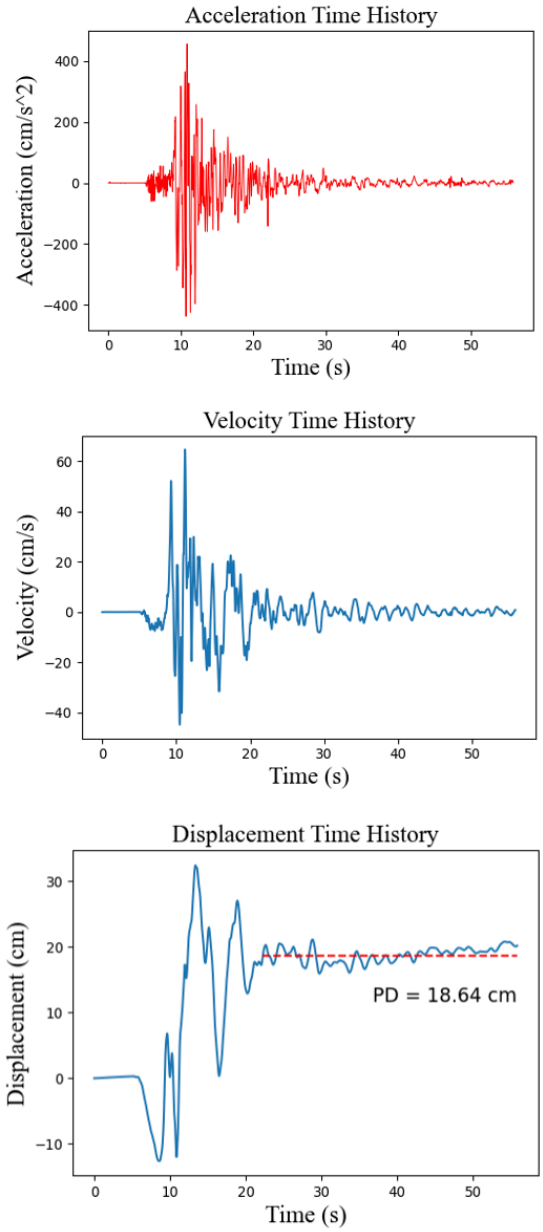

Figure 5.10. Acceleration, velocity and displacement time histories of 1999 Düzce earthquake FN component of the station TK 1401 (PD is permanent displacement)

6. COMPARISON WITH EXISTING FLING STEP PREDICTION MODELS

In this chapter, performance of the existing fling step predictive models of Kamai et al (2014) and Burks and Baker (2016) with earthquakes in Türkiye are evaluated.

6.1. Burks and Baker's (2016) Fling Step Prediction Model and Residual

Burks and Baker (2016) presented a new easy-to-use predictive model for the fling step amplitudes of FN and FP components of the earthquakes by taking into account of moment magnitudes of the events and Rrup distances of the sites. Burks and Baker (2016) identified a combined dataset to create their predictive model. The sources of their dataset consist of 67 real records, 44 high-rate GPS records and 2.2 million ground motion simulations. As a first source they utilized earthquake records which are: 2 records from 2010 Darfield (Mw 7.1) ; 2 records from the 1999 Kocaeli (Mw 7.6) ; and 63 records from 1999 Chi Chi (Mw 7.6) earthquake. In the dataset, the defined fling-containing real records were processed by using the data processing method of Wu and Wu (2007). As the second source of the dataset Burks and Baker (2016) utilized the high-rate GPS records. However, since the GPS stations were located far from the earthquake sources and therefore have very small static offsets, Burks and Baker (2016) used them to evaluate the fling characteristics only at large distances. As the third and the main data source, they utilized ground motion simulations. These simulations consisted of three sets. Two of them are kinematic simulations of 6 earthquake scenarios with rupture geometries similar to 1906 San Francisco and 29 of those on the Hayward fault with varying earthquake parameters, respectively. Thirdly, in addition to these strike slip earthquake simulation sets, reverse type earthquake simulations were computed using the Graves and Pitarka (2010) hybrid broadband method on Southern California Earthquake Center (SCEC) Broadband Platform (BBP). These reverse scenarios consisted of 40 earthquake scenarios with magnitudes ranging between Mw 6 and Mw 7.5. Briefly, the proposed predictive model was mainly based on the strike slip and reverse faults. Based on the defined data sources, Burks and Baker (2016)

constructed the fling step prediction equation as a function of the closest distance of the prediction site to the fault, Rrup, and moment magnitude of the event as follows:

$$ln(D_p) = ln(cot^{-1}(0.3R)) + 1.3M - 5.1 \quad (6.1)$$

where D_p is predicted fling, R is the closest distance, Rrup, and M is moment magnitude, Mw. This proposed equation was based on the functional form suggested by Byerley and De Noyer (1958). Burks and Baker (2016) predictive model is found similar to that of Abrahamson (2002) rather than those of Kamai et al. (2014) since it does depend on neither rupture mechanism nor dip angle. However, after comparison of Abrahamson (2002), Kamai et al. (2014) and their predictive equation on the data source, Burks and Baker (2016) stated that some of the scenarios similar to 1906 San Francisco (Mw 7.9) earthquake tend to follow previous models whereas the others follow their model.

Performance of the Burks and Baker (2016) in Türkiye earthquakes is evaluated by comparison and the residual analyses. Since Burks and Baker (2016) model was created by using predominantly Reverse and Strike Slip type earthquake scenarios, one might consider that the equation is not for normal faulting earthquakes. However, Burks and Baker (2016) did not state any style of faulting limitation. Likewise, although the source data of that equation consisted of the earthquakes with magnitudes ranging between Mw 6 to Mw 8.2, in the study no magnitude limitation was stated. This model is defined for the slip direction components of the earthquake stations. In other words, the model is for Fault Normal (FN) components of dipping and the Fault Parallel (FP) components of strike slip earthquakes. Therefore, firstly, in order to make a comparison between fling amplitudes of Turkish strong motion database and Burks and Baker (2016) fling predictive model, FN and FP components of the stations are defined. This was achieved by the rotating horizontal components by strike angles of the respective earthquake according to Somerville (2002) as:

$$SP = Ncos\varphi + Esin\varphi \quad (6.2a)$$

$$SN = -Nsin\varphi + Ecos\varphi \quad (6.2b)$$

where E, N and φ represent the acceleration time histories in the East-West and North-South directions and strike angle of the earthquake respectively. In the equations SP and SN stand for strike parallel and strake normal respectively. It can be inferred from the Somerville (2002) that the SN and SP also correspond to FN and FP.

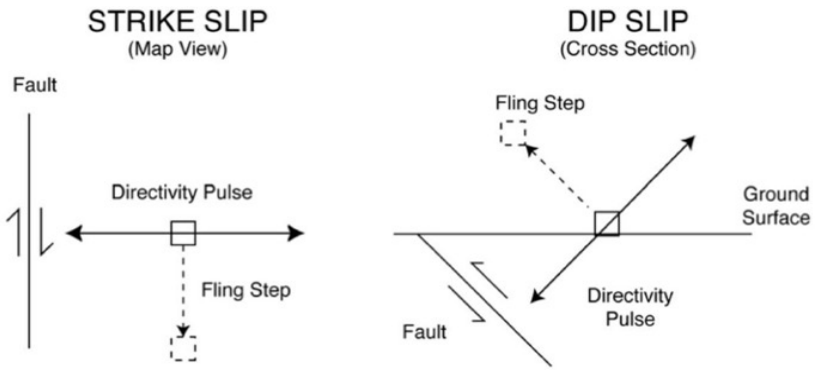

Figure 6.1. Schematic orientation of the rupture directivity pulse and fling step for strike-slip (left) and dip-slip (right) faulting. (Somerville (2002))

Schiappapietra et al. (2021) stated that on account of the large variability in the permanent displacements under 1 cm, only the data having permanent displacement above 1 cm were considered for evaluation of Burks and Baker (2016) predictive model in their study. In this study, however, the permanent displacements of 3 cm and above are considered from an engineering perspective. Previous to evaluation of the permanent displacements in slip direction components of the stations, the predictions of the model are compared with both the FN and FP components of the motions in this study, just like Schiappapietra et al. (2021). Residual analyses are conducted according to Gülerce et al. (2016) by considering each record (i) from each event (j) as follows:

$$R_{ij} = ln(a_{ij}) - ln(p_{ij}) = c_k + \Delta_{Bj} + \Delta_{Wij} \quad (6.3)$$

where R_{ij} is the total residual, a_{ij} is the permanent displacement observed on the processed record and p_{ij} is the predicted value. The total residual is divided into three parts: c_k, the average bias of the real permanent displacements relative to predicted ones, Δ_{Bj}, inter-event residuals, and Δ_{Wj}, intra-event residuals. Figure 6.2 demonstrates the total residuals of the data for the FP

(right) and FN (left) components of the stations with both the moment magnitudes of the events and the Rrup distances of the stations. Figure 6.3 illustrates the inter-event and intra-event residuals of the data in the same directions.

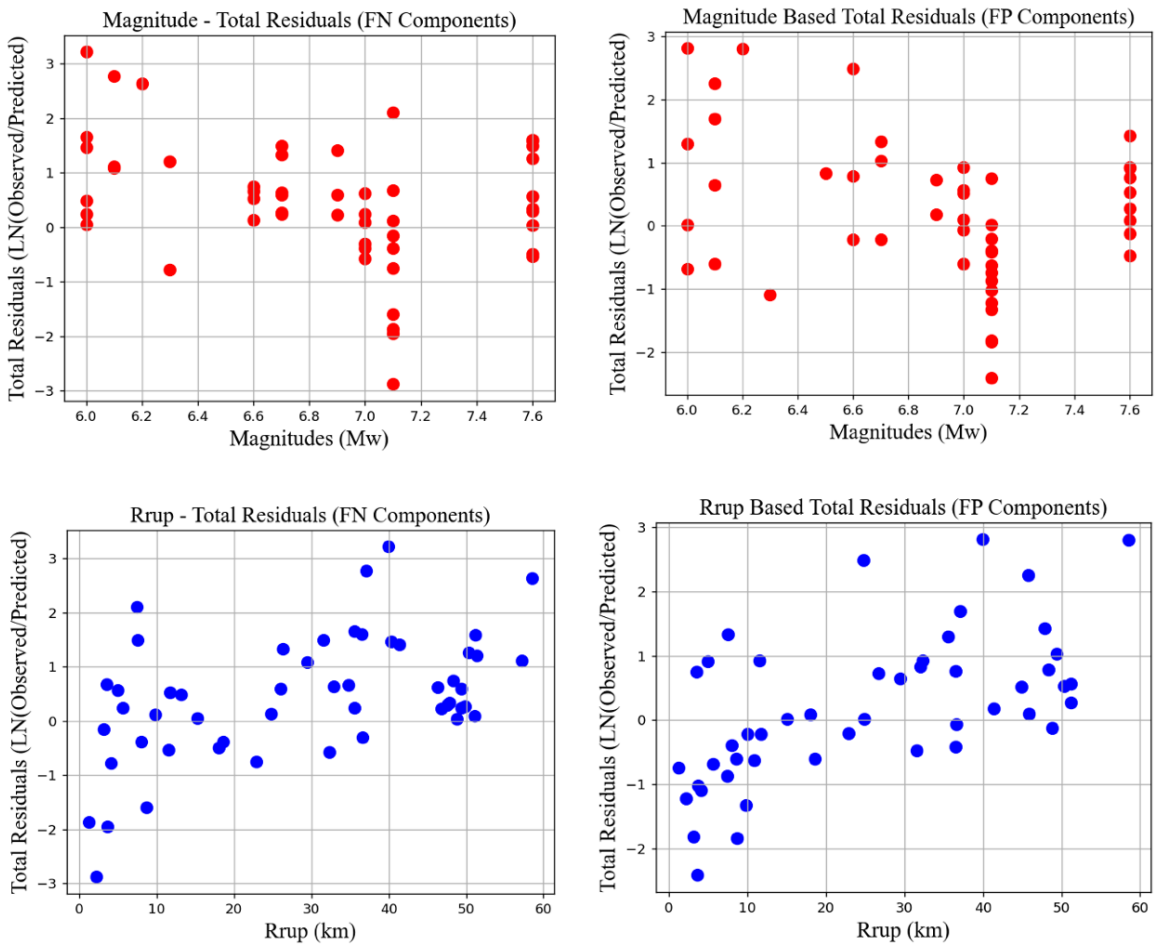

Figure 6.2. Distribution of the total residuals of FN and FP components of the stations with moment magnitudes and the Rrup distances

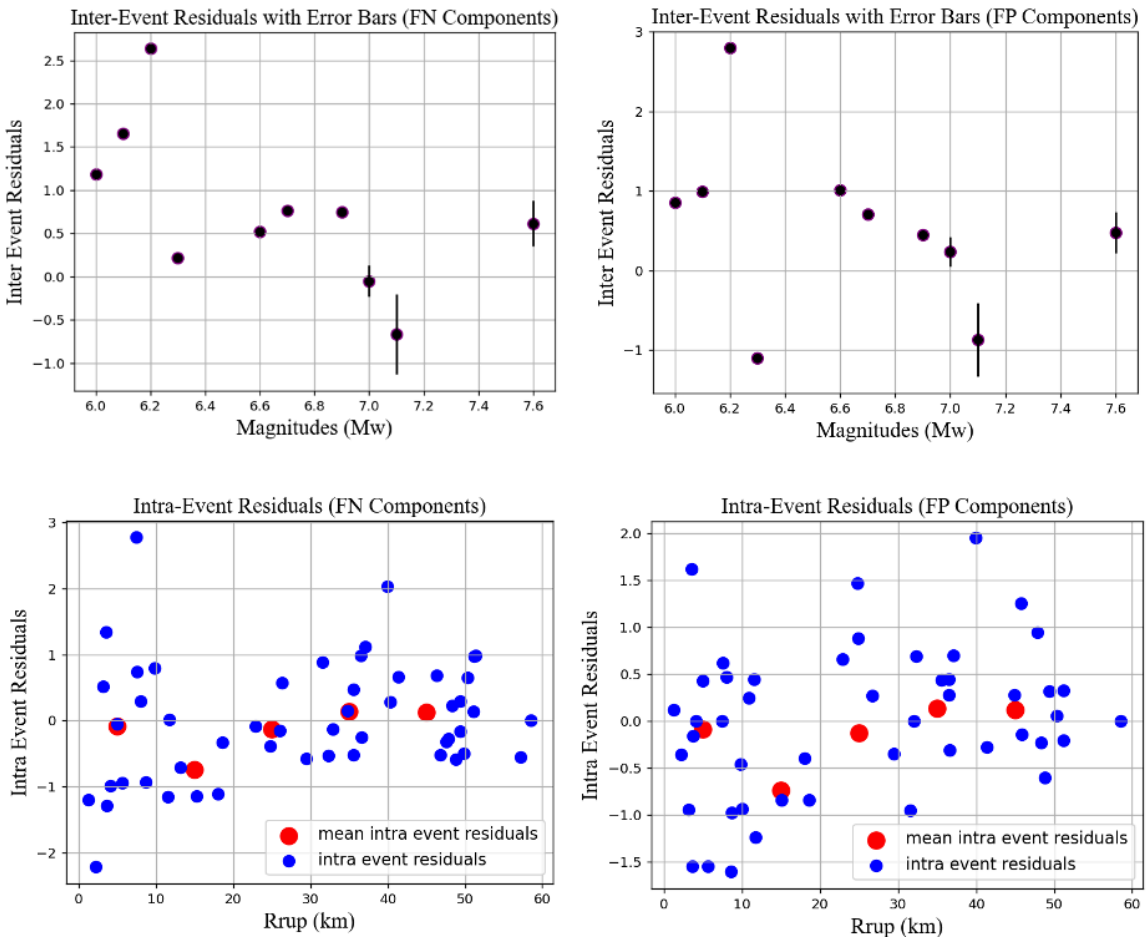

Figure 6.3. Distribution of the inter-event and intra-event residual analyses of FN and FP components of the stations with moment magnitudes and the Rrup distances

As can be seen in Figure 6.2 (left) and 6.3 (left), in terms of FN components, Burks and Baker (2016) relatively well estimates the larger magnitude events than moderate events, especially in the distances between 20 km and 30 km from the rupture surface. Further observation is that the Burks and Baker (2016) estimates permanent displacements of the 1999 Kocaeli (Mw 7.6) earthquake better than the 1999 Düzce (Mw 7.1) earthquake. Moreover, the FN components of the earthquakes with moment magnitudes of above Mw 6.6 are also good estimated by the Burks and Baker (2016).

Similar results also found for the FP components of the earthquakes, as seen in Figure 6.2 (right) and 6.3 (right). The closer distances, especially for the earthquakes with moment magnitudes above Mw 6.6 are well estimated by the Burks and Baker (2016).

Since the existence of permanent displacement has been acknowledged on the slip direction of the earthquakes, Burks and Baker (2016) utilized these directions from the simulation results. However, they did not separate the fling recovered real records by their directions. Since the simulations were defined as the main source of this model, it is considered that evaluating the model with the permanent displacements in slip direction components of Turkish strong motion database results in less discrepancies. The resulting total residual analyses and inter- and intra-event residuals are demonstrated in Figure 6.4 and 6.5, respectively.

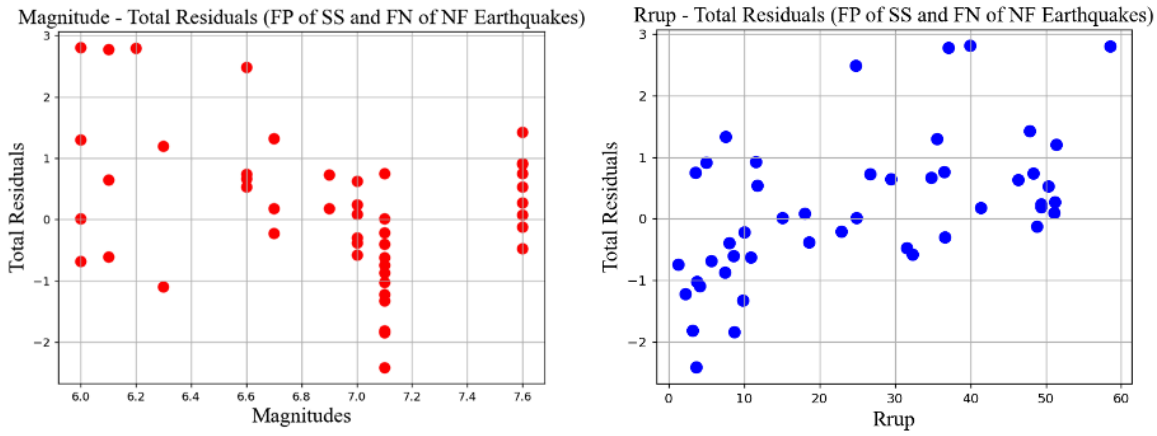

Figure 6.4. Distribution of (left) the total residuals of slip direction with moment magnitudes and the Rrup distances (right)

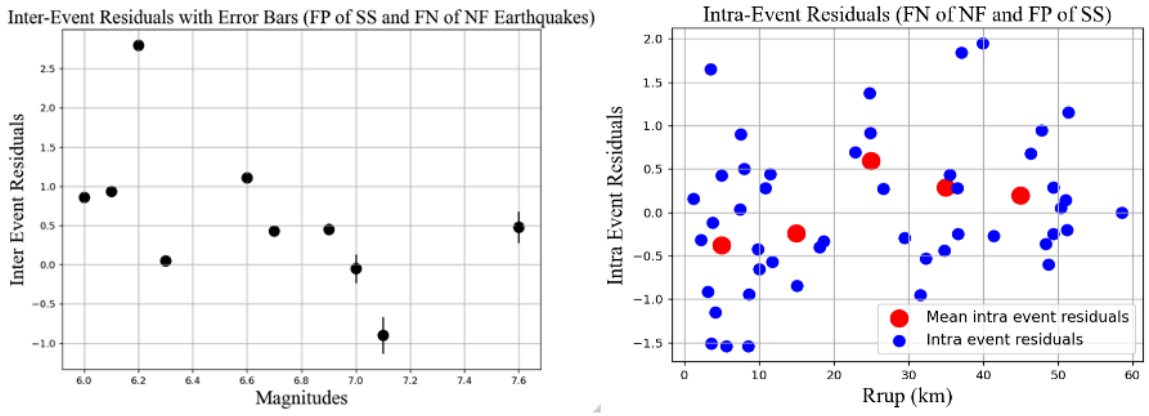

Figure 6.5. Distribution of (right) inter-event and (left) intra-event residual analyses of slip direction components of the stations with moment magnitudes and the Rrup distances

As expected, the estimates of the predictive model are closer to those observed in the slip direction components of the stations. Especially, the 1999 Kocaeli (Mw7.6) and the earthquakes with magnitude ranging between Mw 6.6 to Mw 6.9 are well captured by Burks and Baker (2016) predictive model.

Noteworthy, only one station from the 2011 Van-Erciş (Mw7.1) earthquake is available in the dataset created in this study; nevertheless, it is not utilized in the evaluation of the Burks and Baker (2016) fling step predictive model due to the 3 cm permanent displacement limitation in the FN or FP components.

6.2. Kamai et al. (2014) Fling Step Predictive Model and Residuals

In this section of the study, the performance of the Kamai et al. (2014) for the Türkiye earthquakes are inspected. Firstly, the maximum direction components (RotD100s) of the stations are defined due to the fact that Kamai et. al (2014) predictive model is for these directions. Starting from the Beyer and Bommer (2006), RotD100 component has been defined as the direction of the station in which the maximum spectral ordinate along all possible orientations at each period of the horizontal axis are obtained. Similarly, Kamai et al. (2014) defined that as the rotated horizontal motion which results in the maximum permanent displacement. From this definition, the combination of the horizontal components are rotated

starting from 0° to 360° and each of them is exposed to the processing scheme presented in this study. Among all the rotated waveforms of a station, the RotD100 is defined by comparing the resultant displacements. Kamai et. al (2014) predictive model takes into account of dip angle, magnitude, seismic moment and rupture area of the earthquake as well as the Rrup distance of the station. Earthquake and station parameters defined in this study are utilized in the predictions. In addition, for the earthquakes whose rupture areas are unknown, Wells and Coppersmith (1994) is utilized as recommended by Kamai et al. (2014). This recommendation is also inspected by rupture area-seismic moment approach of Satoh (2020) in Chapter 6.3.

For the evaluation of this model, it is considered that the displacement amplitudes smaller than 10 cm might be more affected by uncertainty in the estimation process. Therefore, the stations of the strike slip earthquakes in Türkiye whose RotD100 direction contains higher than 10 cm permanent displacements in absolute are considered for the aim of this evaluation. As aforementioned in the Chapter 2, the Kamai et al. (2014) was an update study of the fling step model of Abrahamson (2002) and the main aim of that study was recreating synthetic fling-containing ground motion by adding the fling step onto any processed time history. They presented a fling step prediction model and tailored it for the records of the horizontal components of strike-slip earthquakes and both horizontal and vertical components of reverse earthquakes. The presented models are based on the finite-fault simulations, which had been performed on SCEC broadband platform by combining the deterministic approach at low frequencies ($f < 1$ Hz) with stochastic approach at high frequencies ($f > 1$ Hz) according to the hybrid broadband methodology of Graves and Pitarka (2010). In the simulations, they represented the fault rupture kinematically which includes spatial heterogeneity, rupture speed and rise time. Simulations did not contain normal faulting earthquakes and the magnitudes were ranging between Mw 6 and Mw 8.2. Moreover, the dip angles of the simulated events also span from 30° to 90°. Another limitation in the presented models is that they were created only for the surface ruptures as Kamai et al. (2014) found very little fling effect in the buried fault ruptures. At the end, around 25 thousand simulation records were utilized for each of the strike slip and reverse type fling predictive models. In addition, the simulation results were validated by comparing the fling of 84 records of seven earthquakes. Kamai et al. (2014) ground motion records used in validation were processed by Pacific Engineering and Analysis (PE&A)

specifically to maintain the effects of fling in the records. As aforementioned, Kamai et al. (2014) presented one fling step prediction model and tailored it firstly for the sites located in the fault planes of the earthquakes, whether hanging wall (HW) or foot wall (FW), the presented general forms are:

For FW:

$$log(\frac{D_{site}}{D_{fault}}) = log(a_0) + a_2 log(\frac{R_{rup} + a_3}{a_3}) \quad (6.4a)$$

For HW:

$$log(\frac{D_{site}}{D_{fault}}) = log(a_0) + a_2 log(\frac{R_{rup} + a_3}{a_3}) \quad (6.4b)$$

where a_0 defines the displacements on the FW at a distance of $R_{rup} = 0$, a_4 stands for the difference between the HW and the FW displacement at a distance of $R_{rup} = 0$, a_3 allows for the curvature in attenuation, and a_2 stands for the slope of the line or the rate of the attenuation. In the equation, D_{site} is the fling step amplitude, permanent displacement, D_{fault} is the mean slip over the rupture plane derived from the definition of seismic moment (Aki (1966)) as:

$$D_{fault} = \frac{M_0}{\mu LW} \quad (6.5)$$

in which μ is the rigidity of the fault surface, M_0 is the seismic moment of the earthquake, and L and W are the rupture length and width, respectively. D_{fault}, L and W are in cm, M_0 is in dyn.cm and μ is in dyn/cm^2. Kamai et al. (2014) stated that if rupture area of the earthquake is not known, Wells and Coppersmith (1994) can be utilized as an approximation:

$$log(LW) = M_W - 4 \quad (6.6)$$

where LW is in km^2. Moreover, it was also stated that if the seismic moment of the event is unknown, it can be calculated by using Hanks and Kanamori (1979). For these cases the D_{fault} can be calculated as:

$$ln(D_{fault}) = 1.15M - 3.28 \quad (6.7)$$

Input parameters of the earthquakes utilized in the evaluation of Kamai et al. (2014), their references and the calculated D_{fault} values are presented in Table 6.1. As stated previously that rupture areas of some of the earthquakes are calculated by using Wells and Coppersmith (1994) in this study.

Table 6.1. The seismic moments, rupture areas and calculated mean slip values over the rupture planes of the earthquakes utilized in the evaluation of Kamai et al. (2014) predictive model: Mw, moment magnitude; M_0, seismic moment.

Event Name	Mw	Dip (°)	M_0 (N.m)	Reference	Rupture area (LW) (km^2)	Reference	D_{fault} (cm)
2022 Düzce (Gölyaka)	6	83	$1.61x10^{18}$	AUST	100	This study	53.67
1983 Horasan-Narman	6,6	80	$1.37x10^{19}$	Pınar (1995)	13x15	Shortt (1985)	234.19
1992 Doğanbey-Izmir	6	83	$1.61x10^{18}$	ISC-GCMT	100	This study	53.67
1998 Adana-Ceyhan	6,2	81	$2.3x10^{18}$	ISC-CSEM	158.49	This study	48.37
1999 Izmit (Kocaeli)	7,6	87	$2.88x10^{20}$	GCMT	120x15	Erdik (1999)	533.33
1999 Düzce	7,1	65	$1.3x10^{19}$	Birgören et al. (2004)	40.95x 12.6	Birgören et al. (2004)	477.86
2014 Aegean Sea	6,9	85	$2.47x10^{19}$	GCMT	794.33	This study	103.65
2020 Elazığ-Sivrice	6,7	68	$1.47x10^{19}$	Taymaz et al. (2021)	75x20	Taymaz et al. (2021)	32.67

After defining the D_{fault} values, Kamai et al. (2014) defined the coefficients of the Equation 6.4 for horizontal components of strike slip earthquakes as:

$$a_0 = 0.005\delta + 0.05 \quad (6.8a)$$

$$a_2 = 25.29M - 1.577M^2 - 106.22 + 0.02\delta \quad (6.8b)$$

$$a_3 = 50 \quad (6.8c)$$

$$a_4 = 1.35\delta - 0.015\delta \quad (6.8d)$$

where the δ is the fault dip in degrees, and M is the moment magnitude, Mw. For the vertical components of the strike slip scenarios, Kamai et al. (2014) stated that the mean value is expected zero. Therefore, they did not adapt the model for vertical directions of the strike slip earthquakes.

On the other hand, flings in both the vertical and horizontal components of the reverse type earthquakes are parametrized by Kamai et al. (2014) with limitations. For instance, for the fling prediction of the horizontal direction of the reverse faulting earthquakes, only HW stations of the created scenarios are included in the regression. Moreover, for the vertical direction of this type of earthquakes, only FW stations having Rx, the horizontal strike-normal distance from the fault, greater than -10 km are included in the regression analysis. Unfortunately, due to the fact that there is only one station from the reverse type earthquake in this study and its permanent displacements in any direction found below than 10 cm, Kamai et al. (2014) predictive model for the reverse type earthquakes could not be evaluated in this study.

For the normal faulting earthquakes, Kamai et al. (2014) did not present a model. Consequently, Kamai et al. (2014) fling predictive model is evaluated with 23 stations from 5 strike slip earthquakes having permanent displacements higher than 10 cm in the RotD100 direction are used. The list of the stations is presented in Table 6.2.

Table 6.2. The list of the earthquake stations for the test of the performance of the Kamai et al. (2014) against Türkiye earthquakes with the estimated values: Mw, moment magnitude; HW, hanging-wall; FW, foot-wall; PD, permanent displacement. *(Cont.)*

Event Name	Mw/ Dip(°)	Station	Rrup (km)	HW /FW	Reference	$PD_{RotD100}$ (cm)	Rotation Degree	$PD_{Kamai\ et\ al.\ (2014)}$ (cm)
2022 Düzce (Gölyaka)	6/83	TK 8109	5,62	HW	This study	16,21	75	11,01
2022 Düzce (Gölyaka)	6/83	TK 8106	11,42	FW	This study	19,73	240	3,47
2022 Düzce (Gölyaka)	6/83	TK 8105	15,26	HW	This study	18,9	56	2,38
1983 Horasan-Narman	6,6/80	TK 2503	24,74	FW	This study	137,29	161	8,04
1992 Doğanbey-Izmir	6/83	TK 3501	39,94	FW	This study	36,22	36	0,32
1998 Adana-Ceyhan	6,2/81	TK 0105	58,52	HW	This study	32,91	71	0,2
1999 Izmit (Kocaeli)	7,6/87	TK 1404	36,54	HW	Akbas et al. (2023)	67,02	246	44,66
1999 Izmit (Kocaeli)	7,6/87	TK 1612	31,54	HW	Akbas et al. (2023)	165	32	54,56

1999 Izmit (Kocaeli)	7,6/87	ARC	11,52	FW	Akbas et al. (2023)	103,28	28	128,79
1999 Izmit (Kocaeli)	7,6/87	YPT	4,94	FW	Akbas et al. (2023)	187,43	4	188,41
1999 Izmit (Kocaeli)	7,6/87	Maslak-1169	51,19	FW	Akbas et al. (2023)	55,53	105	24,15
1999 Izmit (Kocaeli)	7,6/87	Mecidiye köy	48,76	FW	Akbas et al. (2023)	54,67	314	26,21
1999 Izmit (Kocaeli)	7,6/87	Zeytinburnu	47,84	FW	Akbas et al. (2023)	76,67	39	27,05
1999 Izmit (Kocaeli)	7,6/87	TK 8101	18,05	FW	Akbas et al. (2023)	76,5	108	91,73
1999 Düzce	7,1/87	TK 8101	7,43	HW	Akbas et al. (2023)	267,09	150	182,85
1999 Düzce	7,1/87	A496-8165	3,76	FW	Akbas et al. (2023)	72,48	125	126
1999 Düzce	7,1/87	C1058(Lamont)	1,21	FW	Akbas et al. (2023)	42,23	316	159,54
1999 Düzce	7,1/87	C0375(Lamont)	3,49	FW	Akbas et al. (2023)	197,54	222	129,12

1999 Düzce	7,1/87	D0531	8,02	FW	Akbas et al. (2023)	30,89	19	86,99
2014 Aegen Sea	6,9/87	TK 1701	43,13	FW	Akbas et al. (2023)	18,76	103	2,18
2014 Aegen Sea	6,9/87	TK 2201	26,66	FW	Akbas et al. (2023)	15,3	22	7,66
2020 Elazığ-Sivrice	6,7/87	TK 2308	7,56	FW	Akbas et al. (2023)	116,91	100	5,32
2020 Elazığ-Sivrice	6,7/87	TK 4404	10	FW	Akbas et al. (2023)	14,3	3	4,1

As seen in Table 6.2, the records of 1992 Izmir (Doğanbey) and 1998 Adana-Ceyhan earthquakes could not be estimated by Kamai et al. (2014). Hence, these records are not included in the residual analysis.

Relative locations of the most of the stations in Table 6.2 to the rupture plane, whether HW or FW, are taken from Akbas et al. (2023). The relative location of the other stations are decided based on the R_x distance, the horizontal strike-normal distance from the fault. They are defined based on the R_x distances so that if this distance is lower than 0, the station is assumed on the FW plane and otherwise it is vice versa. For this purpose, R_x distances of the earthquake stations whose fault plane information is not unknown are calculated by utilizing the Kaklamanos et al. (2011) as follows:

$0° \leq \alpha \leq 90°$:

$$R_x = R_{jb}|tan(\alpha)| \tag{6.9a}$$

$90° \leq \alpha \leq 180°$:

$$R_x = R_{jb} tan(\alpha) \left[\alpha - sin^{-1}\left(\frac{W cos(\delta) cos(\alpha)}{R_{jb}}\right) \right] \quad (6.9b)$$

$180° \leq \alpha \leq 360°$:

$$R_x = R_{jb} sin(\alpha) \quad (6.9c)$$

where α is the azimuth angles of the stations, which are calculated by Haversine formula in this study. To verify the calculation of the azimuth degrees, required for above equations, epicentral distances of the AFAD and those calculated by using the Haversine formula are compared. Another input of the above equation, which is down-dip rupture width of the earthquakes, W, is calculated by Wells and Coppersmith (1994). Information for R_x distances and the assigned parameters in their calculation are presented in Table 6.3.

Table 6.3. Calculated Rx distances of the stations whose locations relative to rupture plane are not found in Akbaş et al. (2023) for HW/FW decision. W: down-dip rupture width; Repi: epicentral distance; Rx: Horizontal strike-normal distance from the fault

Event Name	Station	Repi(AFAD)	Repi(Calculated) (km)	Azimuth (°)	W	Rx (km)
2022 Düzce (Gölyaka)	TK 8109	4,75	4.755	190,83	7,24	4,291
2022 Düzce (Gölyaka)	TK 8106	9,63	9,634	130,2	7,24	-10,91
2022 Düzce (Gölyaka)	TK 8105	13,88	13,882	50,24	7,24	0,44
1983 Horasan-Narman	TK 2503	34,55	34,55	180,9	10,52	-21,85
1992 Doğanbey-Izmir	TK 3501	38,74	38,74	135,55	7,24	-5,60
1998 Adana-Ceyhan	TK 0105	48,1	48,1	65,03	8,20	55,15

To see the general performance of the Kamai et al. (2014) models the residual analyses are done. Total residuals versus moment magnitudes of the events and those against Rrup distances are presented in Figure 6.6. In addition to the residual analyses, the predicted curves and the observed permanent displacements from the records of the 1999 Kocaeli and 1999 Düzce earthquakes are illustrated in Figure 6.7.

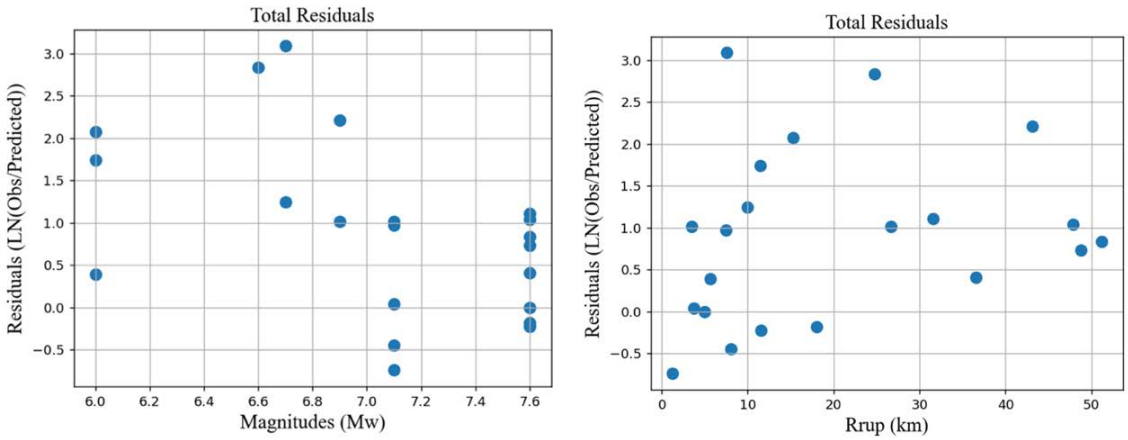

Figure 6.6. Total residuals of the observed and predicted permanent displacements by Kamai et al. (2014) against (left) magnitudes of the earthquakes and (right) Rrup distances

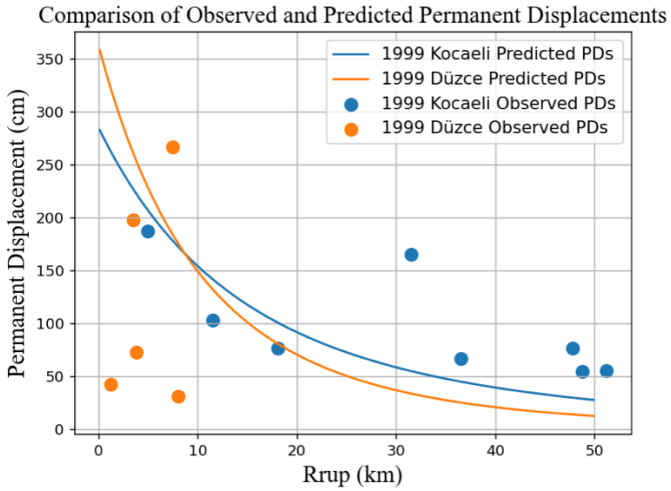

Figure 6.7. Comparison of the observed permanent displacements and the prediction curves of 1999 Kocaeli and 1999 Düzce earthquakes.

6.3. Interpretation of the Performance of Kamai et al (2014) Fling Predictive Model

As can be seen in Figure 6.6 that while Kamai et al. (2014) predictive model is found good for the large magnitude earthquakes in near locations. For the further evaluation of the large earthquakes, 1999 Kocaeli and 1999 Düzce earthquakes are compared with the prediction curve in Figure 6.7, which implied that the estimated values via the model are comparable with the observed permanent displacements from 1999 Kocaeli earthquake.

In addition, capability of using Hanks and Kanomori (1979) for seismic moment approximation is inspected together with the rupture area calculated with Wells and Coppersmith (1994). It is found that this approximation result in low mean slip over the rupture plane, D_{fault}, and thus underestimates the permanent displacements. For instance, the approximation presented in Equation 6.7 results in 235.1 cm mean slip for 1999 Kocaeli earthquake whereas it is calculated as 533.33 cm by using the Equation 6.5, which is the preferred calculation of Kamai et al. (2014). In the approximation case the low D_{fault} paves the way 83.05 cm permanent displacement estimation for YPT stations whereas by using the Equation 5.7 it is found as 188.41 cm. Therefore, the approximation approach for the earthquakes is found ineffective in this study. Moreover, the efficiency of the approximation of fault rupture area by Wells and Coppersmith (1994) is inspected. Utilizing this approximation also gives rise to underestimation of the permanent displacements. To exemplify, D_{fault} is found as 241.14 cm for the 1999 Kocaeli earthquake and permanent displacement is estimated as 85.19 cm for the YPT station. Similarly, Satoh (2020) also inspected the approximations of Kamai et al. (2014) for 6 Japan earthquakes (2000 Tottori-ken Seibu (Mw 6.8), 2004 Niigata-ken Chuetsu (Mw 6.6), 2008 Iwate-Miyagi Nairiku (Mw 6.9), 2011 Fukushima-ken Hamadori (Mw 6.6), 2014 Nagano-ken Hokubu (Mw 6.2), and 2016 Kumamoto (Mw 7.1)). He found that the approximation in Equation 6.7 results in higher rupture areas than the actual ones, which causes conservative estimates of permanent displacements. Instead of using Wells and Coppersmith (1994), Satoh (2020) presented a new seismic moment-rupture area relation using the homogeneous-slip models from geodetic data to be substituted in Kamai et al. (2014) predictive model as:

$$log_{10}S = -10.34 + (2/3)log_{10}M_0 \quad (6.10)$$

where S is the rupture area as km^2, M_0 is the seismic moment as N.m. Even though Satoh (2020) derived this rupture area-seismic relation from some of Japan earthquakes, the proposed rupture area relation for Kamai et al. (2014) fling predictive model is applied in Türkiye earthquakes. It is found that introducing the Equation 6.10 results in lower rupture areas and thus higher predictions than Wells and Coppersmith (1994). Since 78% of the data used in comparison of Kamai et al. (2014) are predicted lower than the observed ones, Satoh (2020)'s approach may be appropriate for some of Türkiye earthquakes. However, it is not always the case. For instance, 1999 Kocaeli earthquake D_{fault} is estimated as 338.34 cm and permanent displacement of YPT station is estimated as 119.53 cm. In other words, rupture area approximation of Satoh (2020) needs a further evaluation for the accuracy.

6.4. Türkiye Adjusted Version of Burks and Baker (2016)

As aforementioned in Chapter 6.1, performance of the fling step predictive model of Burks and Baker is found relatively good for the slip direction components of the Türkiye earthquakes. Nevertheless, it needed to be improved to use in the earthquake engineering perspective. In this study, for the purpose of adjustment of the equation to the Türkiye earthquakes, random-effects regression is executed and plots of the residuals are utilized to evaluate the differences in the magnitudes and distances. Firstly, data which has 3 cm and above permanent displacement in absolute value in the slip direction of the earthquake are inspected. Moreover, since the equation takes into account Rrup distances, the station distances are also re-evaluated before the adjustment. The 1998 Adana-Ceyhan (Mw6.2) earthquake TK 105 station (Rrup = 58.52 km) is not included in the adjustment procedures. The modifications are done with the FN components of the stations recorded normal faulting earthquakes and FP components of those recorded strike slip earthquakes. The records utilized in the modification process are marked with " * " in Table A.3. in Appendix A.

The adjustment is done as followings:

1-Firstly the linear trend found in the distribution of the inter event residuals of the earthquakes is removed. Figure 6.8 (above) illustrates the observed trendline with its equation and the coefficient of determination (R-squared), which demonstrates how well the data fit the line. This trend is removed from by incorporating it in the prediction equation.

2- After the inter event trend is removed, the intra event residuals are inspected. For the intra event residuals, it is found that in the first 10 km, in terms of Rrup distances, the scatter of the data is quite different. Therefore, the intra event residuals are evaluated by separating before and after 10 km, which are demonstrated in Figure 6.8 (left- and right-below, respectively). By removing these trends, the first cycle of the modification is completed.

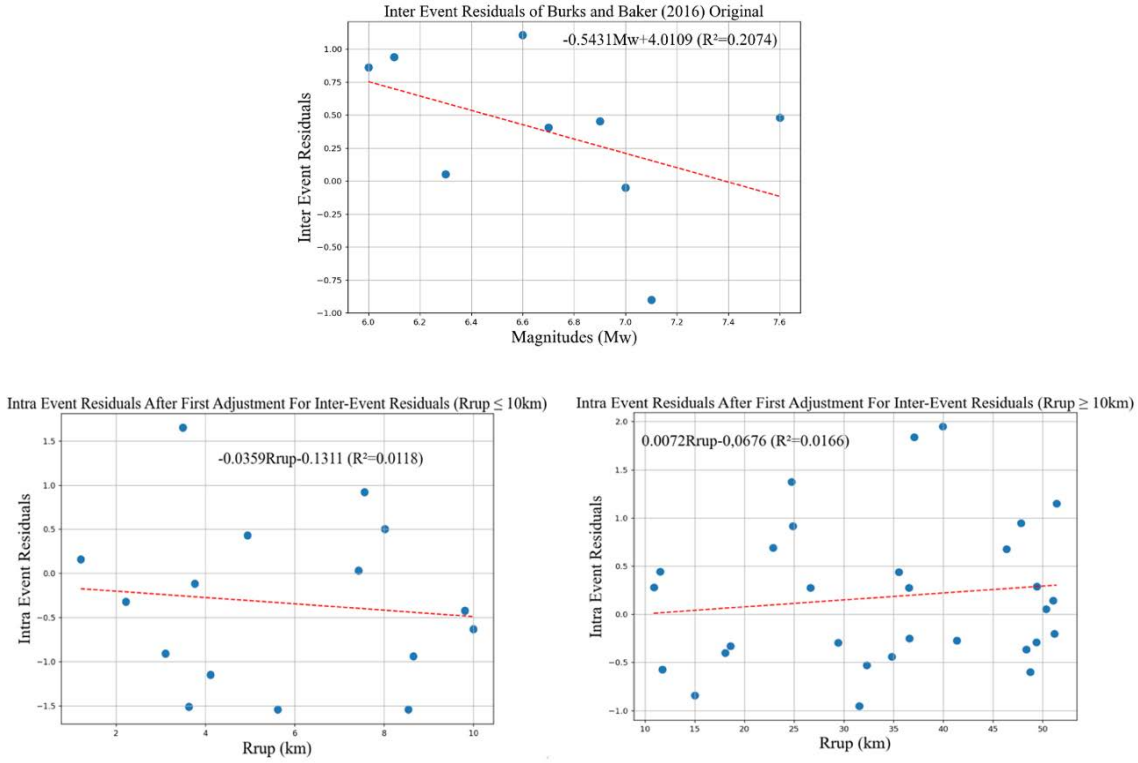

Figure 6.8. Distribution of the inter-event (above) residuals of the Burks and Baker (2016) and intra-event residuals after incorporating it to the equation with observed trendlines, equations and the coefficient of determination (R-squared).

3- As aforementioned, these modifications are done recursively until the best fitted equation is obtained. First two steps are applied again as the second cycle of modification by inspecting inter- and intra-event residuals obtained by the partly adjusted equation which is obtained until this step. Figure 6.9 (left) illustrates the executed second cycle, by inter- and intra-event residuals with the observed trendlines.

4- After the second cycle of the modification is completed, the slope of trendlines are not found as sharp as the previous ones. Nevertheless, the trends are undoubtedly visible. Therefore, the third pair of modifications are done in the same way as the previous cycles. The plots of inter- and intra- event residuals, used in this cycle are shown in Figure 6.9 (right).

5- After the third cycle of the modification is completed, it is decided that that the previous modifications works but additional adjustment cycle will be more reliable. For instance, the intra-event residual within the first 10 km Rrup distance are closer to the zero line, which is an implication of the improvement in the equation, whereas there is still an observable trend line. Thus the fourth pair of modifications are done. The plots of inter- and intra- event residuals, used in this cycle are shown in Figure 6.10 (left).

6- Lastly, the fourth pair of modifications are applied and the adjustment of the Burks and Baker (2016) to Türkiye earthquakes is completed. It resulted in no distinct trend in the inter-event residuals. Moreover, similar result is obtained in intra-event residuals, as seen in Figure 6.10 (right).

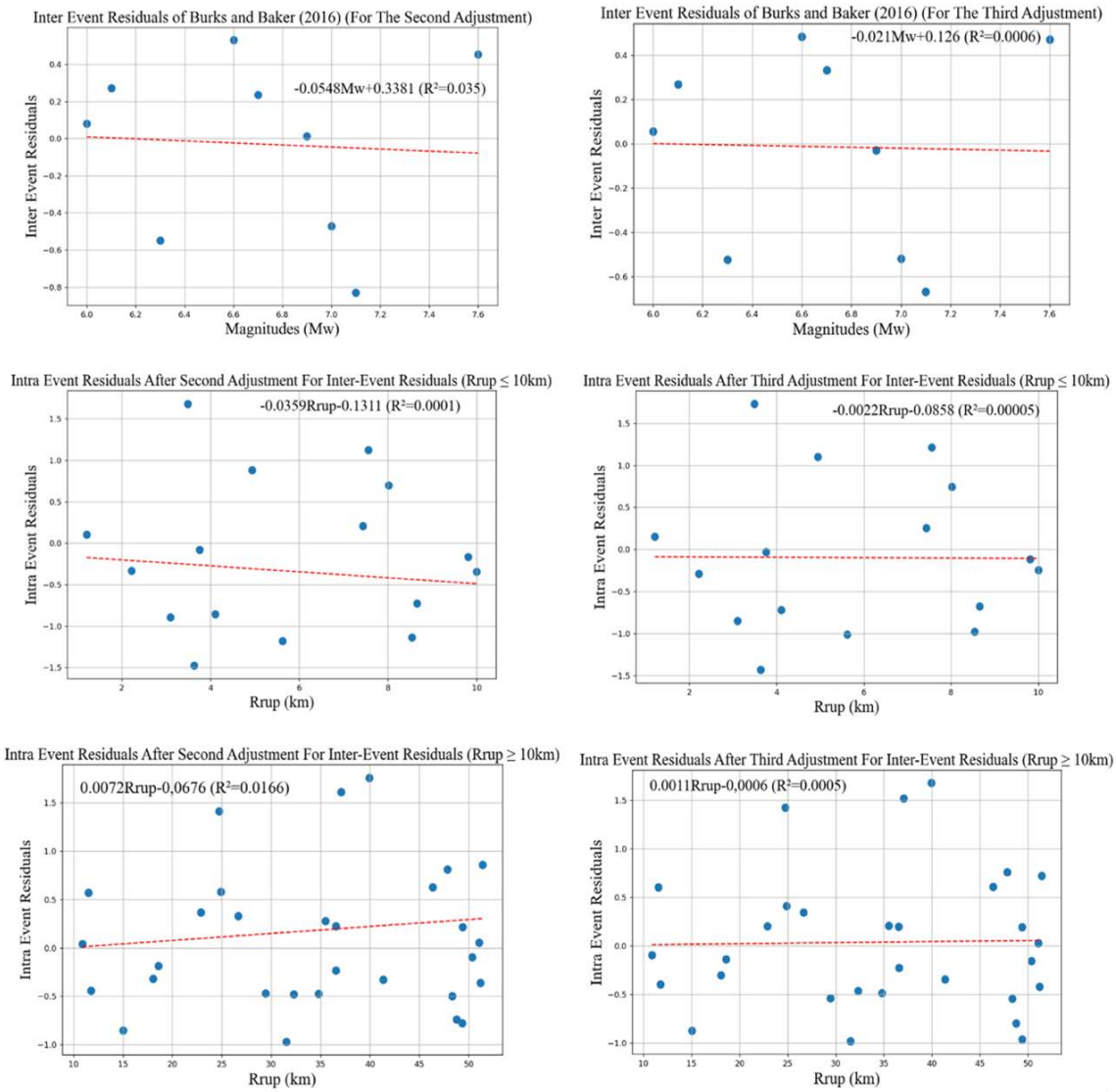

Figure 6.9. Distribution of the inter- and intra-event residuals obtained during the second cycle (left) and the third cycle (right) of the adjustment procedure.

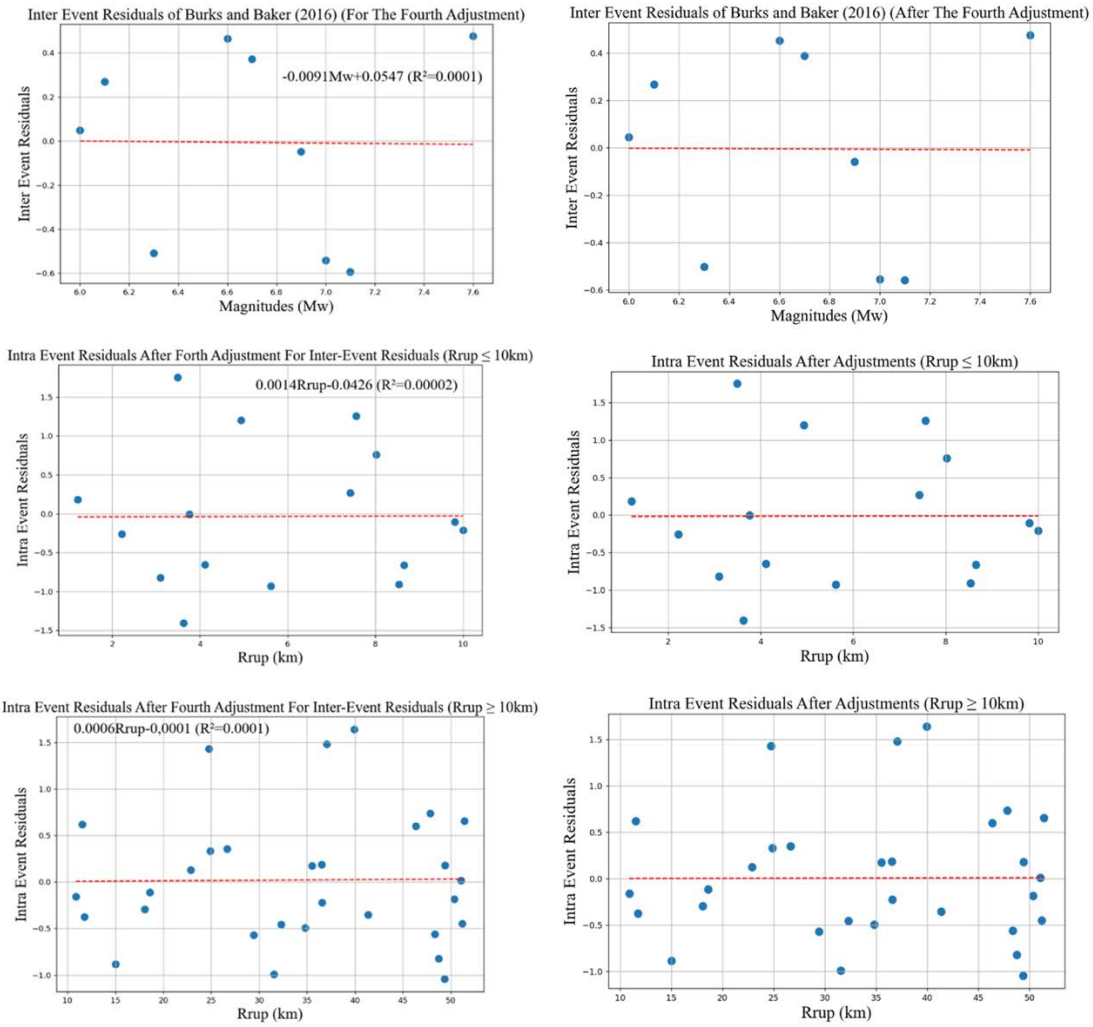

Figure 6.10. Distribution of the inter- and intra-event residuals obtained during the fourth cycle (left) and resulting plots after the adjustment procedure (right).

After the modifications are completed, the adjusted version of Burks and Baker (2016) predictive model is obtained as:

Rrup > 10km:

$$ln(D_p) = Ln(cot^{-1}(0.3Rrup)) + 0.672Mw + 0.0113Rrup - 0.63994 \quad (6.11a)$$

Rrup ≤ 10 km:

$$ln(D_p) = Ln(ot^{-1}(0.3Rrup)) + 0.672Mw + 0.0327Rrup - 0.9847 \quad (6.11b)$$

Comparisons of the inter- and intra-event residuals of Burks and Baker (2016) and its Türkiye adjusted version are presented in Figure 6.11.

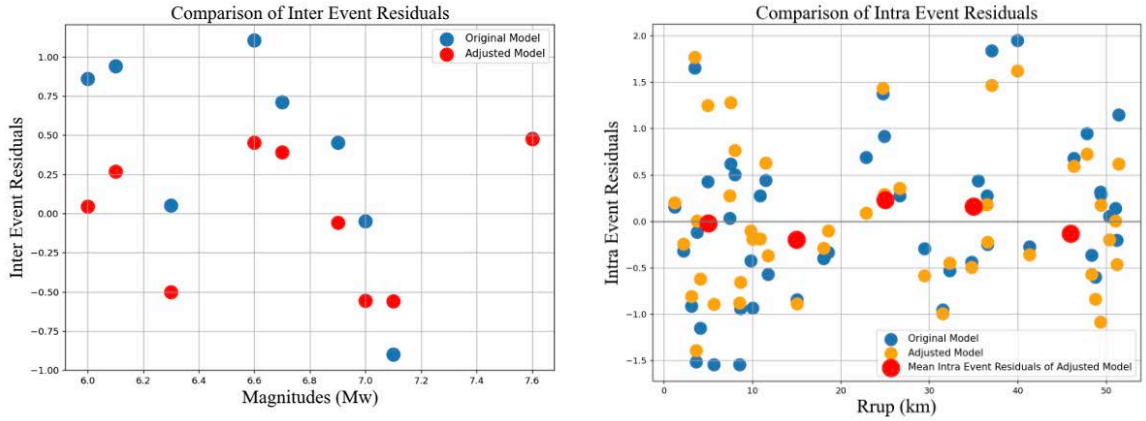

Figure 6.11. The comparison of the inter-event (left) and intra-event (right) residuals of Burks and Baker (2016) and its Türkiye adjusted version

By inspection of Figure 6.11, the conformity of the adjusted equation is found well. Furthermore, the total residuals of the Burks and Baker (2016) and its Türkiye adjusted version are also compared. Figure 6.12 illustrates the total residuals of the both of the equations with Rrup and Mw.

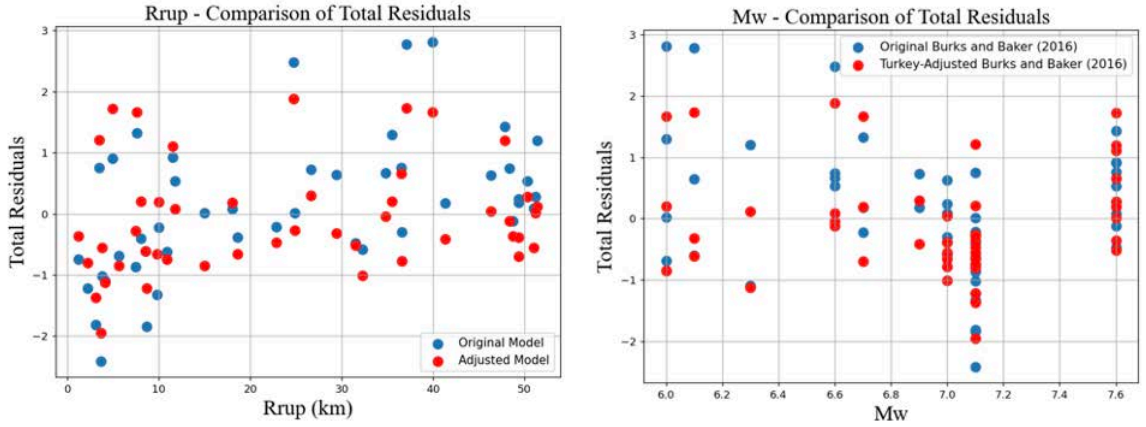

Figure 6.12. Comparison of the total residuals of Burks and Baker (2016) and its Türkiye-adjusted version against (left) Rrup and (right) Mw.

In addition to the comparison of the residual values, the permanent displacements obtained from the records of 1999 Kocaeli and Düzce earthquakes are compared with the predicted ones by Burks and Baker (2016) and its Türkiye adjusted version in Figure 6.13. The adjusted version is found more effective to capture permanent displacements of 1999 Düzce earthquake in the first 10 km. Furthermore, it is also found more useful to predict permanent displacements at sites far than 10 km. To demonstrate the conformity of the adjusted model with the dataset in a broader range, permanent displacements and the estimation curves of the adjusted model for 2020 Elazığ-Sivrice, 2020 Izmir(Samos), and 2022 Düzce-Gölyaka earthquakes are also compared together with 1999 Kocaeli and 1999 Düzce earthquakes in Figure 6.14. Taking into account the utilized data in the adjustment of the equation, in which the only 3 cm and above data are considered, the conformity of the data is found well. Consequently, the adjusted model is found successful to estimate the fling of Türkiye earthquakes.

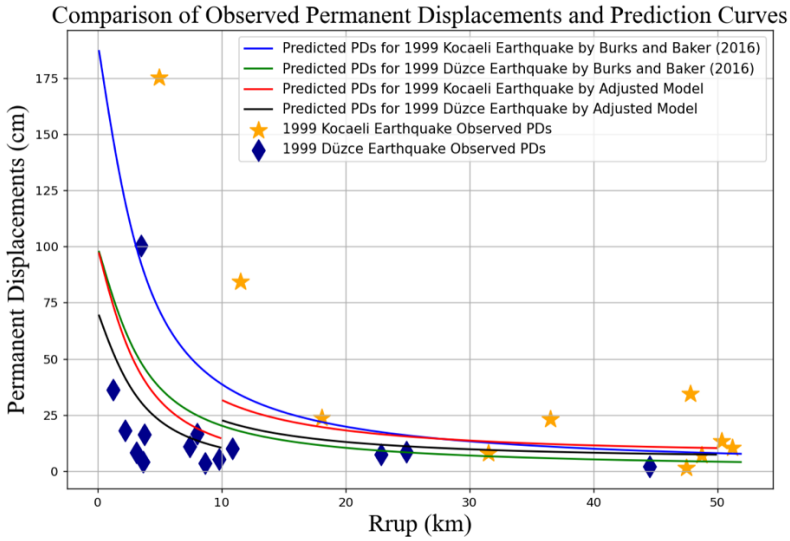

Figure 6.13. The comparison of permanent displacements of 1999 Kocaeli and 1999 Düzce earthquakes with the those predicted by Burks and Baker (2016) and its Türkiye adjusted version (PDs are permanent displacements)

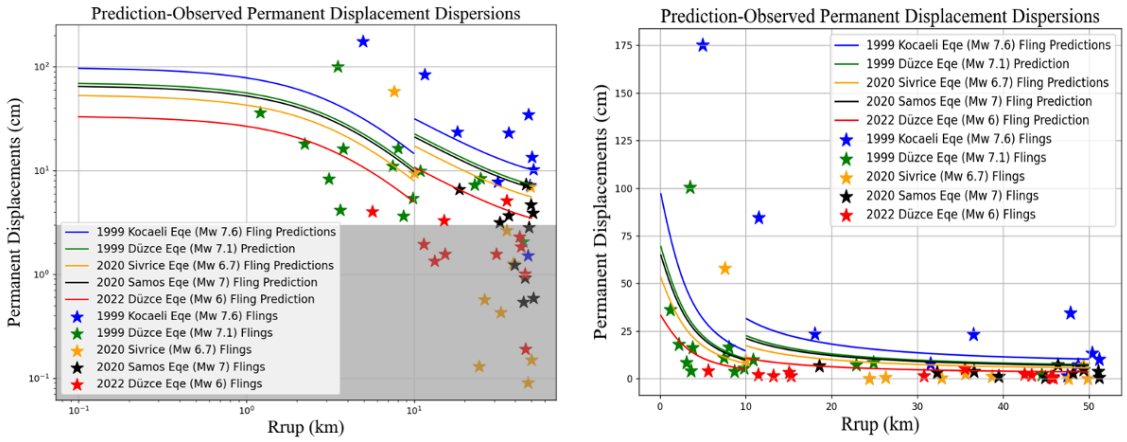

Figure 6.14. General prediction curves of Türkiye-adjusted Burks and Baker (2016) for the 1999 Kocaeli, 1999 Düzce, 2020 Elazığ-Sivrice, 2020 Izmir(Samos), and 2022 Düzce-Gölyaka earthquakes in a (left) logarithmic (gray area covers the permanent displacements that are not included in regression) and (right) linear scales.

6.5. Performance of Türkiye Adjusted Burks and Baker (2016) for February 6, 2023 Kahramanmaraş (Mw 7.7) Earthquake

During the thesis-writing period, the 6 February 2023 Kahramanmaraş (Mw 7.7) earthquake took place. Recordings of this earthquake are utilized for a further evaluation of the Türkiye-adjusted Burks and Baker (2016) fling predictive model. For this purpose, 65 strong motion recordings are detected within 50 km from the fault rupture projection (Rjb≤50km) in ESM and AFAD that used in this study. Among them 29 recordings contain bad quality data. Therefore, 36 earthquake stations are utilized to evaluate the performance of the model. Due to the fact the faulting mechanism of the earthquake is strike slip, FP components of the stations are calculated by following the same scheme as described in Chapter 6.1, in accordance with requirements of the model. In addition, the earthquake parameters are taken from GCMT as: strike angle: 320°; dip angle: 80°; slip angle: 160°. Firstly, the obtained permanent displacements are compared with those derived from satellite images by Geospatial Information Authority of Japan in Figure 6.15. It is found that the displacement traces are similar so that permanent displacements are higher in the south-eastern side of the fault than the north-western side. Moreover, some of the permanent displacements derived from GPS data (Prof. Dr. Semih

Ergintav, personal communication) are also demonstrated on the map. Although there is not a direct co-located GPS station with earthquake recordings, the general displacement distributions are the same as those of obtained from recordings. Then, to evaluate the performance of the model for Kahramanmaraş (Mw 7.7) earthquake, residual analyses are conducted based on the same process as presented in Chapter 6.1. Resulting residual graphic is demonstrated in Figure 6.16. In addition, the distributions of the observed permanent displacements with the estimation curve are illustrated in Figure 6.17. Based on the comparison graphics, Türkiye-adjusted Burks and Baker (2016) prediction model is found successful to capture the observed permanent displacements.

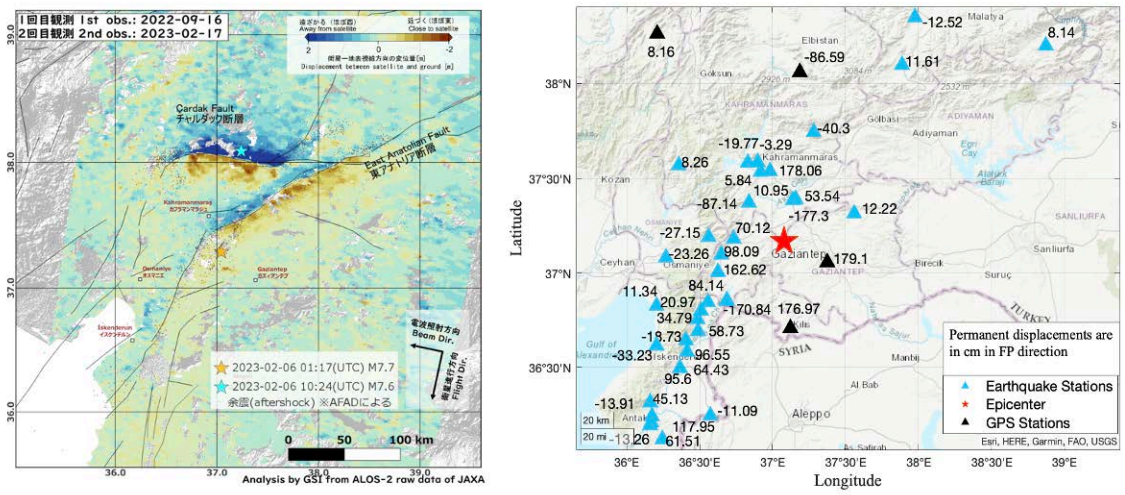

Figure 6.15. Comparison of (left) permanent displacements delineated by pixel offset technique using ALOS-2 (Advanced Land Observing Satellite 2, Japan Aerospace Exploration Agency) imagery and (right) permanent displacements in FP direction of strong motion recordings (blue triangles) and GPS data (black triangles) (Ergintav S., personal communication)

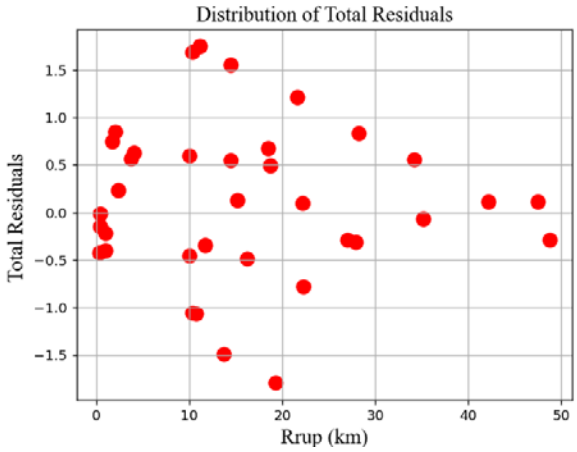

Figure 6.16. Total residuals of Türkiye Adjusted Burks and Baker (2016) and observed permanent displacements of 2023 Kahramanmaraş (Mw 7.7) earthquake with Rrup distances.

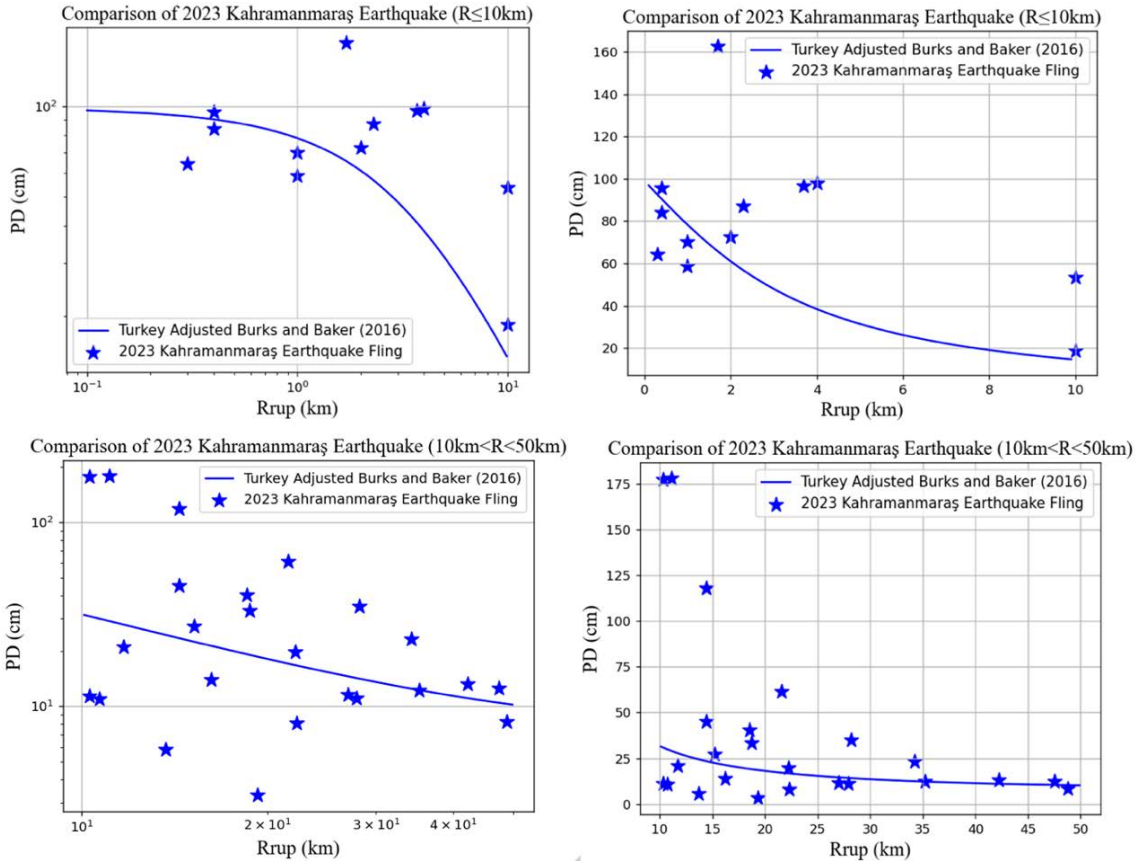

Figure 6.17. Distribution of the observed permanent displacements of 2023 Kahramanmaraş (Mw 7.7) earthquake and prediction curves with Rrup distances.

7. GLOBAL FLING STEP PREDICTION MODEL FOR VERTICAL COMPONENTS

Although early studies defined the fling step in the slip direction of the fault rupture such as Abrahamson (2002) and Hisada and Bielak (2003), findings of this study and previous ones demonstrated that fling step cannot be confined only to slip direction. In other words, permanent displacements are observed in any direction including vertical direction in the sites near to the fault rupture. In terms of vertical direction, a wide range of permanent displacements are observed on processed near fault records in this study. For instance, the obtained permanent displacements in this direction span from 0.003 cm to 68.9 cm. Likewise, NESS 2.0 database also contains permanent displacements between 0.004 cm to 403.48 cm in up-down components of the near fault stations. Nevertheless, only Kamai et al. (2014) presented a fling step predictive model for vertical components. In this chapter, firstly, the effectiveness of Kamai et al. (2014) is evaluated with permanent displacement datasets. Then, a new fling step predictive model for the vertical direction records of global earthquakes is presented.

7.1. Evaluation of Kamai et al. (2014) Permanent Displacement Prediction Model

Kamai et al. (2014) utilized the simulations of strike slip and reverse faulting scenario earthquakes. For the strike slip earthquake simulations, they stated that mean permanent displacements for the vertical direction are found zero and therefore a predictive model for these kinds of earthquakes is not constructed. On the other hand, for reverse faulting earthquakes, they conducted a regression analysis with the simulation results of HW stations and FW ones which have a Rx distance greater than -10 km. They stated that since the mean value of the permanent displacements at farther distances resulted in zero, FW stations having Rx smaller than -10 km are not included in the regression analysis. Based on the results, Kamai et al. (2014) redefined the coefficients of the Equation 6.4 for vertical components of reverse faulting earthquakes as:

$$a_0 = 0.0063\delta - 0.17 \tag{7.1a}$$

$$a_2 = -11.312M^2 + (176.7 - 0.158\delta)M + 1.218\delta - 700 \tag{7.1b}$$

$$a_3 = 100 \tag{7.1c}$$

$$a_4 = -0.003\delta + 1.555 - 0.11M \tag{7.1d}$$

For the sake of increasing the evaluated data, firstly, compatibility of the permanent displacements on the same vertical records that are contained both in NESS 2.0 and database of this study are compared. Even though updated version of eBASCO which is used in NESS 2.0 and proposed processing scheme in this study are different, the obtained permanent displacements in vertical direction are found quite similar. Therefore, NESS 2.0 and the output database of this study are combined to increase the data. Comparison of the permanent displacements on some of the common records are shown in Table 7.1.

Table 7.1. Comparison of permanent displacements obtained on the same vertical records: Mw, moment magnitude; PD, permanent displacement.

Date	Location	Mw	Station	$PD_{NESS\ 2.0}$ (cm)	$PD_{This\ Study}$ (cm)
17.Aug.99	Izmit (Kocaeli)	7,60	ARC	2,79	3,44
17.Aug.99	Izmit (Kocaeli)	7,60	YPT	11,11	12,52
12.Nov.99	Düzce	7,10	TK 1401	20,61	21,92
12.Nov.99	Düzce	7,10	C 1061	-6,84	-4,81

After combining the datasets, permanent displacements are eliminated by the limitations of the predictive model. At last, permanent displacements of 90 records from Türkiye and 449 records from worldwide earthquakes are compared together with predicted ones. Residual analyses are done by considering the style of faulting and without considering it. While Figure 7.1 demonstrates the residuals for all the data in limits of the model for all styles of faulting earthquakes, Figure 7.2 illustrates the residuals for reverse faulting earthquakes.

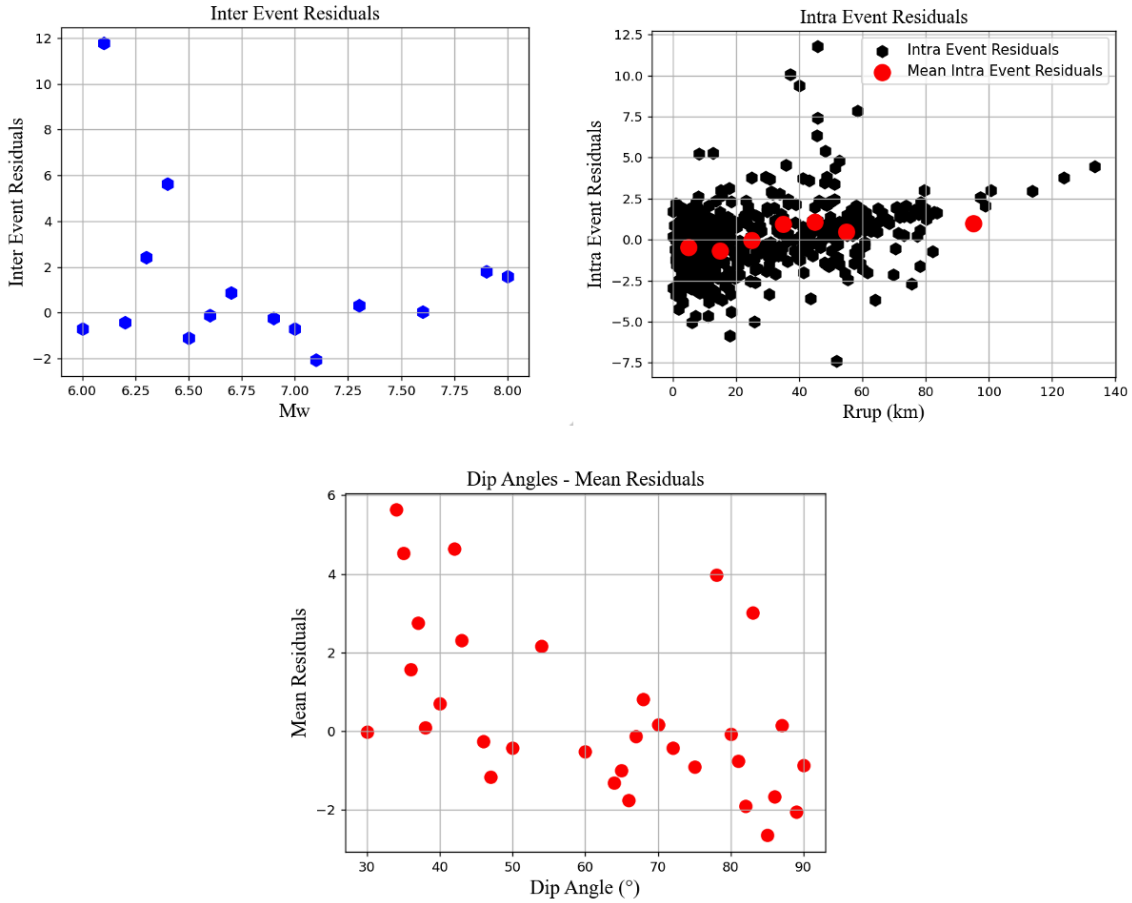

Figure 7.1. Distribution of inter event (above-left), intra event (above-right) and mean residual (below) analyses of the vertical permanent displacements for all styles of faulting earthquakes

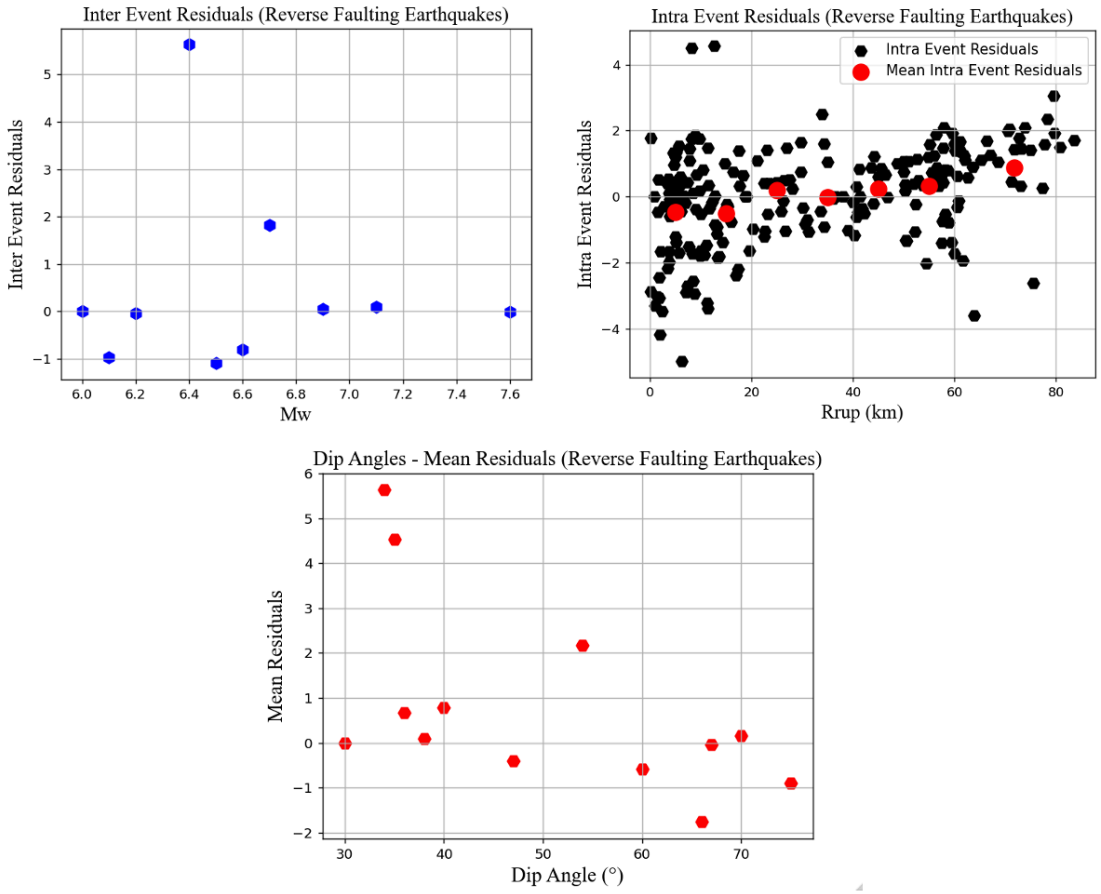

Figure 7.2. Distribution of (above-left) inter event, (above-right) intra event and (below) mean residual analyses of the vertical permanent displacements for reverse faulting earthquakes

As can be seen in Figure 7.1 and Figure 7.2, although Kamai et al. (2014) presented this model for reverse faulting earthquakes, it causes similar results for all styles of faulting earthquakes. Nevertheless, it can be seen that generally the model overestimates the permanent displacements at close distances whereas it underestimates them at farther distances. Moreover, for the earthquakes having Mw smaller than 7, predictive model demonstrates higher discrepancies than others. Another point is that, Kamai et al. (2014) relatively well estimates the vertical permanent displacements from the earthquakes having dip angles of 45° to 60°.

7.2. Proposed Global Fling Step Predictive Model for Vertical Components

Due to the fact that Kamai et al. (2014) predictive model for vertical components shows high discrepancies with the empirical data, a new predictive model based on empirical dataset is proposed in this study. Since the NESS 2.0 contains highly similar permanent displacements to those found in this study for the same records, outputs of this study and NESS 2.0 are combined with the aim of increasing the dataset. Before constructing the new model, the dataset that is combination of NESS 2.0 and outputs of this study is re-evaluated as follows:

- To avoid complexity that is encountered in Kamai et al. (2014), the dataset is evaluated based on absolute permanent displacement values.
- The dataset limited with the records having permanent displacements higher than 3 cm and smaller than 75 cm. Lower limit is set with the same approach that mentioned in Chapter 6.1. Upper limit, on the other hand, is set due to the fact that the fling above this limit did not obey to general trend of the dataset. The reason behind this fact is considered as that the permanent displacements higher than this limit may be caused by uncommon site effects such as liquefaction or settlement.

By considering the above criteria, the dataset that contains 296 records, which can be found in Table A.4. in Appendix A, is acquired. However, due to the fact that only 40 normal faulting earthquake records are found in the combined dataset, which is not considered enough to reflect the general attenuation, this style of faulting earthquakes are eliminated. Moreover, strike slip earthquakes demonstrated very high dispersion. For instance, among the 1999 Kocaeli earthquake records, permanent displacement is found as 12.52 cm in YPT station which is 4.94 km away from the fault rupture trace whereas it is found as 24.73 cm in ZYT station whose Rrup distance is 47.84 km. Therefore, strike slip earthquakes are also not included in the regression analysis. As a result, the prediction equation is obtained by exposing 151 reverse faulting earthquake records to least squares regression analysis. For this purpose, dip angles and Mw of the earthquakes and Rrup of the stations are defined as inputs. As the earthquake parameters attenuate logarithmically, in general, the natural logarithm of the input values are introduced in the regression. Resulting predictive model is found as:

$$PD_{Vertical} = 16.0186ln(M) - 1{,}1497ln(R) + 9{,}1237ln(\delta) - 50{,}696 \qquad (7.2)$$

where M, R and δ are Mw, Rrup and dip angle, respectively. Magnitudes of the events in the utilized dataset are ranging between Mw 5.5 and 7.6. On the other hand, the dip angles of the events are from 30° to 75°. In this study, different from Kamai et al. (2014), it is assumed that the effect of the seismic moment on permanent displacements is compensated with Mw and thus it not included in the model. In addition, the Rrup distances of the involved stations are within 140 km as the it is the upper distance limit in Ness 2.0. After the model is obtained, the dataset is compared with the predicted values. For this purpose, residual analyses are conducted in the same way that defined in Chapter 6.1 and resulting plots are presented in Figure 7.3.

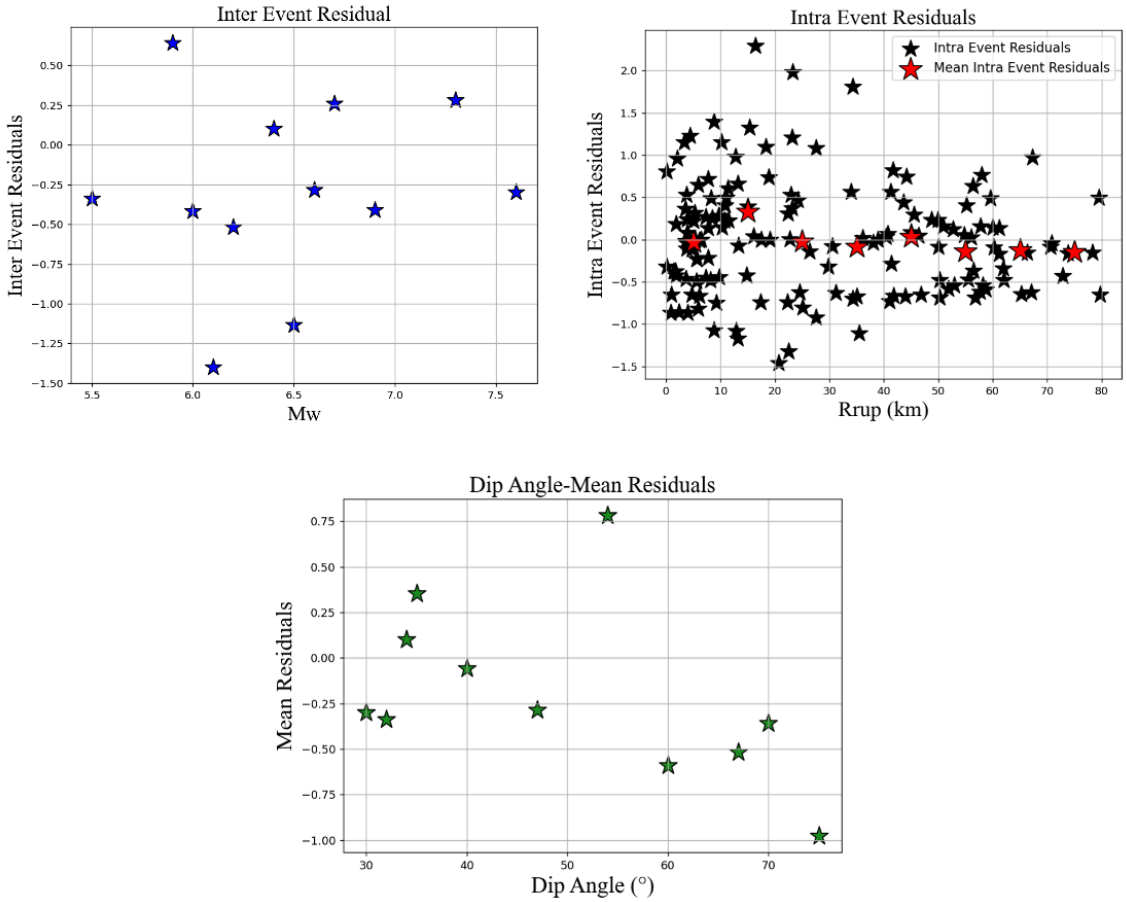

Figure 7.3. Inter event residuals (above-left), intra event residuals (above-right) and mean residuals with dip angles (below) of proposed model and empirical dataset.

As can be seen in Figure 7.3, the proposed model well estimates the permanent displacements in a general manner. Flings from some of the earthquakes with a magnitude of Mw 6 and Mw 6.6 are overestimated and those from the earthquakes with steeper dip angles are somewhat overestimated. Nonetheless, the discrepancies are not remarkably high. Therefore, the constructed model is found effective for estimating the permanent displacements in vertical directions. To demonstrate the effectiveness of the model in a broader sense, total residuals with the three inputs of the model are presented in Figure 7.4.

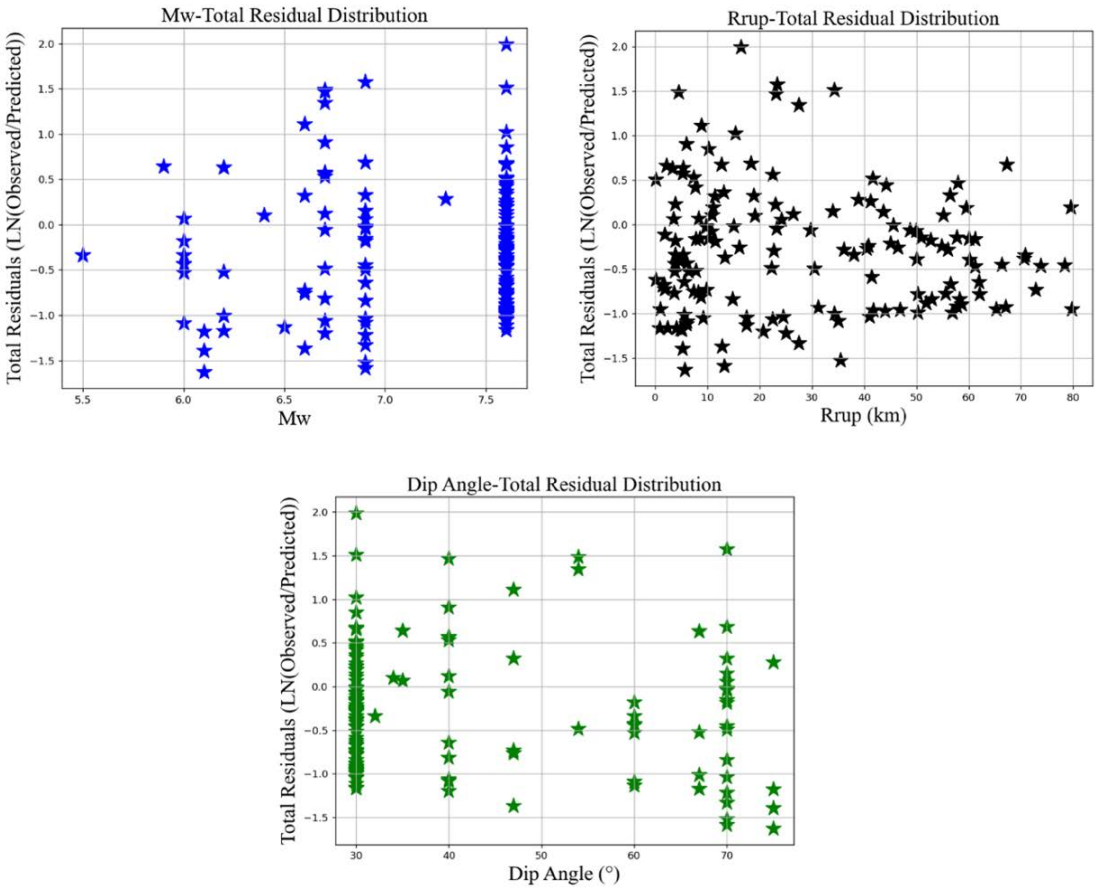

Figure 7.4. Distribution of total residuals of proposed model and empirical dataset with Mw (above-left), Rrup (above-right) and Dip angle (below)

8. CONCLUSION

This study investigated the fling steps in Türkiye earthquakes. The need for the identification of the fling-containing ground motion records to be used in the seismic design of the structures through selecting and scaling is met by the presented inventory.

Because the standard data processing algorithms are not capable of revealing the permanent displacements, special processing methods are inspected. Nevertheless, it is found that the existing procedures have some shortcomings. Thus, an improved data processing scheme is presented. Capability of the proposed scheme to capture the permanent displacements is verified through comparison of permanent displacements that obtained on the processed records and those derived from the co-located GPS data from both Türkiye and worldwide earthquakes. It is found that the proposed scheme is capable of capturing very small displacements to very large ones. In addition, the proposed scheme results in more accurate permanent displacements than the previous procedures, based on the comparison of the common records.

By processing the near fault records of Türkiye earthquakes, for the first time, fling inventory of Türkiye is presented. Totally 288 strong motion records are processed via proposed scheme and it is found that permanent displacements of Türkiye earthquakes are ranging between 0 cm to 264 cm. One of the new findings of this study is that 1999 Düzce earthquake produced the largest permanent displacements among Türkiye earthquakes. Another point of this study is that the permanent displacement dataset named NESS 2.0, which contains fling steps from worldwide earthquakes, can be increased by 22% and 33% in terms of normal faulting and strike slip earthquakes, respectively ignoring differences of the data processing schemes.

Apart from the three components (EW,NS,UD) of the stations, FN and FP components and RotD100 components are also presented to evaluate the performance of Burks and Baker (2016) and Kamai et al. (2014) prediction models for Türkiye, respectively. It is found that fling step can be observed in any direction as opposed to the common acceptance which states that it

is expected in fault parallel direction (Hisada and Bielak (2003), Abrahamson (2002)). Moreover, the observed permanent displacement in FN components can be larger than those in FP components and the maximum one can be in any direction. In terms of the performance of the Kamai et al. (2014) and Burks and Baker (2016) fling predictive models, findings indicate that both of these models are only somewhat successful. In addition, the effect of the input which defines moment magnitude-rupture area relation of Kamai et al. (2014) prediction model is inspected. It is found that this relation should be further investigated by worldwide earthquakes to improve the model. Then, based on the residual analyses, Burks and Baker (2016) prediction model is adjusted to permanent displacement dataset of Türkiye earthquakes. In addition, the effectiveness of the adjusted model is demonstrated by comparing the permanent displacement predictions obtained by the Türkiye-adjusted Burks and Baker (2016) prediction model and acquired permanent displacements on the recordings of 6 February 2023 Kahramanmaraş (Mw 7.7) earthquake.

At last, permanent displacements in vertical components are inspected by view of general trends. It is found that Kamai et al. (2014), which is the only model and valid for reverse faulting earthquakes, is not successful. Therefore, by utilizing the empirical dataset, a new prediction equation is presented. Due to the inconsistency in dispersion of the data from strike slip earthquakes as well the scarcity of data from normal faulting earthquakes, proposed equation is constructed only for reverse faulting earthquakes.

8.1. Future Works

The proposed scheme is going to converted to fully automatic scheme so that the processing of the earthquake records can be introducing in data providers such as AFAD-TADAS.

Created dataset is going to be enlarged by decreasing distance limitation for sake of the safety of long period structures of great importance. For instance, large earthquakes have potential to cause permanent displacements at very far distances, which might be cause high economic loss for some particular structures such as nuclear power plants.

Global fling step prediction models for vertical components of normal faulting and strike slip earthquakes will be presented after processing the up-down records from worldwide earthquakes.

REFERENCES

Abrahamson, N. A., 2002, "Velocity Pulses in Near-Fault Ground Motions", *Proceedings of the UC Berkeley—CUREE Symposium in Honor of Ray Clough and Joseph Penzien: Berkeley, California, UC Berkeley, Consortium of Universities for Research in Earthquake Engineering*, pp. 40–41.

Akbaş B., T. Tetik, F.M. Önder, E. Sopacı, G. Tanırcan, A.A. Ozacar, and Z. Gulerce, 2023, "The New Turkish Strong Motion Dataset (N-TSMD) for Earthquake Engineering Applications". Submitted to *Bulletin of Earthquake Engineering*

Aki. K., 1966, "Generation and Propagation of G-Waves from the Niigata Earthquake of June 16, 1964. Part 2. Estimation of Earthquake Moment, Released Energy, and Stress-Strain Drop from the G-Wave Spectrum", *Bulletin of earthquake Research Institute, Tokyo University*, Vol. 44, 1966, pp. 73-88.

Aktuğ, B., I. Tiryakioğlu, H. Sözbilir, H. Özener, Ç. Özkaymak, C.Ö. Yiğit, M. Softa, 2021, "GPS Derived Finite Source Mechanism of the 30 October 2020 Samos Earthquake, Mw = 6.9, in the Aegean Extensional Region", *Turkish Journal of Earth Sciences*, Vol. 30, pp. 718–737.

American Society of Civil Engineers, 2005, *ASCE-7 Minimum Design Loads for Buildings*, Reston, VA., 2005.

Beyer, K., and J.J. Bommer, 2006, "Relationships Between Median Values and Aleatory Variabilities for Different Definitions of the Horizontal Component of Motion", *Bulletin of Seismological Society of America*, Vol. 96, pp. 1512–1522

Birgören, G., H. Sekiguchi, K. Irikura, 2004, "Rupture model of the 1999 Duzce, Turkey, earthquake deduced from high and low frequency strong motion data", *Geophysical Research Letter*, pp. 31,

Boore D.M. and J.J. Bommer, 2005, "Processing of Strong-Motion Accelerograms: Needs, Options and Consequences", *Soil Dynamics and Earthquake Engineering*, Vol. 25, pp. 93–115.

Boore DM., 2001, "Effect of Baseline Corrections on Displacements and Response Spectra for Several Recordings of the 1999 Chi-Chi, Taiwan", *Earthquake, Bulletin of the Seismological Society of America*, Vol. 91, No. 5, pp. 1199–1211.

Boore, D. M., 1999, "Effect of Baseline Corrections on Response Spectra for Two Recordings of the 1999 Chi-Chi, Taiwan, Earthquake", *U.S. Geological Survey Open-File Report*, pp. 99–545.

Burks, L. S., and Jack W. Baker, 2014, "Fling in Near-Fault Ground Motions and Its Effect on Structural Collapse Capacity", *Proceedings of the 10th National Conference in Earthquake Engineering, Earthquake Engineering Research Institute*, Anchorage, AK.

Burks, L.S. and J.W. Baker, 2016, "A Predictive Model for Fling-Step in Near-fault Ground Motions Based on Recordings and Simulations", *Soil Dynamics and Earthquake Engineering*, Vol. 80, pp. 119–126.

Cauzzi C, E. Faccioli, M. Vanini, A. Bianchini, 2015, "Updated Predictive Equations for Broadband (0.01–10 s) Horizontal Response Spectra and Peak Ground Motions, Based on a Global Dataset of Digital Acceleration Records", *Bulletin of Earthquake Engineering*, Vol. 13, pp. 1587–612.

Cetin, K. O., G. Mylonakis, A. Sextos, J. P. Stewart, (report coordinators), 2020, *Seismological and engineering effects of the M 7.0 Samos Island (Aegean Sea) Earthquake, GEER Report 069, Hellenic Association of Earthquake Engineering, Earthquake Engineering Association of Turkey, Earthquake Foundation of Turkey, Earthquake Engineering Research Institute, Geotechnical Extreme Event Reconnaissance Association*, 2020.

Chao, W. A., Y. M. Wu, and L. Zhao, 2010, "An Automatic Scheme for Baseline Correction of Strong-Motion Records in Coseismic Deformation Determination", *Journal of Seismology*, Vol. 14, No. 3, pp. 495–504.

Chousianitis, K., A. O. Konca, G.A. Tselentis, G.A. Papadopoulos, and M. Gianniou, 2016, "Slip model of the 17 November 2015 Mw = 6.5 Lefkada Earthquake from the Joint Inversion of Geodetic and Seismic Data", *Geophysical Research Letter*, Vol. 43, pp. 7973–7981.

D'Amico, M., C. Felicetta, E. Schiappapietra, F. Pacor, F. Gallovic, R. Paolucci, R. Puglia, G. Lanzano, S. Sgobba, L. Luzi, 2018, "Fling Effects from Near-Source Strong-Motion Records: Insights from the 2016 Mw 6.5 Norcia, Central Italy, Earthquake", *Seismological Research Letters*, Vol. 90, pp. 659–671.

D'Amico, M.C., E. Schiappapietra, C. Felicetta, S. Sgobba, F. Pacor, G. Lanzano, E. Russo, L. Luzi, L, 2021, "NEar-Source Strong-Motion Flat-File from eBASCO (NESS-eBASCO); Version 2.0; Istituto Nazionale di Geofisica e Vulcanologia (INGV)", Milan, Italy.

Dhanya, J., S.T.G. Raghukanth, 2020, "Probabilistic Fling Hazard Map of India and Adjoined Regions", *Journal of Earthquake Engineering*, pp. 1–25.

Disaster And Emergency Management Authority, 1973, "Turkish National Strong Motion Network (Dataset)", Department of Earthquake, Disaster and Emergency Management Authority.

Doğan, B., T.S. Irmak, A. Karakaş, and D. Kalafat, 2016, "Seismo-Tectonic Content by the Source Parameters of the 10 June 2012 Ölüdeniz-Fethiye (Dodecanese Islands) Mw 6.1 Earthquake and Aftershocks (SW-Turkey)", *Acta Geodaetica et Geophysica*, Vol. 51, pp.15–41.

Dogru, A., F. Bulut, C. Yaltirak, B. Aktug, Slip 2021, "Distribution of the 2020 Elazığ Earthquake (Mw 6.75) and Its Influence on Earthquake hazard in the Eastern Anatolia", *Geophysical Journal International*, Vol. 224, No. 1, pp. 389–400.

Dziewonski, A. M., T.A. Chou and J. H. Woodhouse, 1981, "Determination of Earthquake Source Parameters from Waveform Data for Studies of Global and Regional Seismicity", *Journal of Geophysical Research*, Vol. 86, pp. 2825-2852.

Geospatial Information Authority of Japan (2023): "The 2023 Turkey Earthquake: Crustal deformation detected by ALOS-2 data", https://www.gsi.go.jp/cais/topic20230206-e_Turkey.html, Accessed on March 3, 2023.

Graves, R. W., and A. Pitarka, 2010, "Broadband Ground-Motion Simulation Using a Hybrid Approach", *Bulletin of the Seismological Society of America*, Vol. 100, pp. 2095–2123.

Gülerce Z., B. Kargıoğlu., N.A. Abrahamson, 2016, "Turkey-Adjusted NGA-W1 Horizontal Ground Motion Prediction Models", *Earthquake Spectra*, Vol. 32, pp. 75-100.

Hanks, T. C., and H. Kanamori, 1979, "Fault Mechanics", *Journal of Geophysical Research. Solid Earth*, Vol. 84, p. 2145.

Hisada, Y., and J. Bielak, 2003, "A Theoretical Method for Computing Near-Fault Ground Motions in Layered Half-Space Considering Static Offset due to Surface Faulting, with a

Physical Interpretation of Fling Step and Rupture Directivity", *Bulletin of the Seismological Society of America*, Vol. 93, No. 3, pp. 1154–1168.

Hisada, Y., and S. Tanaka (2021). What Is Fling Step? Its Theory, "Simulation Method, and Applications to Strong Ground Motion near Surface Fault Ruptures", *Bulletin of the Seismological Society of America*, Vol. 111, pp. 2486–2506.

INGV16: Istituto Nazionale di Geofisica e Vulcanologia (INGV) Working Group “GPS Geodesy (GPS Data and Data Analysis Center), (2016). *Preliminary Co-seismic Displacements for the October 26 (Mw 5.9) and October 30 (Mw 6.5) Central Italy Earthquakes from the Analysis of GPS Stations*

International Conference of Building Officials, 2006, *International Building Code*, Whittier, CA, 2006.

International Conference of Building Officials, 2007, *California Building Code*, Whittier, CA, 2007.

Iwan W.D., M.A. Moser, C.Y. Peng, 1985, "Some Observations on Strong-Motion Earthquake Measurement Using a Digital Accelerograph", *Bulletin of Seismological Society of America*, Vol. 75, pp. 1225–1246.

Kaklamanos, J., L. G. Baise, and D. M. Boore, 2011, "Estimating Unknown Input Parameters when Implementing the NGA Ground Motion Prediction Equations in Engineering Practice", *Earthquake Spectra*, Vol. 27, pp. 1219–1235.

Kalkan, E., and S. K. Kunnath, 2006, "Effects of Fling Step and Forward Directivity on Seismic Response of Buildings", *Earthquake Spectra*, Vol. 22, No. 2, pp. 367–390.

Kamai, R., N. Abrahamson, R. Graves, 2014, "Adding Fling Effects to Processed Ground-Motion Time Histories", *Bulletin of the Seismological Society of America* , Vol. 104, pp. 1914–1929.

Karasözen, E., E. Nissen, P. Büyükakpınar, M.D. Cambaz, M. Kahraman, E. K. Ertan, B. Abgarmi, E. Bergman, A. Ghods, A.A. Özacar, 2018, "The 2017 July 20 Mw 6.6 Bodrum–Kos Earthquake Illuminates Active Faulting in the Gulf of Gökova, SW Turkey", *Geophysical Journal International,* Vol. 214, pp. 185-199.

Kiratzi, A., 2017, "The 12 June 2017 Mw 6.3 Lesvos Island (Aegean Sea) Earthquake: Slip Model and Directivity Estimated with Finite-Fault Inversion", *Tectonophysics,* Vol. 724–725, pp. 1-10.

Konca, A. O., S. Cetin, H. Karabulut, R. Reilinger, U. Dogan, S. Ergintav, Z. Cakir, E. Tari, 2018, "The 2014 Mw 6.9 North Aegean Earthquake: Seismic and Geodetic Evidence for Coseismic Slip on Persistent Asperities", *Geophysical Journal International*, Vol. 213, No. 2, pp. 1113–1120.

Konca, A. O., S. E. Guvercin, S. Ozarpaci, A. Ozdemir, G. J. Funning, U. Dogan, S. Ergintav, M. Floyd, H. Karabulut, R. Reilinger, 2019, "Slip Distribution of the 2017 Mw 6.6 Bodrum–Kos Earthquake: Resolving the Ambiguity of Fault Geometry", *Geophysical Journal International*, Vol. 219, No. 2, pp. 911–923.

Luzi L., G. Lanzano, C. Felicetta, M. C. D'Amico, E. Russo, S. Sgobba, F. Pacor, and ORFEUS Working Group 5, 2020, *Engineering Strong Motion Database (ESM) (Version 2.0). Istituto Nazionale di Geofisica e Vulcanologia (INGV).*

Özmen B., 2000, "Geology of Düzce-Bolu Region, Active Faults and Damaging Earthquakes, 12 November 1999 Düzce Earthquake Report", *Earthquake Research Department, Ankara, Turkey,* pp. 1- 14 (in Turkish).

Pınar, A., 1995, *Rupture Process and Spectra of Some Major Turkish Earthquakes and Their Seismotectonic Implications. (Ph.D. Thesis), Boğaziçi University, Istanbul, 1995*.

Rathje E. M., J. P. Stewart, M. B. Baturay, J. D. Bray, J. P. Bardet, 2006, "Strong Ground Motions and Damage Patterns from the 1999 Düzce Earthquake in Turkey", *Journal Earthquake Engineering*, Vol. 10, pp. 693-724.

Roussis P. C., M. C. Constantinou, M. Erdik, E. Durukal, M. Dicleli, 2002, "Assessment of Performance of Bolu Viaduct in the 1999 Duzce Earthquake in Turkey", *The Multidisciplinary Center for Earthquake Engineering Research, Buffalo*.

Satoh, T., 2020, "Static Displacement And Long-Period Velocity Pulse Of Crustal Earthquakes In Japan", *Journal of Japan Association for Earthquake Engineering*, Vol. 20, No. 5, pp. 36-58.

Schiappapietra, E., G. Lanzano, S. Sgobba, 2022, "Empirical Predictive Models for Fling Step and Displacement Response Spectra Based on the NESS Database", *Soil Dynamics and Earthquake Engineering*, Vol. 158, 107294.

Schiappapietra, E., C. Felicetta, M. D'Amico, 2021, "Fling-Step Recovering from Near-Source Waveforms Database", *Geosciences*, Vol. 11, No. 67.

Somerville, P.G., 2002, "Characterizing Near Fault Ground Motion For The Design And Evaluation Of Bridges", *Third National Seismic Conference & Workshop on Bridges & Highways*, Portland, Oregon.

Storchak, D.A., D. Di Giacomo, E.R. Engdahl, J. Harris, I. Bondár, W.H.K. Lee, P. Bormann and A. Villaseñor, 201, *The ISC-GEM Global Instrumental Earthquake Catalogue (1900-2009): Introduction, Physics of the Earth and Planetary Interiors*, Vol. 239, pp. 48-63.

Tan, O., Z. Pabuçcu, M.C. Tapırdamaz, S. İnan, S. Ergintav, H. Eyidogan, H., et al., 2011, "Aftershock Study and Seismotectonic Implications of the 8 March 2010 Kovancılar (Elazığ, Turkey) Earthquake (MW= 6.1)", *Geophysical Research Letters*, Vol. 38, L11304.

Taymaz T and O. Tan, 2001, "Source Parameters of June 6, 2000 Orta-Çankırı and December 15, 2000 Sultandağı-Akşehir Earthquakes (Mw = 6.0) Obtained from Inversion of Teleseismic Body Wave Forms", *Symposia on Seismotectonics of the North–Western Anatolia—Aegean and Recent Turkish Earthquakes: Scientific Activities 2001*, pp. 96-107.

Taymaz, T., A. Ganas, S. Yolsal-Çevikbilen, et al., 2021, "Source Mechanism and Rupture Process of the 24 January 2020 Mw 6.7 Doğanyol Sivrice Earthquake Obtained from Seismological Waveform Analysis and Space Geodetic Observations on the East Anatolian Fault Zone (Turkey)", *Tectonophysics*, Vol. 804, 228745.

Trifunac, M. D., and A. G. Brady, 1975, "A Study of the Duration of Strong Earthquake Ground Motion", *Bulletin of the Seismological Society of America*, Vol. 65, pp. 581–626.

Wells, D. L., and K. J. Coppersmith, 1994, "New Empirical Relationships Among Magnitude, Rupture Length, Rupture Width, Rupture Area, and Surface Displacement", *Bulletin of the Seismological Society of America*, Vol. 84, pp. 974–1002.

Wright T.J., B.E. Parsons, J.A. Jackson, M. Haynes, E.J. Fielding, P.C. England, P.J. Clarke, 1999, "Source Parameters of the 1 October Dinar (Turkey) Earthquake from SAR Interferometry and Seismic Body Wave Modelling", *Earth and Planetary Science Letters*, Vol. 171, pp. 23- 37.

Wu Y.M., C.F. Wu, 2007, "Approximate Recovery of Coseismic Deformation from Taiwan Strong-Motion Records", *Journal of Seismology*, Vol. 11, pp. 159–70.

Yılmaz, C., and A. Türer, 2002, "Design Philosophy and Earthquake Behavior of the 2300-meter-long Bolu Viaduct." *ECAS2002 International Symposium on Structural and Earthquake Engineering*: 50-65 (in Turkish)

Yu, S.B., L.C. Kuo, Y.J. Hsu, H.H. Su, C.C. Liu, C.S. Hou, J.F. Lee, T.C. Lai, C.C. Liu, C.L. Liu, T.F. Tseng, C.S. Tsai, and T.C. Shin, 2001, "Preseismic Deformation and Coseismic Displacements Associated with the 1999 Chi-Chi, Taiwan, Earthquake", *Bulletin of the Seismological Society of America.*, Vol. 91, pp. 995-1012.

APPENDIX A

Table A1: The earthquake records which required additional baseline correction. T(A): Additional baseline correction point as seconds *(Cont.)*

Date	Earthquake	Station	Component	T(A) sample point (s)
30.10.1983	Horasan-Narman	TK 2503	EW	15
30.10.1983	Horasan-Narman	TK 2503	NS	15
30.10.1983	Horasan-Narman	TK 2503	UD	7
13.03.1992	Erzincan	TK 2402	EW	24
6.11.1992	Doğanbey-İzmir	TK 0905	EW	10
6.11.1992	Doğanbey-İzmir	TK 0905	NS	16
6.11.1992	Doğanbey-İzmir	TK 0905	UD	10
6.11.1992	Doğanbey-İzmir	TK 3501	EW	4
6.11.1992	Doğanbey-İzmir	TK 3501	NS	4
6.11.1992	Doğanbey-İzmir	TK 3501	UD	3
1.10.1995	Dinar	TK 0302	EW	22
1.10.1995	Dinar	TK 2006	NS	20
17.08.1999	Kocaeli (Izmit)	TK 1404	EW	20
17.08.1999	Kocaeli (Izmit)	TK 1612	EW	42
17.08.1999	Kocaeli (Izmit)	TK 1612	NS	40
17.08.1999	Kocaeli (Izmit)	TK 1612	UD	30
17.08.1999	Kocaeli (Izmit)	TK 8101	EW	9

12.11.1999	Düzce	TK 8101	NS	12
12.11.1999	Düzce	A496-8165	EW	24
12.11.1999	Düzce	A498-8166	NS	35
12.05.2017	Bodrum	TK 4809	NS	18
24.01.2020	Elazığ-Sivrice	TK 4404	NS	50
23.11.2022	Düzce-Gölyaka	TK 1412	NS	50

Table A.2. The information of the earthquake stations utilized in this study AFAD: Earthquake Research Department of General Directorate of Disaster Affairs; IRIGM: Universite Joseph Fourier, Grenoble, France; LDEO: Lamont Doherty Earth Observatory of Columbia University; KOERI: Boğaziçi University Kandilli Observatory and Earthquake Research Institute; ITU: Istanbul Technical University (*Cont.)*

Date	Event Name	Station Code	Data Source	Operator Institution	Rjb (km)	Rrup (km)	Distance Reference
30.10.1983	Horasan-Narman	TK 2503	AFAD	AFAD	22,6	24,74	AFAD
13.03.1992	Erzincan	TK 2402	AFAD	AFAD	3,32	16,82	AFAD
6.11.1992	Doğanbey-İzmir	TK 0905	AFAD	AFAD	38,11	40,32	AFAD
6.11.1992	Doğanbey-İzmir	TK 3501	AFAD	AFAD	37,34	39,94	AFAD
1.10.1995	Dinar	TK 0302	ESM	AFAD	1,67	4,71	Akbaş et al. (2023)
1.10.1995	Dinar	TK 1501	AFAD	AFAD	36,66	37,07	Akbaş et al. (2023)

1.10.1995	Dinar	TK 2006	AFAD	AFAD	45,24	45,8	Akbaş et al. (2023)
27.06.1998	Adana-Ceyhan	TK 0105	AFAD	AFAD	39,99	58,52	AFAD
31.06.1998	Adana	TK 0114	AFAD	AFAD	16,59	24,48	Akbaş et al. (2023)
31.06.1998	Adana	TK 0101	AFAD	AFAD	27,71	33,04	Akbaş et al. (2023)
31.06.1998	Adana	TK 0109	AFAD	AFAD	16,87	24,67	Akbaş et al. (2023)
31.06.1998	Adana	TK 0111	AFAD	AFAD	25,79	31,45	Akbaş et al. (2023)
31.06.1998	Adana	TK 0106	AFAD	AFAD	0,64	18,19	Akbaş et al. (2023)
31.06.1998	Adana	TK 0113	AFAD	AFAD	0,37	18,1	Akbaş et al. (2023)
17.08.1999	Kocaeli (Izmit)	TK 3401	AFAD	AFAD	47,52	47,52	Akbaş et al. (2023)
17.08.1999	Kocaeli (Izmit)	TK 1404	ESM	AFAD	35,96	36,54	Akbaş et al. (2023)
17.08.1999	Kocaeli (Izmit)	TK 1612	ESM	AFAD	30,96	31,54	Akbaş et al. (2023)
17.08.1999	Kocaeli (Izmit)	ARC	ESM	KOERI	11,52	11,52	Akbaş et al. (2023)
17.08.1999	Kocaeli (Izmit)	SKR(TK 5401)	ESM	AFAD	1,8	1,8	Akbaş et al. (2023)
17.08.1999	Kocaeli (Izmit)	YPT	ESM	KOERI	4,94	4,94	Akbaş et al. (2023)

17.08.1999	Kocaeli (Izmit)	Fatih-1160	ESM	KOERI	50,36	50,36	Akbaş et al. (2023)
17.08.1999	Kocaeli (Izmit)	MSK-1169	ESM	ITU	51,19	51,19	Akbaş et al. (2023)
17.08.1999	Kocaeli (Izmit)	MCD	ESM	ITU	48,76	48,76	Akbaş et al. (2023)
17.08.1999	Kocaeli (Izmit)	ZYT	ESM	ITU	47,84	47,84	Akbaş et al. (2023)
17.08.1999	Kocaeli (Izmit)	TK 4106	ESM	AFAD	11,12	7,37	Akbaş et al. (2023)
17.08.1999	Kocaeli (Izmit)	TK 8101	AFAD	AFAD	18,05	18,05	Akbaş et al. (2023)
12.11.1999	Düzce	TK 8101	AFAD	AFAD	3,13	7,43	Akbaş et al. (2023)
12.11.1999	Düzce	TK 1401	AFAD	AFAD	9,81	9,81	Akbaş et al. (2023)
12.11.1999	Düzce	TK 5401	AFAD	AFAD	44,52	44,52	Akbaş et al. (2023)
12.11.1999	Düzce	A487-8164	ESM	IRIGM	2,22	2,22	Akbaş et al. (2023)
12.11.1999	Düzce	A496-8165	ESM	IRIGM	3,76	3,76	Akbaş et al. (2023)
12.11.1999	Düzce	A498-8166	ESM	IRIGM	3,1	3,1	Akbaş et al. (2023)
12.11.1999	Düzce	C 0362	ESM	LDEO	22,87	22,87	Akbaş et al. (2023)

12.11.1999	Düzce	C 1058	ESM	LDEO	1,21	1,21	Akbaş et al. (2023)
12.11.1999	Düzce	C 1059	ESM	LDEO	3,63	3,63	Akbaş et al. (2023)
12.11.1999	Düzce	C 0375	ESM	LDEO	3,49	3,49	Akbaş et al. (2023)
12.11.1999	Düzce	C 1060	ESM	LDEO	24,79	24,89	Akbaş et al. (2023)
12.11.1999	Düzce	C 1061	ESM	LDEO	10,88	10,88	Akbaş et al. (2023)
12.11.1999	Düzce	C 1062	ESM	LDEO	8,65	8,65	Akbaş et al. (2023)
12.11.1999	Düzce	D 0531	ESM	LDEO	8,02	8,02	Akbaş et al. (2023)
6.06.2000	Ankara-Çankırı	TK 1801	AFAD	AFAD	17,87	17,87	Akbaş et al. (2023)
3.02.2002	Afyon(Sultandağ)	TK 301	AFAD	AFAD	30,95	32,07	Akbaş et al. (2023)
1.05.2003	Bingöl	TK 1201	AFAD	AFAD	4,11	4,11	Akbaş et al. (2023)
8.03.2010	Elazığ	TK 1201	AFAD	AFAD	30,91	31,26	Akbaş et al. (2023)
8.03.2010	Elazığ	TK 2303	AFAD	AFAD	17,3	24,2	Akbaş et al. (2023)
23.10.2011	Van-Erciş	TK 6503	AFAD	AFAD	32,1	36,47	Akbaş et al. (2023)

10.06.2012	Fethiye	TK 4803	AFAD	AFAD	17,05	29,44	Akbaş et al. (2023)
10.06.2012	Fethiye	TK 4811	AFAD	AFAD	50,69	57,21	Akbaş et al. (2023)
24.05.2014	Aegean Sea	TK 1701	AFAD	AFAD	42,42	43,13	Akbaş et al. (2023)
24.05.2014	Aegean Sea	TK 1710	AFAD	AFAD	38,08	38,49	Akbaş et al. (2023)
24.05.2014	Aegean Sea	TK 1711	AFAD	AFAD	25,29	26,06	Akbaş et al. (2023)
24.05.2014	Aegean Sea	TK 1713	AFAD	AFAD	40,65	41,36	Akbaş et al. (2023)
24.05.2014	Aegean Sea	TK 1714	AFAD	AFAD	46,07	46,76	Akbaş et al. (2023)
24.05.2014	Aegean Sea	TK 2201	AFAD	AFAD	26,66	26,66	Akbaş et al. (2023)
12.05.2017	Midilli	TK 3503	AFAD	AFAD	51,38	51,42	Akbaş et al. (2023)
12.05.2017	Midilli	TK 3527	AFAD	AFAD	23,41	24,83	Akbaş et al. (2023)
12.05.2017	Midilli	TK 3534	AFAD	AFAD	38,79	38,84	Akbaş et al. (2023)
12.05.2017	Bodrum	TK 0918	AFAD	AFAD	47,96	48,34	Akbaş et al. (2023)
12.05.2017	Bodrum	TK 4806	AFAD	AFAD	42,64	43,06	Akbaş et al. (2023)

12.05.2017	Bodrum	TK 4809	AFAD	AFAD	10,09	11,75	Akbaş et al. (2023)
12.05.2017	Bodrum	TK 4810	AFAD	AFAD	48,64	48,67	Akbaş et al. (2023)
12.05.2017	Bodrum	TK 4812	AFAD	AFAD	15,56	15,56	Akbaş et al. (2023)
12.05.2017	Bodrum	TK 4814	AFAD	AFAD	53,32	52,66	Akbaş et al. (2023)
12.05.2017	Bodrum	TK 4815	AFAD	AFAD	35,93	35,93	Akbaş et al. (2023)
12.05.2017	Bodrum	TK 4817	AFAD	AFAD	34,29	34,81	Akbaş et al. (2023)
12.05.2017	Bodrum	TK 4819	AFAD	AFAD	26,44	27,11	Akbaş et al. (2023)
24.01.2020	Elazığ-Sivrice	TK 0204	AFAD	AFAD	32,7	32,84	Akbaş et al. (2023)
24.01.2020	Elazığ-Sivrice	TK 0205	AFAD	AFAD	49,75	49,84	Akbaş et al. (2023)
24.01.2020	Elazığ-Sivrice	TK 0207	AFAD	AFAD	47,54	47,64	Akbaş et al. (2023)
24.01.2020	Elazığ-Sivrice	TK 0212	AFAD	AFAD	24,21	24,39	Akbaş et al. (2023)
24.01.2020	Elazığ-Sivrice	TK 2104	AFAD	AFAD	49,27	49,36	Akbaş et al. (2023)
24.01.2020	Elazığ-Sivrice	TK 2301	AFAD	AFAD	21,71	26,27	Akbaş et al. (2023)

24.01.2020	Elazığ-Sivrice	TK 2302	AFAD	AFAD	38,6	38,72	Akbaş et al. (2023)
24.01.2020	Elazığ-Sivrice	TK 2308	AFAD	AFAD	6,94	7,56	Akbaş et al. (2023)
24.01.2020	Elazığ-Sivrice	TK 4401	AFAD	AFAD	32,29	35,6	Akbaş et al. (2023)
24.01.2020	Elazığ-Sivrice	TK 4404	AFAD	AFAD	9,54	10	Akbaş et al. (2023)
30.10.2020	Izmir(Samos)	TK 0905	AFAD	AFAD	36,43	36,57	Akbaş et al. (2023)
30.10.2020	Izmir(Samos)	TK 0911	AFAD	AFAD	48,14	48,14	Akbaş et al. (2023)
30.10.2020	Izmir(Samos)	TK 3516	AFAD	AFAD	49,92	51,06	Akbaş et al. (2023)
30.10.2020	Izmir(Samos)	TK 3523	AFAD	AFAD	45,09	46,35	Akbaş et al. (2023)
30.10.2020	Izmir(Samos)	TK 3528	AFAD	AFAD	43,59	44,89	Akbaş et al. (2023)
30.10.2020	Izmir(Samos)	TK 3533	AFAD	AFAD	44,54	45,81	Akbaş et al. (2023)
30.10.2020	Izmir(Samos)	TK 3536	AFAD	AFAD	30,47	32,3	Akbaş et al. (2023)
30.10.2020	Izmir(Samos)	TK 3538	AFAD	AFAD	50,1	51,23	Akbaş et al. (2023)
30.10.2020	Izmir(Samos)	CESE	ESM	KOERI	48	49,4	ESM
30.10.2020	Izmir(Samos)	GMLD	ESM	KOERI	14,2	18,6	ESM

30.10.2020	Izmir(Samos)	KUSD	ESM	KOERI	36,7	39,5	ESM
23.11.2022	Düzce-Gölyaka	TK 1407	AFAD	AFAD	27,74	30,78	AFAD
23.11.2022	Düzce-Gölyaka	TK 5406	AFAD	AFAD	41,45	42,47	AFAD
23.11.2022	Düzce-Gölyaka	TK 8102	AFAD	AFAD	14,98	13,19	AFAD
23.11.2022	Düzce-Gölyaka	TK 8104	AFAD	AFAD	17,17	15,02	AFAD
23.11.2022	Düzce-Gölyaka	TK 8105	AFAD	AFAD	17,45	15,26	AFAD
23.11.2022	Düzce-Gölyaka	TK 8106	AFAD	AFAD	12,87	11,42	AFAD
23.11.2022	Düzce-Gölyaka	TK 8109	AFAD	AFAD	5,94	5,62	AFAD
23.11.2022	Düzce-Gölyaka	TK 8110	AFAD	AFAD	34,29	35,52	AFAD
23.11.2022	Düzce-Gölyaka	TK 5414	AFAD	AFAD	44,91	45,86	AFAD
23.11.2022	Düzce-Gölyaka	TK 1412	AFAD	AFAD	45,63	45,56	AFAD
23.11.2022	Düzce-Gölyaka	TK 8111	AFAD	AFAD	42,28	43,29	AFAD

Table A.3. List of the prepared fling step database for Türkiye earthquakes, which also contains the FN and FP components of the stations in addition to 288 (EW,NS,UD) records and the earthquake and stations parameters: SoF, style of faulting; SS, strike slip; N, normal faulting; R, reverse faulting; Mw, moment magnitude; Vs30, the average seismic shear-wave velocity from the surface to a depth of 30 meters; NEHRP, National earthquake Hazards Reduction Program; Rjb, Joyner and Boore distance that corresponds to the closest distance from the fault rupture projection; Rrup, closest distance to the fault; PD, permanent displacement; EW; East-West; NS, North-South; UD, Up-Down; FN, fault-normal; FP, fault parallel; CR, permanent displacement could not recovered. ("*" shows the records that are used in the Türkiye adjustment process of Burks and Baker (2016) fling step prediction

Earthquake Date/Location	SoF	Mw	Station	Vs30	Soil Class (NEHRP)	Rjb (km)	Rrup (km)	PD of EW (cm)	PD of NS (cm)	PD of UD (cm)	PD of FN (cm)	PD of FP (cm)
30.10.1983/Erzurum (Horasan-Narman)	SS	6,6	TK 2503	316	D	22,6	24,74	55,4	-132,18	34,36	-4,95	*52,07
13.03.1992/Erzincan	SS	6,6	TK 2402	455	C	3,32	16,82	6,52	CR	CR	CR	CR
6.11.1992 /Doğanbey-Izmir	SS	6	TK 3501	196	D	37,34	39,94	20,24	33,91	19,48	31,07	*-20,59
6.11.1992 /Doğanbey-Izmir	SS	6	TK 0905	369	C	38,11	40,32	6,63	8,55	3,26	5,34	0,6
1.10.1995 /Dinar	N	6,1	TK 0302	198	D	1,67	4,71	130,58	CR	CR	CR	CR
1.10.1995 /Dinar	N	6,1	TK 1501	335	D	36,66	37,07	-17,21	40,21	39,02	*24,46	8,26
1.10.1995 /Dinar	N	6,1	TK 2006	395	C	45,24	45,8	8,59	-36,63	30	2,34	-11,67
27.06.1998 /Adana-Ceyhan	SS	6,2	TK 0105	264	D	39,99	58,52	-25,14	-23,68	7,57	15,36	*18,05

Earthquake Date/Location	SoF	Mw	Station	Vs30	Soil Class (NEHRP)	Rjb (km)	Rrup (km)	PD of EW (cm)	PD of NS (cm)	PD of UD (cm)	PD of FN (cm)	PD of FP (cm)
31.07.1998/Adana	SS	6,2	TK 0113	267	D	0,37	18,1	0,006	0,004	0,003	0,01	0,00008
31.07.1998/Adana	SS	6,2	TK 0106	210	D	0,64	18,19	-0,01	0,06	-0,037	0,03	-0,01
31.07.1998/Adana	SS	6,2	TK 0114	483	C	16,59	24,48	0,13	-0,3	0,03	0,25	0,1
31.07.1998/Adana	SS	6,2	TK 0109	253	D	16,87	24,67	0,04	0,08	1,81	0,23	-0,01
31.07.1998/Adana	SS	6,2	TK 0111	461	C	25,79	31,45	0,21	0,12	0,071	-0,27	-0,06
31.07.1998/Adana	SS	6,2	TK 0101	478	C	27,71	33,04	0,17	-0,08	0,175	0,16	0,05
17.08.1999/Izmit (Kocaeli)	SS	7,6	SKR (TK 5401)	412	C	1,8	1,8	186,84	CR	0,11	CR	CR
17.08.1999/Izmit (Kocaeli)	SS	7,6	YPT	297	D	4,94	4,94	-84,73	149	12,52	124,62	*175,16
17.08.1999/Izmit (Kocaeli)	SS	7,6	GBZ (TK 4106)	unknown	-	11,12	7,37	-56,82	CR	23,81	CR	CR
17.08.1999/Izmit (Kocaeli)	SS	7,6	ARC	523	C	11,52	11,52	-16	-100,4	3,44	19,65	*84,44
17.08.1999/Izmit (Kocaeli)	SS	7,6	TK 8101	282	D	18,05	18,05	-17,85	-64,16	-0,3	-13,29	*-23,56
17.08.1999/Izmit (Kocaeli)	SS	7,6	TK 1612	197	D	30,96	31,54	46,34	111,69	42,5	56,1	*-7,81
17.08.1999/Izmit (Kocaeli)	SS	7,6	TK 1404	348	D	35,96	36,54	-41,11	51,78	30,6	53,78	*-23,07
17.08.1999/Izmit (Kocaeli)	SS	7,6	TK 3401	595	C	47,52	47,52	3,2	0,74	2,98	-11,22	1,51

Earthquake Date/Location	SoF	Mw	Station	Vs30	Soil Class (NEHRP)	Rjb (km)	Rrup (km)	PD of EW (cm)	PD of NS (cm)	PD of UD (cm)	PD of FN (cm)	PD of FP (cm)
17.08.1999/Izmit (Kocaeli)	SS	7,6	ZYT	341,56	D	47,84	47,84	11,66	31,56	24,73	11,67	*34,49
17.08.1999/Izmit (Kocaeli)	SS	7,6	MCD	384,86	C	48,76	48,76	-11,2	52,48	21,92	8,39	*7,2
17.08.1999/Izmit (Kocaeli)	SS	7,6	FTH (TK 1160)	386,75	C	50,36	50,36	0,17	7,04	3,87	27,92	*-13,42
17.08.1999/Izmit (Kocaeli)	SS	7,6	MSK (TK 1169)	445,66	C	51,19	51,19	17,65	-7,79	25,86	-37,73	*10,22
12.11.1999/Düzce	SS	7,1	C 1058	529,18	C	1,21	1,21	-27,05	-29,5	-6	-11,71	*36,17
12.11.1999/Düzce	SS	7,1	A 487-8164	690	C	2,22	2,22	1,86	6,25	15,27	3,43	*18,07
12.11.1999/Düzce	SS	7,1	A 498-8166	425	C	3,1	3,1	7,23	11,26	7,65	43,78	*8,35
12.11.1999/Düzce	SS	7,1	TK 8101	282	D	3,13	7,43	-212,66	263,89	68,9	215,09	*11,01
12.11.1999/Düzce	SS	7,1	C 0375	454,2	C	3,49	3,49	91,49	-156,24	-1,3	-93,13	*100,48
12.11.1999/Düzce	SS	7,1	C 1059	551,3	C	3,63	3,63	-1,75	-17,04	3,16	-6,55	*-4,14
12.11.1999/Düzce	SS	7,1	A 496-8165	760	C	3,76	3,76	72,14	36,34	-11,04	2,39	*-16,28
12.11.1999/Düzce	SS	7,1	D 0531	638,39	C	8,02	8,02	-7,66	-12,08	-1,03	-16,75	*16,46
12.11.1999/Düzce	SS	7,1	C 1062	338	D	8,65	8,65	-7,72	-7,29	-1,95	-4,64	*-3,63
12.11.1999/Düzce	SS	7,1	TK 1401	294	D	9,81	9,81	-2,26	3,56	21,92	23,07	*5,41

Earthquake Date/Location	SoF	Mw	Station	Vs30	Soil Class (NEHRP)	Rjb (km)	Rrup (km)	PD of EW (cm)	PD of NS (cm)	PD of UD (cm)	PD of FN (cm)	PD of FP (cm)
12.11.1999/Düzce	SS	7,1	C 1061	481	C	10,88	10,88	-9,25	-2,34	-4,81	2,74	*9,92
12.11.1999/Düzce	SS	7,1	C 0362	517	C	22,87	22,87	3,1	-11,43	2,62	4,23	*-7,3
12.11.1999/Düzce	SS	7,1	C 1060	782	B	24,79	24,89	-1,94	-4,49	1,74	-2,72	*8,42
12.11.1999/Düzce	SS	7,1	TK 5401	412	C	44,52	44,52	8,49	4,41	6,51	-1,23	-2,05
3.02.2000/Afyon-Sultandağ	N	6,5	TK 301	226	D	30,95	32,07	1,87	1,39	-0,92	-0,41	-6,79
6.06.2000/ Ankara-Çankırı	SS	6	TK 1801	348	D	17,87	17,87	2,5	-1,72	1,25	0,13	1,77
1.05.2003 /Bingöl	SS	6,3	TK 1201	529	C	4,11	4,11	-4,26	-2,57	-1,66	-6,91	*5
8.03.2010 /Elazığ	SS	6,1	TK 2303	529	C	8,54	8,54	-1,39	1,5	2,72	1,95	*3,44
8.03.2010 /Elazığ	SS	6,1	TK 1201	529	C	30,91	31,26	0,25	2,05	1,85	0,19	0,34
23.10.2011/Van-Erciş	R	7,1	TK 6503	293	D	32,1	36,47	6,06	7,28	2,54	-0,79	-3,72
10.06.2012/Fethiye	SS	6,1	TK 4803	248	D	17,05	29,44	1,8	4,53	1,8	5,68	*3,64
10.06.2012/Fethiye	SS	6,1	TK 4811	372	C	50,69	57,21	-0,73	-0,01	3,29	2,99	1,26
24.05.2014/Aegen Sea	SS	6,9	TK 1711	403	C	25,29	26,06	7,57	-7,54	0,77	-11,02	1,06
24.05.2014/Aegen Sea	SS	6,9	TK 2201	315	D	26,66	26,66	8,65	-11,53	6,09	2,28	*12,34
24.05.2014/Aegen Sea	SS	6,9	TK 1710	286	D	38,08	38,49	4,51	7,78	2,42	1,42	0,78

Earthquake Date/Location	SoF	Mw	Station	Vs30	Soil Class (NEHRP)	Rjb (km)	Rrup (km)	PD of EW (cm)	PD of NS (cm)	PD of UD (cm)	PD of FN (cm)	PD of FP (cm)
24.05.2014/Aegen Sea	SS	6,9	TK 1713	483	C	40,65	41,36	2,7	2,02	-0,54	-15,75	*4,61
24.05.2014/Aegen Sea	SS	6,9	TK 1701	192	D	42,42	43,13	-4,01	10,86	2,94	0,59	1,54
24.05.2014/Aegen Sea	SS	6,9	TK 1714	429	C	46,07	46,76	-3,03	1,53	1,86	4,29	1,17
12.06.2017/Midilli	N	6,3	TK 3527	207	D	23,41	24,83	0,9	0,29	1,66	-1,26	-0,71
12.06.2017/Midilli	N	6,3	TK 3534	328	D	38,79	38,84	-0,4	-0,22	0,7	0,82	1,77
12.06.2017 /Midilli	N	6,3	TK 3503	193	D	51,38	51,42	2,38	5,47	0,67	*4,74	1,79
20.07.2017/Bodrum	N	6,6	TK 4809	747	C	10,09	11,75	-0,29	15,79	1,14	*15,31	-7,23
20.07.2017/Bodrum	N	6,6	TK 4812	732	C	15,56	15,56	5,81	-2,83	3,45	-2,74	1,41
20.07.2017/Bodrum	N	6,6	TK 4819	219	D	26,44	27,11	9,63	0,56	1,56	-1,94	-0,82
20.07.2017/Bodrum	N	6,6	TK 4817	948	B	34,29	34,81	-0,73	6,9	0,49	*6,03	1,98
20.07.2017/Bodrum	N	6,6	TK 4815	278	D	35,93	35,93	0,6	0,07	-0,83	-1,33	0,09
20.07.2017/Bodrum	N	6,6	TK 4806	323	D	42,64	43,06	-0,08	2,87	1,43	2,58	1,76
20.07.2017/Bodrum	N	6,6	TK 0918	630	C	47,96	48,34	-1,76	3,97	4,24	*4,69	4,9
20.07.2017/Bodrum	N	6,6	TK 4810	393	C	48,64	48,67	0,04	1,46	0,82	2,3	-0,57
20.07.2017/Bodrum	N	6,6	TK 4814	694	C	53,32	52,66	1,12	3,15	1,32	2,2	0,1

Earthquake Date/Location	SoF	Mw	Station	Vs30	Soil Class (NEHRP)	Rjb (km)	Rrup (km)	PD of EW (cm)	PD of NS (cm)	PD of UD (cm)	PD of FN (cm)	PD of FP (cm)
24.01.2020/Elazığ-Sivrice	SS	6,7	TK 2308	450	C	6,94	7,56	57,29	-110,43	5,63	-68,67	*-57,92
24.01.2020/Elazığ-Sivrice	SS	6,7	TK 4404	1380	B	9,54	10	-13,54	1,36	0,97	1,5	*9,51
24.01.2020/Elazığ-Sivrice	SS	6,7	TK 2301	407	C	21,71	26,27	2,27	1,66	5,6	17,63	-0,57
24.01.2020/Elazığ-Sivrice	SS	6,7	TK 0212	433	C	24,21	24,39	1,28	0,3	-0,85	1,31	0,13
24.01.2020/Elazığ-Sivrice	SS	6,7	TK 4401	481	C	32,29	35,6	1,15	-0,16	4,2	4,41	-2,66
24.01.2020/Elazığ-Sivrice	SS	6,7	TK 0204	555	C	32,7	32,84	5,86	3,79	2,83	7,03	0,43
24.01.2020/Elazığ-Sivrice	SS	6,7	TK 2302	907	B	38,6	38,72	-3,31	0,7	1,99	-0,62	1,27
24.01.2020/Elazığ-Sivrice	SS	6,7	TK 0207	660	C	47,54	47,64	1,71	2,26	-0,56	0,62	-0,09
24.01.2020/Elazığ-Sivrice	SS	6,7	TK 2104	519	C	49,27	49,36	1,69	5,48	-0,34	4,53	*6,95
24.01.2020/Elazığ-Sivrice	SS	6,7	TK 0205	660	C	49,75	49,84	-2,64	-2,37	2,5	-3,22	0,15
30.10.2020/Izmir (Samos Island)	N	7	GMLD	816	B	14,2	18,6	11,23	12,61	0,062	*6,61	5,31
30.10.2020/Izmir (Samos Island)	N	7	TK 3536	1141	B	30,47	32,3	4,84	6,7	4,2	*3,15	14,23
30.10.2020/Izmir (Samos Island)	N	7	TK 0905	369	C	36,43	36,57	9,2	2,65	1,26	*-3,68	-4,65
30.10.2020/Izmir (Samos Island)	N	7	KUSD	1052	B	36,7	39,5	-0,8	1,74	5,74	-1,23	2,62
30.10.2020/Izmir (Samos Island)	N	7	TK 3528	532	C	43,59	44,89	2,08	8,7	-3	-0,54	*6,79

Earthquake Date/Location	SoF	Mw	Station	Vs30	Soil Class (NEHRP)	Rjb (km)	Rrup (km)	PD of EW (cm)	PD of NS (cm)	PD of UD (cm)	PD of FN (cm)	PD of FP (cm)
30.10.2020/Izmir (Samos Island)	N	7	TK 3533	415	C	44,54	45,81	-3,36	15,74	1,24	0,92	4,39
30.10.2020/Izmir (Samos Island)	N	7	TK 3523	414	C	45,09	46,35	3,08	7,04	3,85	*7,35	2,91
30.10.2020/Izmir (Samos Island)	N	7	CESE	460	C	48	49,4	-2,36	1,48	-2,7	*-4,68	-0,92
30.10.2020/Izmir (Samos Island)	N	7	TK 0911	307	D	48,14	48,14	0,7	1,23	1,35	2,83	0,62
30.10.2020/Izmir (Samos Island)	N	7	TK 3516	460	C	49,92	51,06	2,41	1,59	-0,65	*3,9	1,07
30.10.2020/Izmir (Samos Island)	N	7	TK 3538	554	C	50,1	51,23	-2,72	14,47	7,23	-0,59	6,24
23.11.2022/Düzce (Gölyaka)	SS	6	TK 8109	183	D	5,94	5,62	7,51	9,94	1,29	10,13	*4,02
23.11.2022/Düzce (Gölyaka)	SS	6	TK 8106	338	D	12,87	11,42	5,09	10,81	4,85	1,4	1,94
23.11.2022/Düzce (Gölyaka)	SS	6	TK 8102	280	D	14,98	13,19	3,56	3,16	2,18	5,97	1,35
23.11.2022/Düzce (Gölyaka)	SS	6	TK 8104	398	C	17,17	15,02	4,08	4,4	3,13	2,35	*3,31
23.11.2022/Düzce (Gölyaka)	SS	6	TK 8105	914	B	17,45	15,26	3,31	11,54	3,91	3,35	1,56
23.11.2022/Düzce (Gölyaka)	SS	6	TK 1407	273	D	27,74	30,78	3,91	1,17	1	2,36	1,57
23.11.2022/Düzce (Gölyaka)	SS	6	TK 8110	407	C	34,29	35,52	-2,12	1,36	-1,91	7,33	*5,1
23.11.2022/Düzce (Gölyaka)	SS	6	TK 5406	272	D	41,45	42,47	1,38	1,06	1,02	2,11	2,3
23.11.2022/Düzce (Gölyaka)	SS	6	TK 8111	unknown	-	42,28	43,29	1,14	1,59	1,66	1,14	1,85

Earthquake Date/Location	SoF	Mw	Station	Vs30	Soil Class (NEHRP)	Rjb (km)	Rrup (km)	PD of EW (cm)	PD of NS (cm)	PD of UD (cm)	PD of FN (cm)	PD of FP (cm)
23.11.2022/Düzce (Gölyaka)	SS	6	TK 5414	unknown	-	44,91	45,86	-1,46	0,71	-2,76	-1,95	0,19
23.11.2022/Düzce (Gölyaka)	SS	6	TK 1412	unknown	-	45,63	45,56	-1,08	1,01	1	1,02	1,01

Table A.4. Permanent displacements, between 3 cm and 100 cm in absolute, in the vertical direction from Turkish strong motion database and NESS 2.0. SoF, style of faulting; Mw, moment magnitude; Rjb, Joyner and Boore distance that corresponds to the closest distance from the fault rupture projection; Rrup, closest distance to the fault; PD_UD, permanent displacement in vertical component. (Earthquake ID of the data taken from Turkish strong motion database is written as "date location") *(Cont.9)*

Earthquake ID	Earthquake Date	SoF	Dip (°)	Country	Mw	Station	Rjb (km)	Rrup (km)	PD_UD (cm)
USGS-usp00066k9	17.01.1994	TF	40	US	6,7	24278	20,04	20,66	3,00332
INT-UT19990920_174715	20.09.1999	TF	30	TW	7,6	E052	75,53	79,73	3,01183
INT-UT19990920_174715	20.09.1999	TF	30	TW	7,6	A086	50,76	56,81	3,05204
INT-UT19990920_174715	20.09.1999	TF	30	TW	7,6	B092	32,14	41,03	3,06204
INT-UT19991022_021856	22.10.1999	TF	75	TW	6,1	C047	0	5,64	3,07788
INT-UT19990920_174715	20.09.1999	TF	30	TW	7,6	F031	43,25	50,25	3,11099
INT-UT19990920_174715	20.09.1999	TF	30	TW	7,6	A072	60,04	65,23	3,11539
INT-UT19990920_174715	20.09.1999	TF	30	TW	7,6	E014	62,08	67,13	3,18025
INT-UT19990920_174715	20.09.1999	TF	30	TW	7,6	F005	35,78	43,98	3,21928
INT-UT19990920_174715	20.09.1999	TF	30	TW	7,6	B083	23,85	34,28	3,23680
INT-UT19990920_174715	20.09.1999	TF	30	TW	7,6	A043	39,27	46,83	3,23917
INT-UT19990920_174715	20.09.1999	TF	30	TW	7,6	G014	51,71	57,7	3,25928
USGS-usp00040t8	18.10.1989	TF	70	US	6,9	CRS0	35,23	35,44	3,26067
INT-UT19990920_174715	20.09.1999	TF	30	TW	7,6	F041	33,04	41,78	3,26540
USGS-usp00040t8	18.10.1989	TF	70	US	6,9	47381	12,62	13,21	-3,29660
EMSC-20080613_0000091	13.06.2008	TF	40	JP	6,9	AKT29	32,8	35,02	3,32861
INT-UT19990920_174715	20.09.1999	TF	30	TW	7,6	A007	52,89	58,72	3,34752
INT-UT19990920_174715	20.09.1999	TF	30	TW	7,6	B095	0	17,41	3,36746
USGS-usp00066k9	17.01.1994	TF	40	US	6,7	638	12,71	22,46	3,41396
INT-UT19990920_174715	20.09.1999	TF	30	TW	7,6	A032	45,17	51,88	3,44068

INT-UT19990920_174715	20.09.1999	TF	30	TW	7,6	B147	17,97	31,22	-3,49665
INT-UT19990920_174715	20.09.1999	TF	30	TW	7,6	B057	4,02	4,02	3,512941
INT-UT19990920_174715	20.09.1999	TF	30	TW	7,6	F023	52,28	58,2	3,532782
INT-UT19990920_174715	20.09.1999	TF	30	TW	7,6	B116	5,95	5,95	3,536289
INT-UT19990920_174715	20.09.1999	TF	30	TW	7,6	A035	46,4	52,95	3,576868
INT-UT19990920_174715	20.09.1999	TF	30	TW	7,6	B059	9,17	9,17	3,597428
INT-UT19990920_174715	20.09.1999	TF	30	TW	7,6	B065	0	2,37	-3,71456
INT-UT19990920_174715	20.09.1999	TF	30	TW	7,6	E051	56,6	62,09	3,716399
INT-UT19990920_174715	20.09.1999	TF	30	TW	7,6	A003	49,36	55,56	-3,79794
INT-UT19990920_174715	20.09.1999	TF	30	TW	7,6	E004	68,21	72,83	3,81279
INT-UT19990920_174715	20.09.1999	TF	30	TW	7,6	G031	43,21	50,22	3,81340
INT-UT19991022_021856	22.10.1999	TF	75	TW	6,1	C038	0	5,17	3,92825
USGS-usp00040t8	18.10.1989	TF	70	US	6,9	1575	27,25	27,52	-4,01896
INT-UT19990920_174715	20.09.1999	TF	30	TW	7,6	B060	0,87	0,88	-4,06208
INT-UT19990920_174715	20.09.1999	TF	30	TW	7,6	F029	50,4	56,52	4,19808
INT-UT19990920_174715	20.09.1999	TF	30	TW	7,6	G042	56,47	61,99	4,25737
IR-2005-0044	22.02.2005	TF	60	IR	6,5	QAD	14,79	17,44	-4,30808
IT-2012-0011	29.05.2012	TF	60	IT	6	SAN0	0	6,08	4,48164
IT-2012-0010	29.05.2012	TF	32	IT	5,5	T0819	3,64	5,29	4,50948
USGS-usp00040t8	18.10.1989	TF	70	US	6,9	HDA0	24,73	25,03	4,53418
EMSC-20110221_0000047	21.02.2011	TF	67	NZ	6,2	CHHC	4,74	4,77	-4,67704
INT-UT19990920_174715	20.09.1999	TF	30	TW	7,6	F055	32,54	41,39	4,76215
USGS-usp00066k9	17.01.1994	TF	40	US	6,7	24087	3,16	8,78	4,85626
INT-UT19991022_021856	22.10.1999	TF	75	TW	6,1	C009	0,51	5,07	4,86895
INT-UT19990920_174715	20.09.1999	TF	30	TW	7,6	E031	74,06	78,33	4,97052
INT-UT19990920_174715	20.09.1999	TF	30	TW	7,6	B053	0	0,99	-4,97174
INT-UT19990920_174715	20.09.1999	TF	30	TW	7,6	E064	69,28	73,84	4,97598
INT-UT19990920_174715	20.09.1999	TF	30	TW	7,6	B042	0	7,32	-4,99515

INT-UT19990920_174715	20.09.1999	TF	30	TW	7,6	A041	55,61	61,18	-5,08464
INT-UT19990920_174715	20.09.1999	TF	30	TW	7,6	E037	61,23	66,34	5,09842
INT-UT19990920_174715	20.09.1999	TF	30	TW	7,6	B100	3,67	3,67	5,26709
INT-UT19990920_174715	20.09.1999	TF	30	TW	7,6	E044	65,8	70,58	5,41281
EMSC-20110221_0000047	21.02.2011	TF	67	NZ	6,2	SHLC	5,55	5,57	-5,43844
USGS-usp00040t8	18.10.1989	TF	70	US	6,9	57066	24,21	24,52	-5,44748
INT-UT19990920_174715	20.09.1999	TF	30	TW	7,6	A014	54,51	60,18	-5,49775
INT-UT19990920_174715	20.09.1999	TF	30	TW	7,6	F045	66,03	70,8	5,64924
INT-UT19990920_174715	20.09.1999	TF	30	TW	7,6	F056	42,99	50,01	-5,67203
JP-2004-0002	23.10.2004	TF	47	JP	6,6	NIG14	7,12	8,16	5,72133
JP-2004-0002	23.10.2004	TF	47	JP	6,6	NIG1D	1,06	9,77	5,80745
INT-UT19990920_174715	20.09.1999	TF	30	TW	7,6	B075	0	1,86	-5,86440
INT-UT19990920_174715	20.09.1999	TF	30	TW	7,6	E067	28,13	37,99	-6,1806616
INT-UT19990920_174715	20.09.1999	TF	30	TW	7,6	A010	49,89	56,03	6,21818
INT-UT19990920_174715	20.09.1999	TF	30	TW	7,6	B050	1,72	1,72	6,23953
INT-UT19990920_174715	20.09.1999	TF	30	TW	7,6	C006	7,73	7,74	-6,26682
EMSC-20080613_0000091	13.06.2008	TF	40	JP	6,9	IWT34	5,49	5,53	6,28695
INT-UT19990920_174715	20.09.1999	TF	30	TW	7,6	B054	0	1,36	-6,34220
INT-UT19990920_174715	20.09.1999	TF	30	TW	7,6	F051	48,47	54,8	6,45437
INT-UT19990920_174715	20.09.1999	TF	30	TW	7,6	F030	38,78	46,45	-6,52859
INT-UT19990920_174715	20.09.1999	TF	30	TW	7,6	C100	40,42	40,42	-6,56376
INT-UT19990920_174715	20.09.1999	TF	30	TW	7,6	B085	25,57	36,13	6,59275
INT-UT19990920_174715	20.09.1999	TF	30	TW	7,6	F039	31,71	40,74	6,77716
INT-UT19990920_174715	20.09.1999	TF	30	TW	7,6	B015	0	13,34	6,81683
INT-UT19990920_174715	20.09.1999	TF	30	TW	7,6	F020	37,02	44,99	6,85043
INT-UT19990920_174715	20.09.1999	TF	30	TW	7,6	A094	55,6	61,17	-6,87932

INT-UT19990920_174715	20.09.1999	TF	30	TW	7,6	B018	12,31	22,67	6,88190
USGS-usp00040t8	18.10.1989	TF	70	US	6,9	57382	14,3	14,83	-6,89036
INT-UT19990920_174715	20.09.1999	TF	30	TW	7,6	F002	46,04	52,67	6,95141
INT-UT19990920_174715	20.09.1999	TF	30	TW	7,6	F026	54,34	60,05	6,95574
INT-UT19990920_174715	20.09.1999	TF	30	TW	7,6	F011	51,76	57,73	7,06782
INT-UT19990920_174715	20.09.1999	TF	30	TW	7,6	G022	44,06	50,94	7,20786
INT-UT19990920_174715	20.09.1999	TF	30	TW	7,6	B138	4,68	4,68	-7,3112
INT-UT19990920_174715	20.09.1999	TF	30	TW	7,6	C092	16,09	16,09	-7,45595
USGS-iscgem787038	9.02.1971	TF	54	US	6,7	JPC0	22,07	22,27	7,76378
INT-UT19990920_174715	20.09.1999	TF	30	TW	7,6	G001	42,9	49,95	7,77984
INT-UT19990920_174715	20.09.1999	TF	30	TW	7,6	F058	41,52	48,76	7,83977
IT-2012-0011	29.05.2012	TF	60	IT	6	MIRH	0	3,75	8,18596
INT-UT19990920_174715	20.09.1999	TF	30	TW	7,6	B038	0	0,11	8,29170
INT-UT19990920_174715	20.09.1999	TF	30	TW	7,6	F035	37,7	45,55	8,39880
IT-1976-0030	15.09.1976	TF	35	IT	6	BUI	5,08	8,25	8,59697
IR-2004-0043	28.05.2004	TF	34	IR	6,4	POO	6,26	19,06	-8,66667
IT-2012-0011	29.05.2012	TF	60	IT	6	MIR01	0	6,06	8,67507
INT-UT19990920_174715	20.09.1999	TF	30	TW	7,6	B123	10,24	10,24	8,67920
EMSC-20110221_0000047	21.02.2011	TF	67	NZ	6,2	LPCC	2,85	6,39	8,76779
INT-UT19990920_174715	20.09.1999	TF	30	TW	7,6	B109	7,75	7,75	8,91930
IT-2012-0011	29.05.2012	TF	60	IT	6	MIR02	0	3,7	8,95853
USGS-usp00066k9	17.01.1994	TF	40	US	6,7	24157	23,23	29,74	8,97811
INT-UT19990920_174715	20.09.1999	TF	30	TW	7,6	F049	48,91	55,19	9,13967
USGS-usp00040t8	18.10.1989	TF	70	US	6,9	SLA0	30,24	30,49	-9,23728
INT-UT19990920_174715	20.09.1999	TF	30	TW	7,6	B078	0	10,7	-9,36317
INT-UT19990920_174715	20.09.1999	TF	30	TW	7,6	E007	75,3	79,51	9,48000
INT-UT19990920_174715	20.09.1999	TF	30	TW	7,6	F032	35,35	43,63	9,78575
INT-UT19990920_174715	20.09.1999	TF	30	TW	7,6	F019	53,77	59,54	9,81121
IT-2012-0011	29.05.2012	TF	60	IT	6	MIRE	0	3,86	9,87385

INT-UT19990920_174715	20.09.1999	TF	30	TW	7,6	B046	0	9,83	-9,94163
INT-UT19990920_174715	20.09.1999	TF	30	TW	7,6	B106	9,67	9,67	10,04786
INT-UT19990920_174715	20.09.1999	TF	30	TW	7,6	B036	0	1,86	-10,83966
USGS-usp00066k9	17.01.1994	TF	40	US	6,7	24538	17,15	26,38	10,92299
USGS-usp00040t8	18.10.1989	TF	70	US	6,9	57007	0,17	3,9	11,11357
INT-UT19990920_174715	20.09.1999	TF	30	TW	7,6	F034	32,32	41,22	11,14641
INT-UT19990920_174715	20.09.1999	TF	30	TW	7,6	B107	10,85	10,85	11,21398
INT-UT19990920_174715	20.09.1999	TF	30	TW	7,6	F048	50,26	56,39	11,44848
IT-2012-0011	29.05.2012	TF	60	IT	6	MRN	0	3,86	-11,53012
INT-UT19990920_174715	20.09.1999	TF	30	TW	7,6	C026	22,94	22,95	11,60131
INT-UT19990920_174715	20.09.1999	TF	30	TW	7,6	B102	0	3,52	12,12233
INT-UT19990920_174715	20.09.1999	TF	30	TW	7,6	B089	0	11,08	-12,2517
INT-UT19990920_174715	20.09.1999	TF	30	TW	7,6	F027	51,99	57,94	13,0405
INT-UT19990920_174715	20.09.1999	TF	30	TW	7,6	F006	36,03	44,18	13,25658
USGS-usp00040t8	18.10.1989	TF	70	US	6,9	47380	10,83	11,51	-13,48256
USGS-usp00040t8	18.10.1989	TF	70	US	6,9	58065	7,56	8,5	14,16707
INT-UT19990920_174715	20.09.1999	TF	30	TW	7,6	B079	0	13,14	-14,17129
INT-UT19990920_174715	20.09.1999	TF	30	TW	7,6	B067	0	3,78	-14,28037
INT-UT19990920_174715	20.09.1999	TF	30	TW	7,6	C111	41,67	41,67	14,37932
USGS-usp00040t8	18.10.1989	TF	70	US	6,9	57425	22,86	23,19	-14,78108
USGS-usp00040t8	18.10.1989	TF	70	US	6,9	47125	8,36	14,96	-15,59709
IT-1976-0027	15.09.1976	TF	35	IT	5,9	GMN	3,25	5,37	-15,65775
INT-UT19990920_174715	20.09.1999	TF	30	TW	7,6	D018	67,32	67,32	15,69402
INT-UT19990920_174715	20.09.1999	TF	30	TW	7,6	B131	0	7,7	-15,92231
USGS-usp00040t8	18.10.1989	TF	70	US	6,9	SVL0	23,85	24,17	-16,26226
JP-2004-0002	23.10.2004	TF	47	JP	6,6	NIG15	10,09	11,35	16,40050
USGS-usp00066k9	17.01.1994	TF	40	US	6,7	24688	13,55	22,44	17,36760
USGS-usp00040t8	18.10.1989	TF	70	US	6,9	58127	33,7	33,92	17,41027

USGS-usp00066k9	17.01.1994	TF	40	US	6,7	24088	5,33	7,31	-18,95862
INT-UT19990920_174715	20.09.1999	TF	30	TW	7,6	B045	0	12,72	19,53031
USGS-usp00066k9	17.01.1994	TF	40	US	6,7	24514	1,51	5,22	20,49286
USGS-iscgem893168	21.07.1952	TF	75	US	7,3	TAF0	38,44	38,91	-21,64631
USGS-usp00040t8	18.10.1989	TF	70	US	6,9	57383	18,44	18,85	-21,66308
INT-UT19990920_174715	20.09.1999	TF	30	TW	7,6	B049	0	2,08	-23,24829
INT-UT19990920_174715	20.09.1999	TF	30	TW	7,6	B061	10,18	10,18	23,83365
INT-UT19990920_174715	20.09.1999	TF	30	TW	7,6	B133	0	0,11	-25,51445
INT-UT19990920_174715	20.09.1999	TF	30	TW	7,6	HSN0	3,36	15,33	26,95591
USGS-usp00066k9	17.01.1994	TF	40	US	6,7	24279	3,22	5,95	28,24580
EMSC-20110221_0000047	21.02.2011	TF	67	NZ	6,2	HVSC	0	3,35	29,22998
USGS-usp00040t8	18.10.1989	TF	70	US	6,9	58135	11,95	18,34	31,16827
JP-2004-0002	23.10.2004	TF	47	JP	6,6	NIG13	0	8,83	36,91627
INT-UT19990920_174715	20.09.1999	TF	30	TW	7,6	NCU0	23,85	34,28	39,66855
USGS-usp00066k9	17.01.1994	TF	40	US	6,7	5263	14,44	23,12	42,71490
USGS-iscgem787038	9.02.1971	TF	54	US	6,7	SNT0	27,36	27,52	-47,51397
USGS-iscgem787038	9.02.1971	TF	54	US	6,7	24207	3,27	4,44	63,97223
INT-UT19990920_174715	20.09.1999	TF	30	TW	7,6	B074	0	16,35	-70,45243
USGS-usp00040t8	18.10.1989	TF	70	US	6,9	SJH0	22,95	23,28	74,36140
30 October 2020 Izmir(Samos-Sisam)	30.10.2020	NF	43	TR	7	TK 3528	43,59	44,89	-3
IT-1984-0005	11.05.1984	NF	43	IT	5,5	VLB	4,43	10,52	3,07901
IT-2009-0009	6.04.2009	NF	50	IT	6,1	AQA	0	5,74	-3,08539
IT-2009-0009	6.04.2009	NF	50	IT	6,1	AQV	0	5,43	-3,20063
EMSC-20161030_0000029	24.08.2016	NF	47	IT	6,5	T1244	0,03	0,03	-3,35677
20 July 2017 Bodrum	20.07.2017	NF	37	TR	6,6	TK 4812	15,56	15,56	3,45
USGS-us20005iis	15.04.2016	NF	64	JP	7	KMM1C	14,91	14,94	3,51734
EMSC-20161030_0000029	24.08.2016	NF	47	IT	6,5	MZ63	11,85	12,38	-3,64919
IT-1997-0006	26.09.1997	NF	40	IT	6	CLF	1,63	3,89	3,84303
30 October 2020 Izmir(Samos Island)	30.10.2020	NF	43	TR	7	TK 3523	45,09	46,35	3,85

30 October 2020 Izmir(Samos Island)	30.10.2020	NF	43	TR	7	TK 3536	30,47	32,3	4,2
20 July 2017 Bodrum	20.07.2017	NF	37	TR	6,6	TK 0918	47,96	48,34	4,24
USGS-us20005iis	15.04.2016	NF	64	JP	7	KMM1F	38,87	38,88	-4,45255
GR-1986-0006	13.09.1986	NF	45	GR	5,9	KAL1	0	6,06	-4,48972
EMSC-20161030_0000029	24.08.2016	NF	47	IT	6,5	T1213	4,41	10,25	-4,72358
EMSC-20160824_0000006	24.08.2016	NF	50	IT	6	AMT	1,38	4,62	-4,93876
USGS-us20005iis	15.04.2016	NF	64	JP	7	KMM1A	14,21	14,24	5,10379
USGS-us20005iis	15.04.2016	NF	64	JP	7	KMM09	29,43	29,45	-5,22016
EMSC-20161026_0000095	24.08.2016	NF	47	IT	5,9	CNE	0	2,81	-5,6994
30 October 2020 Izmir(Samos Island)	30.10.2020	NF	43	TR	7	KUSD	36,7	39,5	5,74
EMSC-20170118_0000034	18.01.2017	NF	48,78	IT	5,5	PCB	0	2,66	-5,8034
EMSC-20161030_0000029	24.08.2016	NF	47	IT	6,5	T1299	9,79	11,27	-6,17152
IT-1997-0004	35699,023	NF	46	IT	5,7	CLF	0,31	1,67	-6,79066
GR-1995-0047	34865,011	NF	43	GR	6,5	AIGA	13,61	13,61	6,80049
30 October 2020 Izmir(Samos Island)	30.10.2020	NF	43	TR	7	TK 3538	50,1	51,23	7,23
EMSC-20161030_0000029	24.08.2016	NF	47	IT	6,5	NRC	2,84	9,1	7,41491
USGS-us20005iis	15.04.2016	NF	64	JP	7	KMM18	8,75	8,79	8,55046
USGS-us20005iis	15.04.2016	NF	64	JP	7	KMM06	8,98	9,03	8,63396
USGS-us20005iis	15.04.2016	NF	64	JP	7	KMM15	0	1,27	9,05476
EMSC-20161030_0000029	24.08.2016	NF	47	IT	6,5	ACC	2,19	5,73	-9,90738
USGS-us20005iis	15.04.2016	NF	64	JP	7	KMM19	16,44	16,86	-10,1035
EMSC-20161030_0000029	24.08.2016	NF	47	IT	6,5	NOR	3,14	9,32	12,93121
IT-2009-0009	6.04.2009	NF	50	IT	6,1	AQK	0	4,44	-13,8051
EMSC-20161030_0000029	24.08.2016	NF	47	IT	6,5	MZ102	1,05	5,62	-17,8422
USGS-us20005iis	15.04.2016	NF	64	JP	7	KMM17	0,58	6,5	-25,4953
EMSC-20161030_0000029	24.08.2016	NF	47	IT	6,5	CNE	0	2,13	-28,247
1 October 1995 Dinar	1.10.1995	NF	43	TR	6,1	TK 2006	45,24	45,8	30

1 October 1995 Dinar	1.10.1995	NF	43	TR	6,1	TK 1501	36,66	37,07	39,02
EMSC-20161030_0000029	24.08.2016	NF	47	IT	6,5	T1214	0	4,54	-43,439
USGS-us20005iis	15.04.2016	NF	64	JP	7	KMM10	0	4,68	-49,6792
USGS-us20005iis	15.04.2016	NF	64	JP	7	KMM16	2,29	8,38	-73,7623
EMSC-20161113_0000048	13.11.2016	SS	36	NZ	8	HOCS	121,81	123,78	3,06662
EMSC-20161113_0000048	13.11.2016	SS	36	NZ	8	KIRS	77,25	80,29	-3,33866
EMSC-20161113_0000048	13.11.2016	SS	36	NZ	8	MRZ	131,65	133,47	-3,67404
EMSC-20161113_0000048	13.11.2016	SS	36	NZ	8	BTWS	94,81	97,36	-4,33285
EMSC-20161113_0000048	13.11.2016	SS	36	NZ	8	PHHS	45,24	50,31	-4,38312
EMSC-20161113_0000048	13.11.2016	SS	36	NZ	8	MAVS	81,86	82,67	4,43246
EMSC-20161113_0000048	13.11.2016	SS	36	NZ	8	TFSS	38,38	44,26	-5,15725
EMSC-20161113_0000048	13.11.2016	SS	36	NZ	8	NLMS	98,07	100,55	-5,40098
EMSC-20161113_0000048	13.11.2016	SS	36	NZ	8	LHUS	46,82	51,74	-5,56214
EMSC-20161113_0000048	13.11.2016	SS	36	NZ	8	UHSS	64,34	68	7,48935
EMSC-20161113_0000048	13.11.2016	SS	36	NZ	8	TMDS	73,16	76,4	-7,72979
EMSC-20161113_0000048	13.11.2016	SS	36	NZ	8	BOWS	37,79	43,75	-12,50977
EMSC-20161113_0000048	13.11.2016	SS	36	NZ	8	LRSS	47,4	52,26	-12,70059
EMSC-20161113_0000048	13.11.2016	SS	36	NZ	8	MKBS	41,88	47,32	-13,66046
EMSC-20161113_0000048	13.11.2016	SS	36	NZ	8	WTMC	0	11,99	-14,49212
EMSC-20161113_0000048	13.11.2016	SS	36	NZ	8	LIRS	47,77	52,6	16,01891
EMSC-20161113_0000048	13.11.2016	SS	36	NZ	8	LNBS	50,69	55,26	18,44572
EMSC-20161113_0000048	13.11.2016	SS	36	NZ	8	SEAS	35,28	41,48	-18,51459
EMSC-20161113_0000048	13.11.2016	SS	36	NZ	8	SEDS	21,54	30,84	-38,27768
USGS-usp0002vtg	8.07.1986	SS	46	US	6,7	WWT0	0	5,92	3,03269
USGS-usp0002vtg	8.07.1986	SS	46	US	6,7	NPS0	0	4,04	6,65103
USGS-usp0002vtg	8.07.1986	SS	46	US	6,7	MVF0	3,5	11,95	-9,00192
USGS-usp0002vtg	8.07.1986	SS	46	US	6,7	12025	10,33	11,08	13,70094

12 November 1999 Düzce	12.11.1999	SS	65	TR	7,1	C1059	0	4,63	3,16
12 November 1999 Düzce	12.11.1999	SS	65	TR	7,1	C1061	6,01	6,63	-4,81
12 November 1999 Düzce	12.11.1999	SS	65	TR	7,1	C1058	0	4,66	-6
12 November 1999 Düzce	12.11.1999	SS	65	TR	7,1	5401	40,54	41,2	6,51
12 November 1999 Düzce	12.11.1999	SS	65	TR	7,1	A498-8166	3,1	3,1	7,65
12 November 1999 Düzce	12.11.1999	SS	65	TR	7,1	A496-8165	3,76	3,76	-11,04
12 November 1999 Düzce	12.11.1999	SS	65	TR	7,1	487	0,09	4,91	15,27
12 November 1999 Düzce	12.11.1999	SS	65	TR	7,1	1401	24,85	24,85	21,92
12 November 1999 Düzce	12.11.1999	SS	65	TR	7,1	TK 8101	3,13	7,43	68,9
24 January 2020 Elazığ-Sivrice	24.01.2020	SS	68	TR	6,7	TK 4401	32,29	35,6	4,2
24 January 2020 Elazığ-Sivrice	24.01.2020	SS	68	TR	6,7	TK 2301	21,71	26,27	5,6
24 January 2020 Elazığ-Sivrice	24.01.2020	SS	68	TR	6,7	TK 2308	6,94	7,56	5,63
EMSC-20110613_0000006	13.06.2011	SS	72	NZ	6	NBLC	0	3,88	-3,77353
EMSC-20110613_0000006	13.06.2011	SS	72	NZ	6	HPSC	1,55	4,18	-5,14657
EMSC-20110613_0000006	13.06.2011	SS	72	NZ	6	LPOC	8,59	11,32	7,31729
EMSC-20110613_0000006	13.06.2011	SS	72	NZ	6	PARS	4,46	7,85	14,92803
10 June 2012 Fethiye	10.06.2012	SS	78	TR	6,1	TK 4811	50,69	57,21	3,29
USGS-usp000128g	6.08.1979	SS	80	US	5,8	G040	4,81	5,72	6,50115
USGS-usp00013ee	15.10.1979	SS	80	MX	6,5	E030	10,09	12,14	-3,46489
USGS-usp00013ee	15.10.1979	SS	80	MX	6,5	CHIH	7,26	7,26	4,09389
USGS-usp00013ee	15.10.1979	SS	80	MX	6,5	5053	10,85	10,85	-6,08825
USGS-usp00013ee	15.10.1979	SS	80	MX	6,5	E100	9,26	9,26	-6,12646
USGS-usp00013ee	15.10.1979	SS	80	MX	6,5	E040	4,2	6,34	6,20918
USGS-usp00013ee	15.10.1979	SS	80	MX	6,5	E020	12,59	14,6	8,574448
USGS-usp00013ee	15.10.1979	SS	80	MX	6,5	E080	4,59	4,59	10,92866
USGS-usp00013ee	15.10.1979	SS	80	MX	6,5	BRA0	8,58	10,39	-20,37541
USGS-usp00013ee	15.10.1979	SS	80	MX	6,5	HVP0	4,95	7,09	22,02650
USGS-usp00013ee	15.10.1979	SS	80	MX	6,5	EDA0	5,8	5,8	22,64186
USGS-usp00013ee	15.10.1979	SS	80	MX	6,5	ELC0	8,19	8,19	33,75211

USGS-usp00013ee	15.10.1979	SS	80	MX	6,5	CPRI	15,14	15,14	38,32799
USGS-usp00013ee	15.10.1979	SS	80	MX	6,5	5054	0,12	2,35	45,60728
USGS-usp00013ee	15.10.1979	SS	80	MX	6,5	6618	0	0,49	46,02162
30October1983Horasan-Narman	30.10.1983	SS	80	TR	6,6	TK 2503	22,6	24,74	34,36
27 June 1998 Adana-Ceyhan	27.06.1998	SS	81	TR	6,2	TK 0105	39,99	58,52	7,57
EMSC-20140824_0000036	24.08.2014	SS	82	US	6,1	NHC	3,69	5	-4,39637
EMSC-20100903_0000044	3.09.2010	SS	82,2	NZ	7,1	REHS	19,51	19,51	-4,32742
EMSC-20100903_0000044	3.09.2010	SS	82,2	NZ	7,1	SPFS	29,77	29,77	6,59699
EMSC-20100903_0000044	3.09.2010	SS	82,2	NZ	7,1	DFHS	11,64	11,64	-10,76782
EMSC-20100903_0000044	3.09.2010	SS	82,2	NZ	7,1	ROLC	0	2	-18,52271
EMSC-20100903_0000044	3.09.2010	SS	82,2	NZ	7,1	RHSC	13,58	13,58	23,03383
EMSC-20100903_0000044	3.09.2010	SS	82,2	NZ	7,1	GDLC	1,08	1,08	-46,71756
23 Novemver2022Düzce	22.11.2022	SS	83	TR	6	TK 8104	17,17	15,02	3,13
6 November 1992 Doğanbey-Izmir	6.11.1992	SS	83	TR	6	TK 0905	38,11	40,32	3,26
23 Novemver 2022 Düzce	22.11.2022	SS	83	TR	6	TK 8105	17,45	15,26	3,91
23 Novemver 2022 Düzce	22.11.2022	SS	83	TR	6	TK 8106	12,87	11,42	4,85
6 November 1992 Doğanbey-Izmir	6.11.1992	SS	83	TR	6	TK 3501	37,34	39,94	19,48
24 May 2014 Aegen Sea	24.05.2014	SS	85	TR	6,9	TK 2201	26,66	26,66	6,09
EMSC-20190706_0000043	6.07.2019	SS	85	US	7,1	WRC2	8,63	8,63	-3,02570
EMSC-20190706_0000043	6.07.2019	SS	85	US	7,1	WNM	14,13	16,37	-5,20914
EMSC-20190706_0000043	6.07.2019	SS	85	US	7,1	TOW2	7,04	9,31	6,36349
EMSC-20190706_0000043	6.07.2019	SS	85	US	7,1	CLC	2,52	2,52	-36,2524
IR-2003-0041	26.12.2003	SS	85,5	IR	6,5	BAM	0	1,47	-9,84755
17 August 1999 Izmit (Kocaeli)	17.08.1999	SS	87	TR	7,6	ARC	11,52	11,52	3,44
TK-1999-0077	17.08.1999	SS	87	TR	7,6	YKP	63,92	64,74	3,70990
17 August 1999 Izmit (Kocaeli)	17.08.1999	SS	87	TR	7,6	Fatih-1160	50,36	50,36	3,87
17 August 1999 Izmit (Kocaeli)	17.08.1999	SS	87	TR	7,6	YPT	4,94	4,94	12,52
TK-1999-0077	17.08.1999	SS	87	TR	7,6	KMP	64,22	64,9	15,49114

17 August 1999 Izmit (Kocaeli)	17.08.1999	SS	87	TR	7,6	MCD	63,63	48,76	21,92
17 August 1999 Izmit (Kocaeli)	17.08.1999	SS	87	TR	7,6	Gebze(marmar atübita kTK41 06)	11,12	7,37	23,81
17 August 1999 Izmit (Kocaeli)	17.08.1999	SS	87	TR	7,6	ZYT	47,84	47,84	24,73
17 August 1999 Izmit (Kocaeli)	17.08.1999	SS	87	TR	7,6	MSK	51,19	51,19	25,86
17 August 1999 Izmit (Kocaeli)	17.08.1999	SS	87	TR	7,6	TK 1404	35,96	36,54	30,6
17 August 1999 Izmit (Kocaeli)	17.08.1999	SS	87	TR	7,6	TK 1612	30,96	31,54	42,5
USGS-nc51147892	28.09.2004	SS	89	US	6	36138	1,38	2,86	3,25723
USGS-nc51147892	28.09.2004	SS	89	US	6	36420	3,84	4,69	-3,52871
USGS-nc51147892	28.09.2004	SS	89	US	6	36448	0,66	2,62	3,96124
USGS-nc51147892	28.09.2004	SS	89	US	6	36412	3,82	4,66	4,86998
USGS-nc51147892	28.09.2004	SS	89	US	6	36449	3,73	4,49	5,12744
USGS-nc51147892	28.09.2004	SS	89	US	6	36431	1,61	2,97	-5,59102
USGS-nc51147892	28.09.2004	SS	89	US	6	36176	4,12	4,93	6,20761
USGS-nc51147892	28.09.2004	SS	89	US	6	36445	0,4	2,55	6,58899
USGS-nc51147892	28.09.2004	SS	89	US	6	36415	0,57	2,56	-6,84108
USGS-nc51147892	28.09.2004	SS	89	US	6	36453	3,73	4,49	11,76983
USGS-nc51147892	28.09.2004	SS	89	US	6	36228	1,55	2,94	15,48676
USGS-usp0001dcq	26.04.1981	SS	90	US	5,9	WSM0	5,96	6,29	-9,77230
USGS-usp0001dcq	26.04.1981	SS	90	US	5,9	WLF0	8,08	8,32	-16,98262
USGS-usp000566s	23.04.1992	SS	90	US	6,1	5295	6,76	6,76	-4,62132
JP-2000-0007	6.10.2000	SS	90	JP	6,6	SMN02	23,3	23,31	3,09980
JP-2000-0007	6.10.2000	SS	90	JP	6,6	SMN0 A	16,16	16,16	-3,20401
JP-2000-0007	6.10.2000	SS	90	JP	6,6	TTR02	0,98	1,1	17,73054
USGS-usp0003afe	24.11.1987	SS	90	US	6,6	5051	0,65	0,65	-32,4515
USGS-usp00059sn	28.06.1992	SS	90	US	7,3	22074	16,25	16,28	68,61822